Università degli Studi di Cagliari

DOTTORATO DI RICERCA

in

Scienze e Tecnologie Chimiche e Farmaceutiche

Ciclo **XXIII**

Smart nanostructured drug delivery systems based on non-ionic surfactants

Settore/i scientifico disciplinari di afferenza

CHIM-02 Chimicha Fisica

Presentata da: **Pradip Hiwale**

Coordinatore Dottorato: **Prof. Mariano Casu**

Tutor: **Prof.ssa. Maura Monduzzi**

Dr. Sergio Murgia

Dr. Andrea Salis

Esame finale anno accademico 2009 – 2010

SMART NANOSTRUCTURED DRUG DELIVERY SYSTEMS BASED ON NON-IONIC SURFACTANTS

Pradip Hiwale

PhD in Chemical Sciences and Pharmaceutical Technology

A dissertation

submitted to

University of Cagliari

in partial fulfillment of the requirements
for the degree of

Doctor of philosophy

Department of Chemical Sciences
University of Cagliari
SS 554 Bivio Sestu
09042 Monserrato (CA)
ITALY

XXIII Cycle

2008-2010

Dedicated to my beloved parents

& my loving grandmother

Acknowledgement

Pursuing a Ph.D. project is a unique experience full of everyday happenings. To reach at this stage of highest academic accomplishment, was possible only because of support of many people who always stood beside me whenever I required their guidance, help or assistance.

First of all, I'd like to give my sincere thanks to my respectable supervisor, Prof Maura Monduzzi, who accepted me as her Ph.D. student. She has always offered me ideas and suggestions which were foundations to my research. Every time I met her for discussions, she has motivated and encouraged me. Without her help I could not have finished my dissertation successfully.

I must give special thanks to Dr Sergio Murgia. He is the one whom I met first, when I arrived in Cagliari and from that day he has always helped me in every possible way. His encouragement and help made me feel confident to realize my desire of completing doctorate degree.

I also appreciate very much to Dr Andrea Salis. Our brainstorming discussions and conversations have boosted my knowledge and vision. I'd like to give my sincere thanks to him for his support and supervision.

Thanks are due to Gabriele Conti, Marco Piludu and Prof Alessandro Riva for the precious collaborations in the Electron Microscopy measurements, and to Prof Anna Maria Fadda and Carla Caddeo for rheological measurements.

My thanks to my colleagues Sandrina Lampis, Maura Carboni, Mariana Mamusa, Daniela Steri, Luca Medda and

Francesca Cugia. I will always remember the good time spent with them in last three years.

I would like to thank MIUR for providing me 'Young Indian Researcher Fellowship' for years 2008 and 2009. Thanks are due to Projects MIUR DM28142 of the Sardinian Biomedicine District, MIUR Prin 2008, grant number 2006030935, for financial support. Sardegna Ricerche Polaris is thanked for free access to the instruments belonging to the Nanobiotechnology laboratories. In addition thanks are due to CSGI and CNBS for general expertise support.

I need to mention my sincere thanks to Prof. Arvind K. Bansal, who has recommended me to pursue PhD in University of Cagliari. His teachings will always remain fundamental for me.

I give my heartfelt thanks to all my friends and well-wishers. However, this list is not complete; I would like to mention some names: Prof. Sanjay Kasture, Amit Khairnar, Ajita, Shaji, Manishankar, Brajesh, Amita, Amit Kumar, Shailendra, Saumya, Yogesh, Pallab, Amit Phatale, Abhijeet and Amol.

I am very much grateful to my parents. Their understanding and affection encouraged me to work sincerely and to continue pursuing Ph.D. abroad.

Last but not the least, I would like to express thanks to my wife Kavita, who lived apart from me, even after the marriage. Her love and support has enabled me to work hard.

-Pradip Hiwale

TABLE OF CONTENTS

INTRODUCTION

Smart nanostructured materials refer to the materials that can respond to external stimuli or to their environment, and owing to their small size and very large interfacial area; they possess specific properties and functions. These materials are useful for biomedical applications, for instance, site-specific drug delivery and tissue engineering. The mechanisms used to achieve novel drug delivery systems typically incorporate one or more of the following materials: biologics, polymers and/or silica based materials.

The aim of this PhD work was to modify existing nanostructured materials by altering specific parameters. Three different types of non-ionic surfactants were utilized in this work to obtain diverse nanostructured drug delivery systems. Triblock copolymers of polyoxyethylene and polyoxypropylene viz. Pluronic F127 and Pluronic P123 were used to prepare thermoreversible gels and templates for the synthesis of mesoporous silica materials, respectively. A sorbitan alkyl ester - span 80 was used in the preparation of gelatin microspheres. The monoglyceride surfactant monoolein was used to formulate different liquid crystalline structures and W/O emulsions stabilized by liquid crystalline phases.

The model protein lysozyme and the small hydrophilic drug caffeine were used to evaluate loading and release performances. Three different types of formulations, mainly obtained using non-ionic surfactants, were characterized by techniques such as polarized light microscopy (PLM), scanning- and transmission electron microscopy (SEM and TEM), infrared (IR) spectroscopy, potentiometry, rheology, small angle X-ray scattering (SAXS), nuclear magnetic resonance (NMR) spectroscopy and N_2 adsorption/desorption. Structural features were then correlated with the *in vitro* release properties to study the effect of different variables.

1. GENERAL BACKGROUND

1.1. Colloidal Systems

The term *colloid* applies broadly to systems containing at least two components, in any state of matter, one dispersed in the other, where the dispersed component consists of large molecules or small particles [1]. Thus, they consist of *a dispersed phase* (or *discontinuous phase*) distributed uniformly in a finely divided state in a *dispersing medium* (or *continuous phase*). Colloids are broadly classified into three major classes viz. *simple colloids*, *network colloids* and *multiple colloids*. In case of *simple colloids*, for example emulsions and colloidal suspensions, a clear distinction between the dispersed phase and dispersing medium can be made. Another important example is *association colloids*, where molecules of surface active agents come together to form small aggregates (*micelles*) in water. The nanostructures formed by surfactant molecules can adopt an ordered structure to form *liquid crystals*. In case of *network colloids*, such as certain gels, it is hardly possible to distinguish the two phases as they consist of interpenetrating networks, the elements of each being of colloidal dimension. *Multiple colloids* involve co-existence of three phases of which two (and sometimes three) phases are finely divided. For example, multiple emulsions where water in oil emulsion is dispersed in water or oil in water emulsion is dispersed in oil [2].

The colloidal dispersed phase normally, but not necessarily, in all cases lie between 10-10000 nm [3]. It is not obligatory for all three dimensions to lie in these limits, since colloidal behavior is observed in some systems containing fibers in which only one dimension is in colloidal range. An alternative classification of colloids is based upon the type of dispersing medium *i.e. lyophobic* (or *hydrophobic* when dispersing medium is water) and lyophilic *i.e. lyophilic* (or *hydrophilic* when dispersing medium

is water) colloids, depending on whether particles can be described in the former case as ‘solvent hating’ or in the latter case as ‘solvent loving’ [2].

1.2. Surfactants and self-assembly

Surfactants are low to moderate molecular weight compounds which contain one hydrophobic part, which is generally readily soluble in oil but sparingly soluble or insoluble in water, and one hydrophilic (or polar) part, which is sparingly soluble or insoluble in oil but readily soluble in water (Fig.1.1) [4].

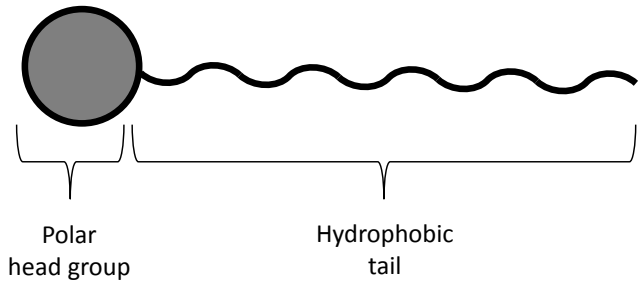

Fig.1.1. Schematic illustration of a surfactant molecule.

Due to this ‘‘schizophrenic’’ nature of surfactant molecules, they experience suboptimal conditions when dissolved molecularly in aqueous solution. If the hydrophobic segment is very large the surfactant will not be water-soluble, whereas for smaller hydrophobic moieties, the surfactant is soluble, but the contact between the hydrophobic block and the aqueous medium is energetically less favorable than the water-water contacts. Alternatives to a molecular solution, where the contact between the hydrophobic group and the aqueous surrounding is reduced, therefore offer ways for these systems to reduce their free energy. Consequently, surfactants are surface active, and tend to accumulate at various polar-apolar interfaces, where the water contact is reduced [4].

Another way to reduce the oil-water contact is self-assembly, through which the hydrophobic domains of the surfactant molecules can associate to form various structures, which allow a reduced oil-water contact. Various structures can be formed, including micelles, microemulsions, and a range of liquid crystalline phases (Fig.1.2). The type of structures formed depends on a range of parameters, such as the size of the hydrophobic tail, the nature and size of the polar head group, temperature, salt concentration, pH, etc. Through varying these parameters, one structure may also turn into another, which offers interesting opportunities in triggered drug delivery [4].

The primary mechanism for surfactants to reduce the energy in most cases will be adsorption at the available interfaces. However, when all interfaces begin to be saturated, the overall energy reduction may continue through other mechanisms as illustrated in Fig.1.2 [3].

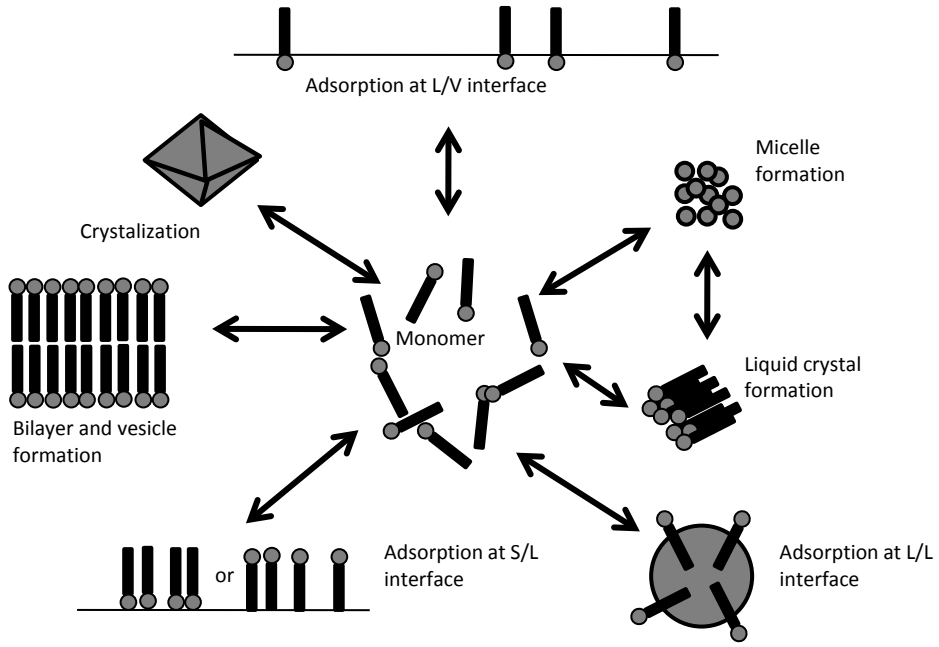

Fig.1.2. Modes of surfactant action for reduction of surface and interfacial energies.

Micelles and liquid crystals formation is a process of thermodynamic random self-assembly whereas the formation of emulsions often involves a tricky, kinetically driven process.

In the following sections these self-assembly structures are discussed individually in order of the complexity of the structures.

1.2.1. Micelles and reverse micelles

1.2.1.1. Micelles

A micelle is a colloidal-size object that is formed by spontaneous association of surfactant molecules. When dissolved in aqueous medium part of the initially added surfactant molecules are adsorbed onto the air–liquid interface and form an adsorbed monolayer. Since the space for the monolayer formation is limited at the surface, the rest of the molecules remain in the solution as a free form of molecules (monomers). In general, the main attractive driving force for the micellization (micelle formation) is the hydrophobic interaction (Fig.1.3).

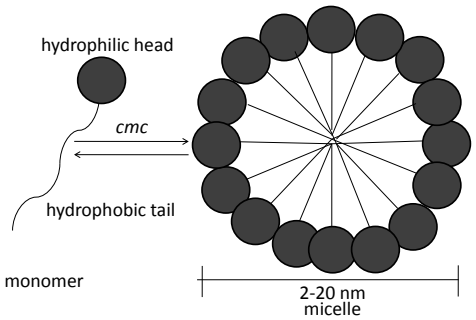

Fig.1.3. Micelle formation: micellization.

As the concentration of surfactant increases, the monomers come close together because of this interaction. This also brings closely together the head groups, which can be either ionic (for ionic surfactants) or hydrated (for nonionic surfactants). Thus, the repulsive force between the head groups begins to arise on the surface of the self-assembled aggregate

(micelle). The transition of monomers into this self-assembled aggregate form occurs when these two opposite forces are balanced. The micelle is at equilibrium with monomers. For most of the surfactants, the initially formed micelle has spherical or near-spherical shape (close to ellipsoidal in the case of longer chain length). The monomer concentration where the first micelle begins to appear is defined as *critical micelle concentration* or *cmc*. Since pre-micellar aggregates are formed in many cases, this point for the *cmc* is not always clear cut. Thus, the *cmc* is often determined by the empirical average of the narrow ranges of concentration. Typical *cmc* ranges are from 10^{-5} to 10^{-2} mole/liter for most of the single-chain surfactants and the amphiphilic polymers, such as the Pluronic series. The aggregation number is the number of surfactant or polymer molecules within a micelle. It ranges 50-10,000. No micelle has a clear-cut aggregation number. It always shows a Gaussian-type distribution. Thus, the aggregation numbers from the references are the average number. Naturally, this is quite dependent on the measurement method and calculation process. So is the *cmc.* Studies using various techniques show that the state of the micelle core region is close to that of the bulk hydrocarbon. The microviscosity of the micelle core of typical surfactants ranges ~10 - ~50 cP at room temperature.

Ninham et al. has proposed the concept of the surfactant (or micelle) packing parameter [5-7].

$$P = \frac{v}{a_0\, l} \tag{1}$$

where v is the volume of the hydrocarbon chain of the surfactant monomer in the micelle, a_o is the area occupied by the head group on the micelle surface, and l is the apparent length of the hydrocarbon chain of the surfactant monomer in the micelle. All these are the simple molecular

parameters of surfactant. The term $a_o l$ has the dimension of volume; thus, P becomes a dimensionless parameter.

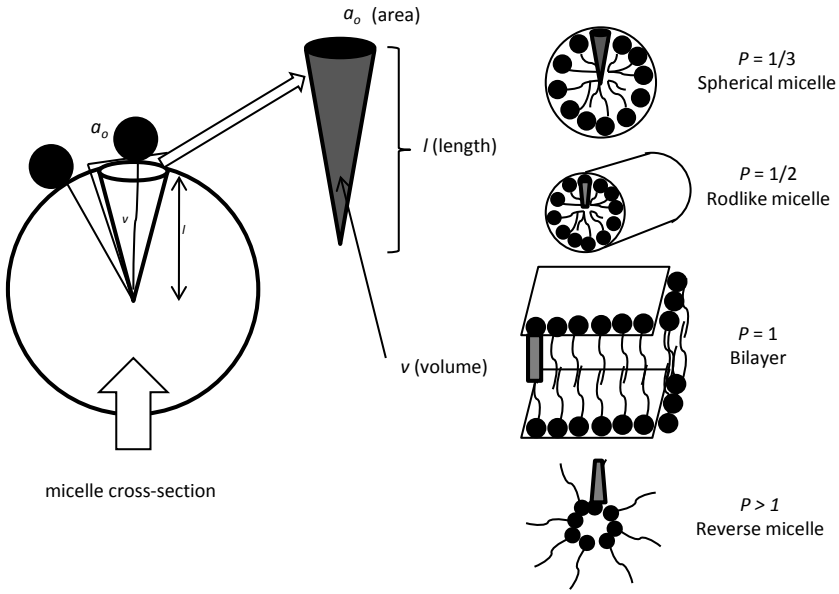

Fig.1.4. Surfactant packing parameter (P).

Once the three sub-parameters v, a_o and l are estimated, it is possible to predict the most favored nanostructure using the surfactant packing parameter (Fig.1.4). For example, when the P-value is close to 1/3, one can predict the formation of a spherical micelle by the simple geometrical consideration of packing of cone-type monomer into three - dimensional self-assembled aggregate. Similarly, when the P-value is close to 1/2, one can predict that rod-like micelles will be formed. When the P-value is close to 1, the unit packing shape becomes the cylinder type; thus a bilayer-type nanostructure is the most likely structure to be assembled. $P > 1$ results in reverse nanostructures (micelle).

1.2.1.2. Reverse micelles

The ideal reverse micelle should be composed of the surfactant molecules that are positioned in reverse compared with those of normal

micelles (Fig.1.12). To have thermodynamically stable reverse micelles that can be counterparts of normal micelles, there should be at least a minimum number of hydrated water molecules that can balance the repulsive force with the attractive hydrophobic force. When the content of water molecules increases, the core region of reverse micelles can hold additional water molecules that are not needed for the hydration of the polar head groups. This water droplet thus can be named as *confined* or *nanoscale* medium.

1.2.2. Bilayers

Typical surfactants are classified as cationic, anionic or zwitterionic , based on the intrinsic charge of their head groups (Fig.1.5).

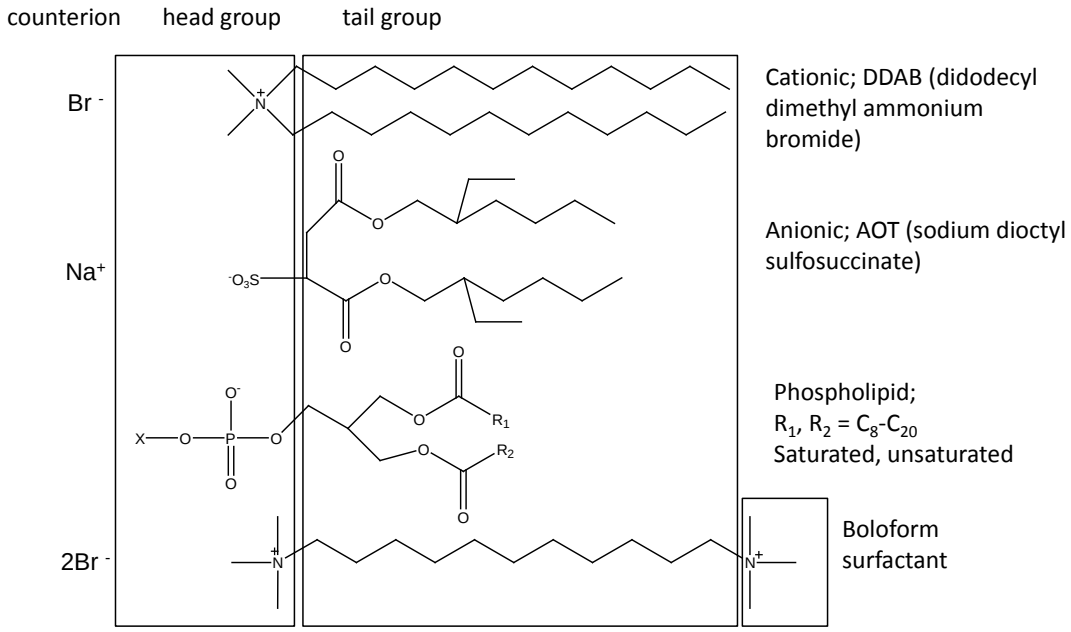

Fig.1.5. Typical surfactants which form bilayers.

Those possessing $P \approx 1$ usually have the capability to form bilayers. But they often require specific conditions that can ensure the increased hydrophobic interaction between surfactant hydrocarbon chains and/or the

decreased repulsive interaction between head groups. Thus, typical binary-phase diagrams of such surfactants with water at these conditions show a wide range of micelle region (spherical, rodlike, wormlike, etc.) that is followed by a liquid crystal region at higher concentration [8].

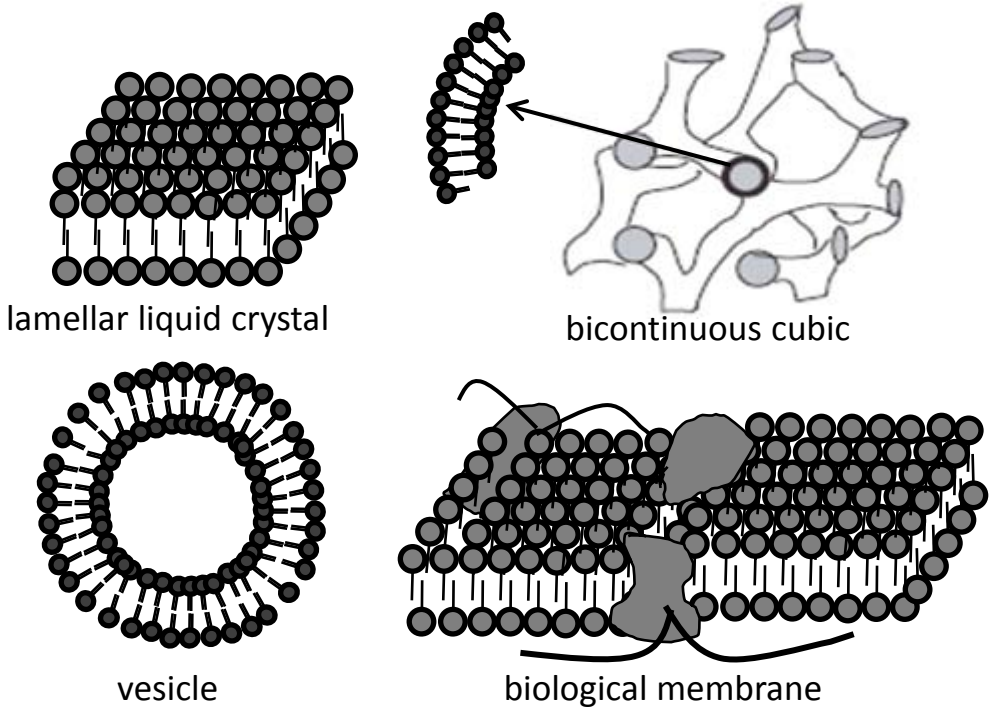

Fig.1.6. Schematic representation of different types of bilayers.

Bilayers serve as a basic repeating or building unit for a variety of macroscopic self-assembled structures. Fig.1.6 shows some examples of different types of bilayers. Lamellar liquid crystals are a stacked form of extended bilayer self-assembled units with one-dimension symmetry. The other two axes of the lamellar structures are dimensionless. Bicontinuous cubic liquid crystals consist of a regularly curved bilayer unit with clearly defined three-dimension geometry. Three typical geometries of bicontinuous cubic phases are Ia3d, Pm3n, and Im3m. There is one bicontinuous cubic melted phase referred as L3 or sponge phase, which consist of three-dimensional random multiply connected bilayer dividing the

solvent into two sub-volumes [9]. Some gels (hydrogel and organogel) are also stabilized by the action of the bilayer unit. A vesicle is a metastable suspension of spherical (globular) enclosed bilayers. A basic structure of biological membranes is a bilayer of various lipids with embedded proteins.

1.2.3. Vesicles, liposomes, and niosomes

When the packing geometry becomes slightly less than 1 for the outer layer and slightly more than 1 for the inner layer, vesicles are formed. Liposome refers to vesicles that are composed solely of lipids (both natural and synthetic).

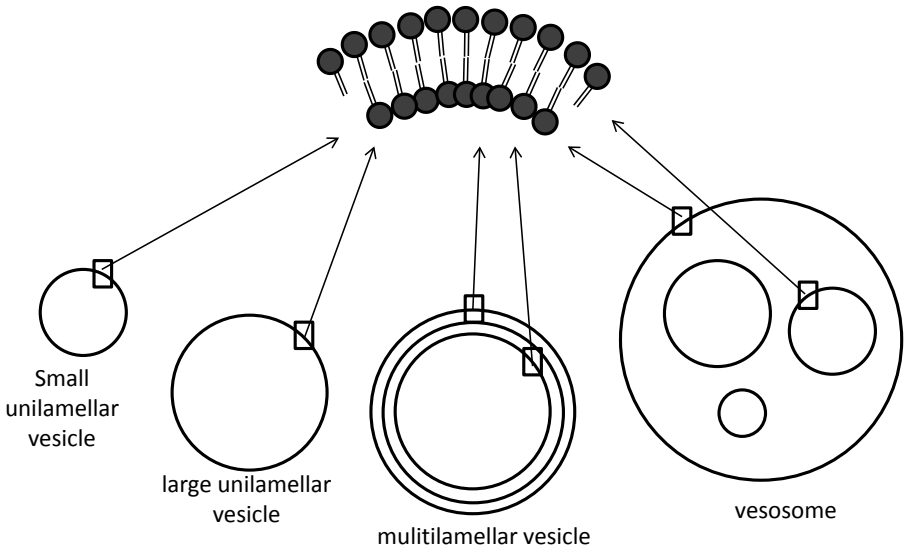

Fig.1.7. Schematic representation of different types of vesicles.

Niosomes are vesicles formed by solely nonionic surfactants. The size of vesicles can range ~ 20 nm – ~ 50 μm in diameter, but the thickness of each single layer is limited to 3 – 5 nm [10].

Fig.1.7 shows schematic representations of typical types of vesicles. They are usually classified in three groups based on their size and geometry: small unilamellar vesicle (those with radius below ~100 nm),

large unilamellar vesicle (those with radius above ~ 100 nm), and multilamellar vesicle [11]. A large unilamellar vesicle with different sizes of smaller unilamellar vesicles inside is named a vesosome.

Vesicles, in most cases, are thermodynamically unstable but kinetically stable self-assembled aggregates. A vesicle “solution” is a dispersion of those aggregates. Thus, a variety of physicochemical properties of vesicles depend on preparation and post-preparation techniques such as sonication, filtration, extrusion, and so forth. These treatments in turn provide useful means to control size and shape of vesicles for given applications.

1.2.4. Liquid crystals

Liquid crystals show both crystalline solid and isotropic liquid characteristics at ambient temperature and pressure. They display some degree of geometrical ordering but with some degree of molecular mobility. Liquid crystals are thermodynamically stable and their phases are referred as mesophases. No strong bonds as those are involved in the solid state are responsible for the liquid crystalline state. Weak intermolecular forces are the only interactions responsible of this state. Their macroscopic appearance often looks like a gellish solid but with some degree of fluidity, and some of them show crystalline solid-like properties such as optical anisotropy. Based on the origin of intermolecular interactions that induce the ordering, liquid crystals are classified as thermotropic and lyotropic liquid crystals. Thermotropic liquid crystals are induced by temperature changes, while lyotropic liquid crystals are formed by the change of concentrations in the presence of a solvent.

Surfactant liquid crystals have more variety of structural diversity than thermotropic liquid crystals and usually exist in equilibrium with monomers. They are often in equilibrium with other self-assembled

aggregates, including normal micelles, reverse micelles, vesicles, and microemulsions.

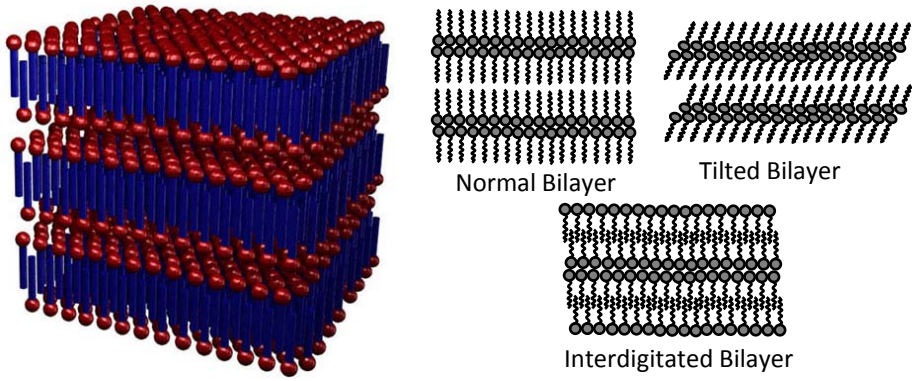

Fig.1.8. (a) Structure of lamellar phase showing bilayers and (b) typical lamellar gel phase structures.

Lamellar phases are the most common lyotropic mesophases and consist of surfactant bilayers separated by solvent layers (Fig.1.8.a). The lamellar phase has a bilayer structure, which has directional order and localized layer disorder. The surfactant head groups are located at the polar-apolar interface. The solvent layer thickness of a typical lamellar liquid crystal can vary from around 8 Å to greater than 100 Å depending on the composition, while the surfactant bilayer thickness is generally about 10-50% less than twice the all-trans chain length.

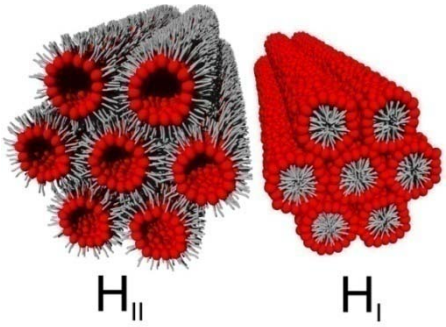

Fig.1.9. Reverse hexagonal (H_{II}) and nomal hexagonal (H_{I}) phases.

In many systems, at temperatures below that at which the lamellar phase forms, a gel phase (L_β) exists. Such phases consist of similar bilayer structures to those in lamellar phases: however, the alkyl chains are frozen in an all-trans configuration (Fig.1.8.b) [12].

Lyotropic hexagonal mesophases consist of infinite liquid cylinders organized on a hexagonal lattice with surfactant polar heads located at the interface of the cylinders. For packing parameter P < 1, (hydrophilic surfactants), oil in water self-assembly structured (normal hexagonal or H_I) phases are formed. Lipophilic surfactants (P > 1) form reverse self-assembly structures (water in oil) commonly referred as the reverse hexagonal structure (H_{II}) (Fig.1.9).

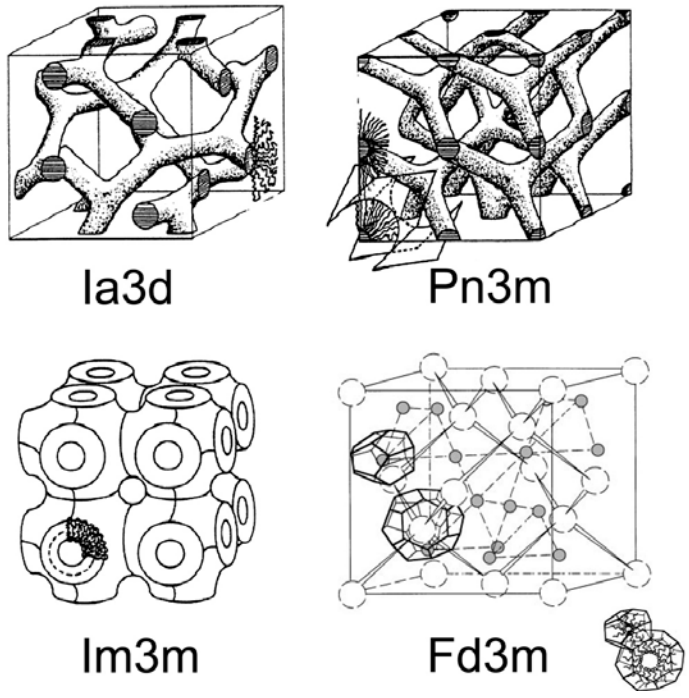

Fig.1.10. Various types of cubic phases

In case of lyotropic cubic phases, micelles arrange themselves in a cubic pattern. There are two distinct micellar aggregation shapes: the first one is spherical and forms the cubic discrete micellar (I) phase while the

second one is rod-like, interconnected in a three dimensional scheme and form the bicontinuous cubic (*V*) phase. The three common structures of bicontinuous cubic phases include double diamond (Pn3m), gyroid (Ia3d) and primitive (Im3m), whereas the common example of discrete cubic micellar phase is face centered cubic (fcc) or Fd3m (Fig.1.10). From an optical point of view, all types of cubic phases present no texture, since they are isotropic and can be distinguished from the isotropic micellar solutions only by their high viscosity. The cubic phases *I* and *V* can be correctly identified one from another by their precise location among other phases. In the hypothesis of increasing progressively the surfactant concentration, the *I* phase location is between the isotropic micellar solution and the hexagonal one, while the *V* phase location is between the hexagonal phase and the lamellar one. However, only small angle X-ray scattering (SAXS) technique can assign the type of cubic liquid crystalline structure univocally.

1.2.5. Emulsions

A surfactant can be used to stabilize the mixture of two immiscible liquids (such as oil and water). The surfactants are self-assembled into protective layers at the interface between the two liquids, and dramatically decrease the interfacial tension between the two liquids, which stabilizes the water or oil droplets. The head group of the surfactant is toward water side, while the tail group is toward the oil phase. These systems are referred as emulsions. Two types of emulsion are possible, based on the ratio of water to oil phase. When the water is the disperse phase while oil forms the droplets, it is defined as oil-in-water emulsion (O/W). Water-in-oil (W/O) is the reverse situation, with water droplets in the oil-disperse phase. Emulsions are also classified as microemulsions and macroemulsions, depending on the size of the droplets and the thermodynamic properties.

In order to understand mechanism of formation and breakdown of macroemulsion, consider a system in which an oil is represented by a large drop 2 of area A1 immersed in a liquid 2, which is now subdivided into a large number of smaller droplets with total area A2 (such that A2 >> A1), as shown in Fig.1.11. The interfacial tension γ_{12} is same for the large and smaller droplets as the latter are generally in the region of 0.1 μm to few microns in size.

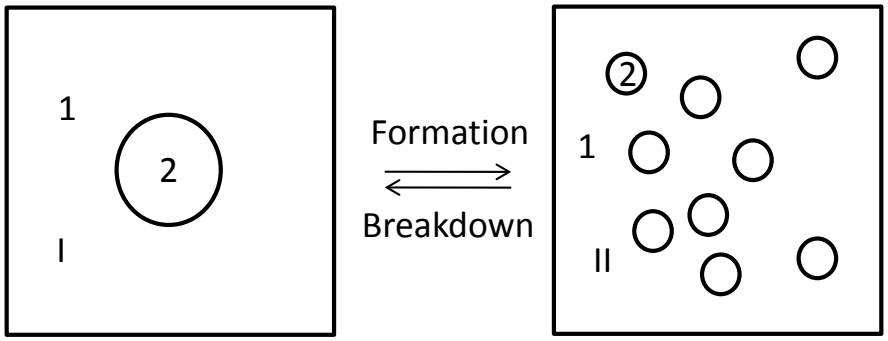

Fig.1.11. Schematic representation of emulsion formation and breakdown.

The change in free energy in going from state I to state II is given by two contributions: a surface energy term (that is positive) that is equal to $\Delta A\gamma_{12}$ (where ΔA=A2–A1); an entropy of dispersions term which is also positive (since the production of a large number of droplets is accompanied by an increase in configurational entropy) which is equal to $T\Delta S^{conf}$.

From the second law of thermodynamics,

$$\Delta G^{form} = \Delta A\gamma_{12} - T\Delta S^{\mathrm{conf}} \quad (2)$$

In most cases, $\Delta A\gamma_{12} >> T\Delta S^{conf}$, which means that ΔG^{form} can be positive – that is, the formation of emulsions is nonspontaneous, unless a strong decrease of γ_{12} occurs. When spontaneous emulsification takes place, a microemulsion, that is, thermodynamically stable system forms.

When the surfactant is not efficient enough in decreasing γ_{12}, work must be added to obtain emulsification. In the last case, macroemulsions, that are kinetically stable systems only, are formed. Fig.1.12 illustrates the two situations just described. Typically, to obtain a microemulsion, γ_{12} must decrease at least 3-4 orders of magnitude with respect to the usual O/W values which range between 20-40 mN/m.

For many micro- and macroemulsions, a fourth important component named *co-surfactant* is needed to achieve satisfactory stability.

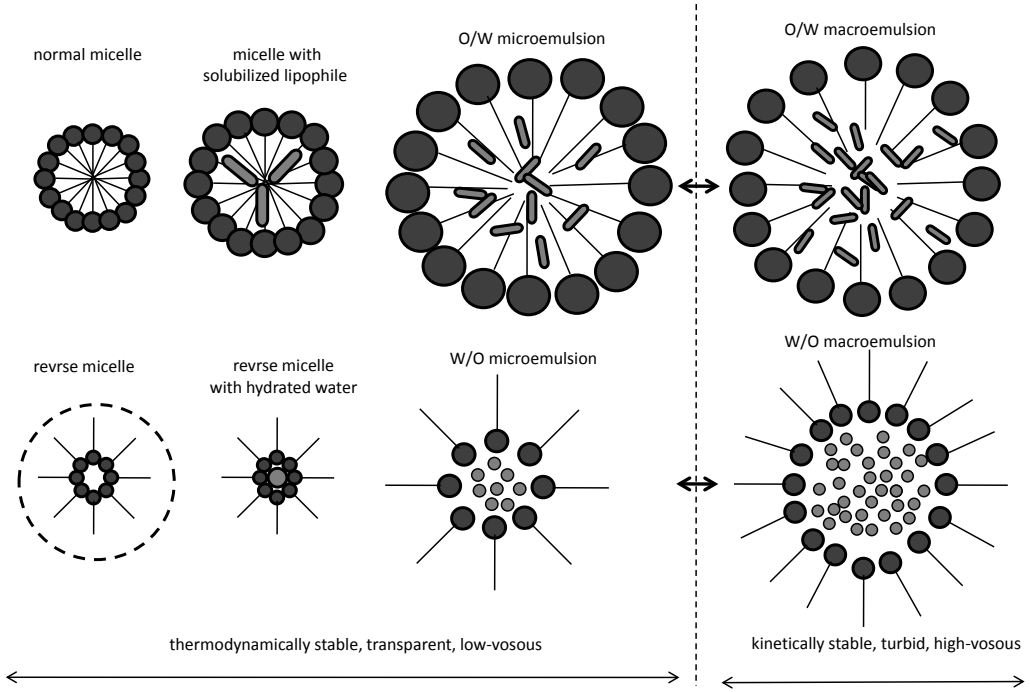

Fig.1.12. Schematic representation of the relation of micelles, microemulsions, and macroemulsions.

1.2.5.1. Microemulsions

Microemulsion is a thermodynamically stable, transparent, low-viscous and isotropic emulsion. Fig.1.12 shows the schematic representation of the formation of emulsions. When a small amount of oil is introduced into normal micellar solution, most likely a swollen micelle is first

formed as the oil (or hydrophobic molecule) is solubilized inside the normal micelle. This is a typical micellar solubilization. As more oil is solubilized, the micelle swells further, and oil droplets begin to be formed inside the micelle. This oil droplet stays in almost a pure oil phase, but not as the mixture of oil and hydrocarbon chain of surfactant. This ideal state thus can be regarded as the oil droplets emulsified (or stabilized) by surfactant layers in the water phase. This is the O/W microemulsion. In case of these thermodynamically stable systems also bicontinuous nanostructures, as in the case of cubic liquid crystals, have been reported.

1.2.5.2. Macroemulsions

Macroemulsion may be defined as an opaque, heterogeneous system of two immiscible liquid phases (oil and water) where one of the phases is dispersed in the other as drops of microscopic or colloidal size (typically around 1 μm). There are two kinds of simple macroemulsions *viz.* oil-in-water (O/W) and water-in-oil (W/O), depending on which phase comprise the drops. Macroemulsions made by the agitation of the pure immiscible liquids are very unstable and break rapidly to the bulk phases. They may be stabilized by the addition of surfactants, which protect the newly formed droplets from coalescence [13].

In the absence of any stabilization mechanism, the emulsion will break by flocculation, coalescence, Ostwald ripening, or a combination of all these processes.

This situation is illustrated graphically in Fig.1.13 where several paths for emulsion breakdown processes are represented. In the presence of a stabilizer (surfactant), an energy barrier is created between the droplets and therefore the reversal from state II to state I become non-continuous as a result of the presence of these energy barriers (Fig.1.11).

Thus, in the presence of the energy barriers, the system becomes kinetically stable.

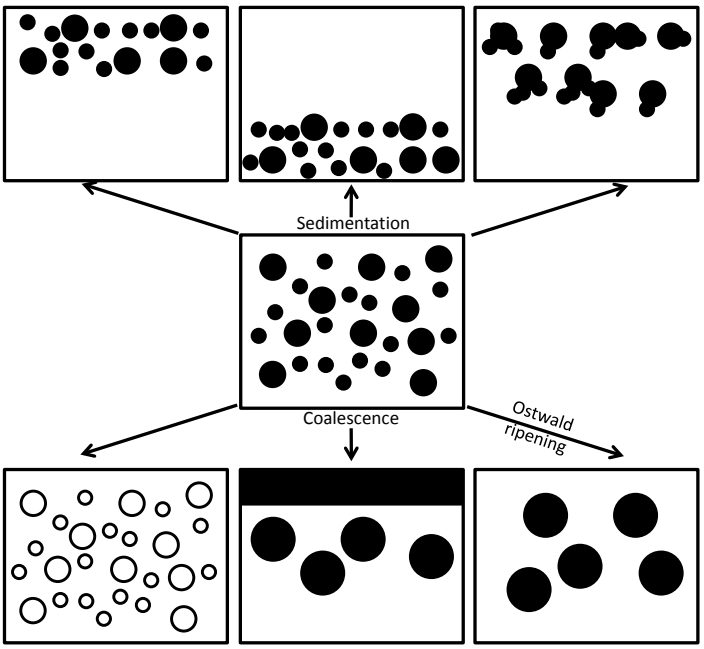

Fig.1.13. Schematic representation of the various breakdown processes in emulsions.

The physical phenomena involved in each breakdown process are not simple, and requires an analysis of the various surface forces involved. In addition, these processes may take place simultaneously rather than consecutively, which in turn complicates the analysis. Model macroemulsions, with monodisperse droplets, cannot be easily produced and hence any theoretical treatment must take into account the effect of polydispersity. In addition, the measurement of surfactant adsorption in macroemulsion is not simple, and such information must be extracted from measurements made at a planar interface [14].

A summary of each of the breakdown processes is provided in the following sections, together with details of each process.

1.2.5.3.1. Creaming and Sedimentation

Creaming is the process by which buoyant macroemulsion droplets tend to rise to the top of a container. It is the same process as sedimentation, but in the opposite direction [15]. This process results from external forces, usually gravitational or centrifugal. When such forces exceed the thermal motion of the droplets (Brownian motion), a concentration gradient builds up in the system such that the larger droplets move more rapidly either to the top (if their density is less than that of the medium) or to the bottom (if their density is greater than that of the medium) of the container. In the limiting cases, the droplets may form a close-packed (random or ordered) array at the top or bottom of the system, with the remainder of the volume occupied by the continuous liquid phase.

1.2.5.3.2. Flocculation

This process refers to aggregation of the droplets (without any change in primary droplet size) into larger units. It is the result of the van der Waals attractions which are universal with all disperse systems. Flocculation occurs when there is not sufficient repulsion to keep the droplets apart at distances where the van der Waals attraction is weak. Flocculation may be either strong or weak, depending on the magnitude of the attractive energy involved.

1.2.5.3.3. Ostwald Ripening

Ostwald ripening in macroemulsions is the growth of one droplet at the expense of a smaller one due to the difference in chemical potential of the continuous phase between different droplets arising from their different radii of curvature. This chemical potential increases with decreasing radius and consequently the solubility of the material comprising the droplet phase increases. The smaller droplets thus tend to dissolve and their material

diffuses through the bulk phase and re-deposits onto a larger droplet, resulting in an overall increase in the average radius of the macroemulsion. Ostwald ripening generally proceeds with the cube of the average radius varying linearly with time. As the radius of the emulsion droplets increases, the rate of change in droplet radius falls rapidly since $dr/dt = (1/r^2)dr^3/dt;$ thus, for a given rate of ripening, the rate of change in radius falls as r^{-2} [16].

1.2.5.3.4. Coalescence

This refers to the process of thinning and disruption of the liquid film between the droplets, with the result that fusion of two or more droplets occurs to form larger droplets. The limiting case for coalescence is the complete separation of the emulsion into two distinct liquid phases. The driving force for coalescence is the surface or film fluctuations; this results in a close approach of the droplets whereby the van der Waals forces are strong and prevent their separation.

1.2.5.3.5. Phase Inversion

Phase inversion refers to the phenomenon when an O/W macroemulsion, quite suddenly changes its morphology and becomes a W/O macroemulsion [17]. In many cases, phase inversion passes through a transition state whereby multiple emulsions are produced.

1.3. Drug delivery systems

Successful drug delivery requires consideration of numerous aspects. Depending on the route of administration, the disease or disorder, the properties of the drug, and many other aspects, various strategies have to be developed. Without doubt the most generically important aspects of any therapy are its efficacy and safety [4]. First and foremost, the drug concentration should be sufficiently high at the site of action in order to

have a therapeutic effect, but at the same time it should not be too high, since this may result in detrimental side effects. For a safe and efficient therapy, the drug concentration should preferably lie essentially constant within ‘‘therapeutic window’’ over the time of action (Fig.1.14).

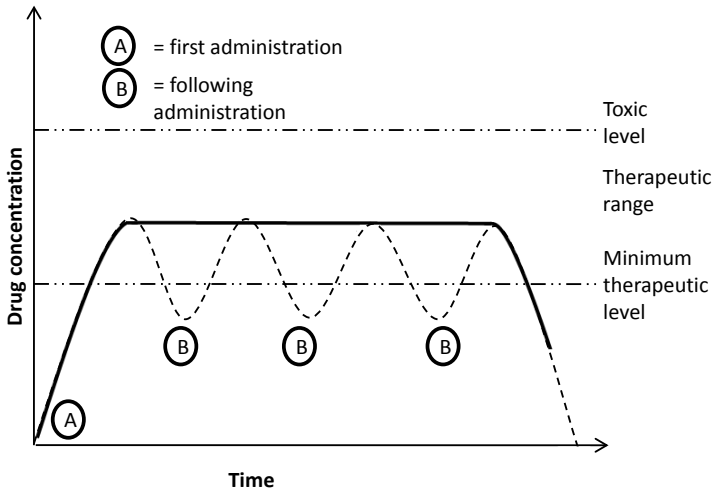

Fig.1.14. Schematic illustration of the drug level for an ideal sustained release formulation (solid line) and of a more typical situation demanding repeated administration (dotted line).

The goal of a constant drug concentration within the therapeutic window at the site of action over a suitable therapeutic time puts requirements not only on the drug but also on the drug formulation. The drug delivery system should preferably be designed so that a preferential accumulation of the drug is reached at the site of action, whereas the drug concentration elsewhere in the body should be as low as possible. The reason for this need of ‘‘targeting’’ is that a high concentration of the drug in tissues or cells other than those being targeted may cause problems related to side effects. A typical example of the latter is cancer therapy, where accumulation of chemotherapeutic agents in areas other than the tumor frequently causes severe side effects, some of which may be dose limiting, thereby limiting also the efficacy of the treatment [18]. Furthermore, the drug should be stable against degradation during storage and

administration, and the formulation designed so that drug degradation is minimized. Once the drug has performed its action, however, it should either be straightforwardly excreted or metabolized to harmless compounds. There are also many other aspects to a drug delivery system, e.g., in relation to the route of administration. Naturally, the preferred situation is that the drug is straightforwardly administrable by the patient himself/herself, without unpleasant sensations. However, depending on a number of different aspects also other routes may be chosen. The complete therapeutic strategy therefore involves choice not only of the drug but also of the drug delivery system and the administration route. Different routes of administration put different requirements on the drug delivery system, and consequently different drug delivery systems tend to have their primary application within a given route of administration, and within a certain type of indication. For example, in oral drug delivery, the drug and the drug carrier have to pass through the stomach, with its quite low pH, which tends to affect drug stability and drug solubility, as well as the properties of the drug carrier system. Also, the uptake in the intestine puts some rather demanding requirements on the drug and the drug formulation, not the least for hydrophobic drugs and/or large molecules (e.g., protein and peptide drugs). In topical administration the penetration over the stratum corneum poses a severe limitation in the therapy efficacy, which puts special demands on the drug delivery system. In intravenous drug delivery, the uptake of the drug and the drug carrier in the reticuloendothelial system frequently reduces the drug bioavailability and results in dose-limiting side effects.

For this thesis work, three different drug delivery systems mainly based upon non-ionic surfactants were studied and are briefly described in following sections.

1.3.1. Microspheres suspended in thermosensitive gels

Microspheres are usually solid, approximately spherical particles containing dispersed drug in either solution or microcrystalline form. Incorporation of drugs can be achieved by entrapment during production (polymerization, gelation, or encapsulation techniques, such as coacervation and phase separation) and by covalent and ionic attachment. Microspheres may be prepared from natural polymers such as gelatin and albumin [19-20] and from synthetic polymers such as polylactic and polyglycolic acid [21-22]. The drug is either totally encapsulated within a distinct capsule wall or is dispersed throughout the microsphere. Drug release is controlled by dissolution and diffusion of the drug through the microsphere matrix or the microcapsule wall, or by polymer degradation. Microspheres range in size between approximately 1 and 1000 μm. Consequently, these systems are outside the conventional colloidal size range. In the pharmaceutical literature, however, microcapsules with sizes up to approximately 15 μm are considered as colloidal-delivery systems [23].

Chemical or physical crosslinking of some polymers leads to hydrogel formation which absorbs a considerable amount of water while maintaining their shape. Injectable hydrogels are of great interest as potential materials for protein delivery [24]. Especially, thermo-sensitive and sol–gel transition water soluble polymers can provide in-situ forming hydrogels for delivery of therapeutic molecules upon injection into the body without an invasive surgical procedure [25]. Physically crosslinked hydrogels self-assembled as a result of intermolecular ionic interactions, hydrogen bonding, and hydrophobic interactions are advantageous for macromolecular delivery systems, since they provide a more benign environment for encapsulation of proteins, compared to chemically

crosslinked hydrogels. Various synthetic thermo-sensitive polymers such as poly(N-isopropylacrylamide) [26], polyphosphazenes[27], poly(ethylene oxide) (PEO)/poly(propylene oxide) (PPO) tri-block copolymers [28], and PEO/poly(d,l-lactide-co-glycolide) (PLGA) tri-block copolymers [29] have been extensively studied for use as injectable sol–gel transition hydrogel systems for pharmaceutical and biomedical applications. Among these, a series of PEO–PPO–PEO tri-block copolymers (or Pluronics) has been widely exploited as *in-situ* forming drug delivery carriers because they exhibit unique sol–gel transition behaviors in response to temperature variations in aqueous solution. These tri-block copolymers form spherical micelles in aqueous solution by hydrophobic interaction between the middle PPO segments [30]. Above a critical gelation temperature and concentration, the self-assembled micelles are closely packed to produce a physically crosslinked gel structure. This consists of discrete cubic micellar phase, as described in section 1.2.4. However, the Pluronic hydrogels are very soft and easily disintegrated and dissolved out upon contact with excess amount of buffer solution. This is due to the fact that the concentration of Pluronic copolymers is immediately diluted to below the critical gelation concentration, resulting in the dis-assembling of the micellar structure. Thus, when a highly concentrated aqueous solution of Pluronic copolymer is injected into the body tissue as a sol state, the *in-situ* formed gel structure cannot be maintained for the desired period to achieve sustained release of encapsulated drugs.

A combination of microspheres and hydrogel has been attempted by many researchers for various reasons. The examples include 5-Fluorouracil in chitosan microspheres and Pluronic F127 (PF127) gel [31], insulin in calcium-alginate microspheres and PF127 gel [32], Baclofen in poly(lactide-co-glycolide) (PLGA) microspheres dispersed in chitosan and PF127 gels

[33], timolol maleate in Poly(adipic anhydride) microspheres and gelrite gel [34], oxybenzone in gelatin microspheres and aloe vera gel [35].

1.3.2. Ordered mesoporous materials

The porosity of a ceramic matrix can be ordered or disordered. It is clear that a well-ordered pore distribution in a ceramic matrix favors the homogeneity of the adsorption and release stages [36]. Ordered silica mesoporous materials are potentially excellent candidates in the field of controlled drug delivery systems for pharmaceutical drugs, proteins and other biogenic molecules. Since the discovery of ordered mesoporous silica materials in 1990s, synthesis and applications of mesoporous solids have received intensive attention due to their highly ordered structures, larger pore size, and high surface area [37].

Table 1 Porous structures of mesoporous materials.

Mesoporous solid	Space group	Pore diameter (nm)	Structure
MCM-41	*P6mm*	2-5	Hexagonal 1D channel
MCM-48	*Ia3d*	2-5	Bicontinuous 3D
SBA-15	*P6mm*	5-10	Hexagonal 1D channel
SBA-16	*Im3m*	Min 1-6; max 4-9	Body centre arrangement of cages
SBA-1	*Pm3m*	2-4	Cubic 3D
SBA-3	*P6mm*	2-4	2D hexagonal
MSU	*P6mm*	2-5	2D hexagonal
HMS	*P6mm*	2-5	Hexagonal

Table 1 presents the porous structure of some mesoporous materials, which have been employed for drug delivery [37]. Vallet-Regi et al. in 2000 has reported the application of MCM-41 as a new drug delivery system [38]. This has stimulated many researchers to develop different types of mesoporous materials with varying porous structure and functionality for sustained drug released and stimuli-responsive release. MCM-41 shows hexagonal arrays of cylindrical mesopores. The structure of

the wall of the pores consists of a disordered network of siloxane bridges and free silanol groups that could act as reacting nuclei against appropriate guest chemical species, behaving as a matrix for controlled adsorption and liberation of organic molecules. The pore morphology and clearance determine the type of molecules that can fit into these materials and, therefore, those that are eligible for the adsorption process; however, the maximum amount accepted depends on the pore volume, which is generally described in terms of cm^3g^{-1} of material. In systems that only contain mesopores, the total pore volume is evidently equal to the mesopore total volume, but this is not generally the case. Frequently, there are also micropores or even macropores (pores with diameter larger than 50 nm); this last type of pore is usually associated to interparticle porosity, and its contribution to the total pore volume increases with decreasing particle size in the material. Undoubtedly, the specific surface is a parameter that influences the adsorption properties of the material, since it is a surface phenomenon itself. The concept of surface encompasses not only the outer surface of the material, but also the inner surface of its cavities and channels, provided that the nitrogen-based molecules used in these measurements can pass freely through these inner areas [39].

1.3.3. Liquid crystals and emulsions

The description about various liquid crystals has been given in section 1.2.4. The stabilization of emulsions by lamellar liquid crystals has been reported by Friberg et al. [40]. In order to further stabilize emulsions, crystallization of lamellar liquid crystalline phases located at the water/oil interface resulting in the formation of a so-called gel phase has been reported [41-43]. It has been demonstrated by Engels et al. that changes in the type and concentration of the co-emulsifier caused the formation of a lamellar gel phase surrounding the oil droplets inside an oil-in-water (O/W)

emulsion which increased the stability of the emulsion from 5 days to more than 1 month [43]. It was found that the physico-chemical properties of the system remained unaffected by the change of the co-surfactant. It was proved that the presence of the lamellar liquid crystalline phase causes the observed increase in emulsion stability. The viscous lamellar film surrounding the emulsion droplets may be several layers thick and reduces the attraction potential between the droplets. As a result, the lamellar layer acts as a barrier against coalescence [44].

Emulsions containing a third phase or multimolecular layers of lyotropic liquid crystals are often found in cosmetic products and are therefore widely used by the cosmetics industry to adjust or optimize specific properties of the product such as viscosity or consistency, storage stability or application convenience [45].

Recently, it has been reported that the long-term stable W/O emulsions can be obtained by dispersing water in the lamellar and reverse hexagonal phases formed by monoolein-based systems [46-47]. Skin permeation experiments demonstrated that emulsions containing liquid crystalline phases compared to an emulsion without liquid crystals, showed enhanced skin penetration of the hydroquinone and octadecenedioic acid. The increase in skin penetration was attributed to an increased partitioning of the drugs into the skin. In the case of salicylic acid, no effect of liquid crystalline phases in emulsion on penetration was observed. This effect was suggested to be due to different interaction of drug and surfactants forming liquid crystalline phases in emulsions [48].

1.4. References

[1] J. Swarbrick, Encyclopedia of pharmaceutical technology, CRC Pr I Llc, 2007.
[2] D.H. Everett, Basic Principles of Colloid Science, Royal Society of Chemistry Paperbacks, London.

[3] D. Myers, D. Meyers, Surfaces, interfaces, and colloids: principles and applications, Wiley-VCH Weinheim, Germany, 1999.
[4] M. Malmsten, Surfactants and polymers in drug delivery, Informa HealthCare, 2002.
[5] J.N. Israelachvili, D.J. Mitchell, B.W. Ninham, Theory of self-assembly of hydrocarbon amphiphiles into micelles and bilayers., J Chem Suc Faraday Trans 2, 57 (1976) 1525.
[6] J. Israelachvili, Intermolecular and Surface Forces, Second Edition: With Applications to Colloidal and Biological Systems (Colloid Science), {Academic Press}, 1992.
[7] D.J. Mitchell, B.W. Ninham, Micelles, vesicles and microemulsions, J Chem Soc Faraday Trans 2 Mol Chem Phys, 77 (1981) 601-629.
[8] G. Burducea, Lyotropic liquid crystals II: Structural Polymorphism, Rom Rep Phys, 56 (2004) 87-100.
[9] H.F. Mahjoub, K.M. McGrath, M. Kléman, Phase Transition Induced by Shearing of a Sponge Phase, Langmuir, 12 (1996) 3131-3138.
[10] I.F. Uchegbu, S.P. Vyas, Non-ionic surfactant based vesicles (niosomes) in drug delivery, Int J Pharm, 172 (1998) 33-70.
[11] J.H. Van Zanten, Characterization of vesicles and vesicular dispersions via scattering techniques, in: M. Rosoff (Ed.) Vesicles, Marcel Dekker, New York, 1996, pp. 239–294.
[12] S. Fuller, Y. Li, G.J.T. Tiddy, E. Wyn-Jones, R.D. Arnell, Formulation of Lyotropic Lamellar Phases of Surfactants as Novel Lubricants, Langmuir, 11 (1995) 1980-1983.
[13] B. Binks, Emulsions—Recent Advances in Understanding, Modern Aspects of Emulsion Science; Binks, BP, Ed.; The Royal Society of Chemistry: Cambridge, England, (1998).
[14] T. Tadros, Emulsion Science and Technology: A General Introduction, Emulsion Science and Technology, (2009) 1.
[15] M.M. Robins, Emulsions -- creaming phenomena, Curr Opin Colloid Interface Sci, 5 (2000) 265-272.
[16] P. Taylor, Ostwald ripening in emulsions, Colloids Surf A Physicochem Eng Asp, 99 (1995) 175-185.
[17] F. Groeneweg, W.G.M. Agterof, P. Jaeger, J.J.M. Janssen, J.A. Wieringa, J.K. Klahn, On the Mechanism of the Inversion of Emulsions, Chem Eng Res Des, 76 (1998) 55-63.
[18] M. Ferrari, Cancer nanotechnology: opportunities and challenges, Nat Rev Cancer, 5 (2005) 161-171.
[19] K. Ulubayram, I. Eroglu, N. Hasirci, Gelatin Microspheres and Sponges for Delivery of Macromolecules, Journal of Biomaterials Applications, 16 (2002) 227-241.
[20] R. Arshady, Albumin microspheres and microcapsules: Methodology of manufacturing techniques, J Control Release, 14 (1990) 111-131.

[21] I. Soriano, M. Llabres, C. Evora, Release control of albumin from polylactic acid microspheres, Int J Pharm, 125 (1995) 223-230.
[22] S. Hunter, M. Andracki, S.K. Hunter, Nasal or IM administration of streptococcal surface protein, C5A peptidase, encapsulated within biodegradable polyglycolic acid microspheres induces strong antibody response in mice: a potential new GBS vaccine, Am J Obstet Gynecol, 189 (2003) S100-S100.
[23] D. Burgess, A. Hickey, Microsphere technology and applications, Encyclopedia of Pharmaceutical Technology. New York, NY: Marcel Dekker, (1994) 1-29.
[24] A.S. Hoffman, Hydrogels for biomedical applications, Adv Drug Deliv Rev, 54 (2002) 3-12.
[25] H.J. Chung, Y. Lee, T.G. Park, Thermo-sensitive and biodegradable hydrogels based on stereocomplexed Pluronic multi-block copolymers for controlled protein delivery, J Control Release, 127 (2008) 22-30.
[26] T.G. Park, A.S. Hoffman, Deswelling characteristics of poly(N-isopropylacrylamide) hydrogel, J Appl Polym Sci, 52 (1994) 85-89.
[27] L. Qiu, Novel degradable polyphosphazene hydrogel beads for drug controlled release, J Appl Polym Sci, 87 (2003) 986-992.
[28] J.G.W. Wenzel, K.S.S. Balaji, K. Koushik, C. Navarre, S.H. Duran, C.H. Rahe, U.B. Kompella, Pluronic® F127 gel formulations of Deslorelin and GnRH reduce drug degradation and sustain drug release and effect in cattle, J Control Release, 85 (2002) 51-59.
[29] B. Jeong, Y.H. Bae, D.S. Lee, S.W. Kim, Biodegradable block copolymers as injectable drug-delivery systems, Nature, 388 (1997) 860-862.
[30] P. Alexandridis, T. Alan Hatton, Poly(ethylene oxide)-poly(propylene oxide)-poly(ethylene oxide) block copolymer surfactants in aqueous solutions and at interfaces: thermodynamics, structure, dynamics, and modeling, Colloids Surf A Physicochem Eng Asp, 96 (1995) 1-46.
[31] A.P. Rokhade, N.B. Shelke, S.A. Patil, T.M. Aminabhavi, Novel hydrogel microspheres of chitosan and pluronic F-127 for controlled release of 5-fluorouracil, J Microencapsulation, 24 (2007) 274-288.
[32] Y. Wang, J.-Q. Gao, F. Li, S.-H. Ri, W.-Q. Liang, Triblock copolymer Pluronic®F127 sustains insulin release and reduces initial burst of microspheres—in vitro and in vivo study, Colloid Polym Sci, 285 (2006) 233-238.
[33] F. Lagarce, N. Faisant, J.-C. Desfontis, L. Marescaux, F. Gautier, J. Richard, P. Menei, J.-P. Benoit, Baclofen-loaded microspheres in gel suspensions for intrathecal drug delivery: In vitro and in vivo evaluation, Eur J Pharm Biopharm, 61 (2005) 171-180.

[34] A.-C. Albertsson, J. Carlfors, C. Sturesson, Preparation and characterisation of poly(adipic anhydride) microspheres for ocular drug delivery, J Appl Polym Sci, 62 (1996) 695-705.
[35] M. Patel, S.K. Jain, A.K. Yadav, D. Gogna, G.P. Agrawal, Preparation and Characterization of Oxybenzone-Loaded Gelatin Microspheres for Enhancement of Sunscreening Efficacy, Drug Deliv, 13 (2006) 323 - 330.
[36] U. Ciesla, F. Schüth, Ordered mesoporous materials, Microporous Mesoporous Mater, 27 (1999) 131-149.
[37] S. Wang, Ordered mesoporous materials for drug delivery, Microporous Mesoporous Mater, 117 (2009) 1-9.
[38] M. Vallet-Regi, A. Rámila, R.P. del Real, J. Pérez-Pariente, A New Property of MCM-41: Drug Delivery System, Chemistry of Materials, 13 (2000) 308-311.
[39] M. Vallet-Regí, Ordered mesoporous materials in the context of drug delivery systems and bone tissue engineering, Chem Eur J, 12 (2006) 5934-5943.
[40] S. Friberg, L. Mandell, M. Larsson, Mesomorphous phases, a factor of importance for the properties of emulsions, J Colloid Interface Sci, 29 (1969) 155-156.
[41] K. Larsson, Stability of emulsions formed by polar lipids, Prog Chem Fats Other Lipids, 16 (1978) 163-169.
[42] K. Shinoda, S. Friberg, Emulsions and solubilization, Wiley New York et al., 1986.
[43] T. Engels, T. Förster, W. von Rybinski, The influence of coemulsifier type on the stability of oil-in-water emulsions, Colloids Surf A Physicochem Eng Asp, 99 (1995) 141-149.
[44] S. Friberg, Liquid crystalline phases in emulsions, J Colloid Interface Sci, 37 (1971) 291-295.
[45] T. Engels, W. Rybinski, Liquid crystalline surfactant phases in chemical applications, J Mater Chem, 8 (1998) 1313-1320.
[46] S. Mele, S. Murgia, M. Monduzzi, Monoolein based liquid crystals to form long-term stable emulsions, Colloids Surf A Physicochem Eng Asp, 228 (2003) 57-63.
[47] S. Mele, S. Murgia, F. Caboi, M. Monduzzi, Biocompatible Lipidic Formulations: Phase Behavior and Microstructure, Langmuir, 20 (2004) 5241-5246.
[48] A. Otto, J. Wiechers, C. Kelly, J. Dederen, J. Hadgraft, J. du Plessis, Effect of Emulsifiers and Their Liquid Crystalline Structures in Emulsions on Dermal and Transdermal Delivery of Hydroquinone, Salicylic Acid and Octadecenedioic Acid, Skin Pharmacology and Physiology, 23 (2010) 273-282.

2. THEORETICAL BACKGROUND

2.1. Microscopy

2.1.1. Polarized light microscopy

Polarized light microscopy (PLM) is one of the important techniques for identification of lyotropic liquid crystals (except cubic mesophases) because anisotropic liquid crystals show birefringence similar to crystalline solids. Each liquid crystal shows typical black and white textures. In the case of an additional λ-plate with strong birefringent properties, color effects of the textures can also be observed [1]. Hexagonal mesophases can be recognized by their typical fan shape texture (Fig.2.1.a) [2]. Lamellar mesophases typically show oily streaks with inserted maltese crosses (Fig.2.1.b). The latter result from defect structures, called confocal domains that arise from concentric rearrangement of plane layers [3]. In some lamellar mesophases these defects prevail. Hence no oily streaks occur but mosaic pattern can be observed (Fig. 2.1.c). A drawback of PLM is that it is restricted to particle dimensions in the micron or submicron range whereas colloidal dimensions of liquid crystals are only resolved by transmission electron microscopy (TEM).

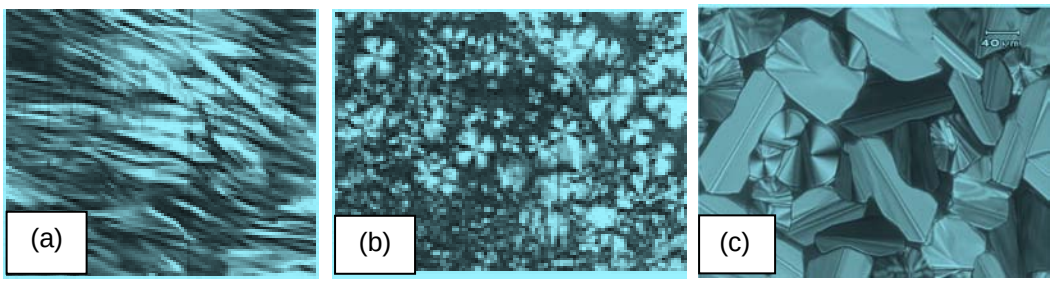

Fig.2.1. Characteristic pattern of liquid crystalline phases (a) hexagonal fan-like structure, (b) lamellar maltese crosses and (c) lamellar mosaic pattern.

2.1.2. Electron Microscopy

There are two types of electron microscopes – the scanning electron microscope (SEM) and the transmission electron microscope (TEM). These

devices require measurements to be undertaken in a vacuum, except for the environmental SEM. Also, the samples must be conducting (in order to accelerate the electrons onto the sample) and, hence, a sample must have a metal layer deposited on its surface if it is to be investigated by SEM or TEM. In the TEM, the sample is a very thin specimen and contrast within the image is due to the spatial variations in intensity of the transmitted electron beam through the specimen, as the beam is raster scanned over the specimen. In the SEM, the image may be produced in a number of ways – from variations in the intensity of secondary electrons back-scattered from the specimen through to X-ray emission produced by inelastic collisions of the primary beam with bound electrons in the specimen. The idea that gave rise to the electron microscope is that, just as light is refracted and focused by an optical lens, the electron, due to its charge, will have its path deviated by either a magnetic field or an electric field. Therefore, with careful design of appropriate electric and magnetic fields within the instrument, an electron beam may be focused like an optical beam [4].

In case of TEM microscope, the electrons are emitted by an incandescent cathode source, and accelerated towards more positive grids through either electrostatic or magnetic field lens onto an object. The specimen is supported on a very thin film to minimize the scattering of the electrons as they pass through the sample. Depending on the thickness and composition of the object, the electron beam experiences different attenuation as a function of position. The beam travels through two more lenses before being imaged onto a fluorescent screen (in original models) or photographic plate or directly onto a scintillator placed on the face of a photomultiplier tube or a CCD device. (A scintillator is a semi-transparent material, which emits a flash of light when a charged particle traverses it.)

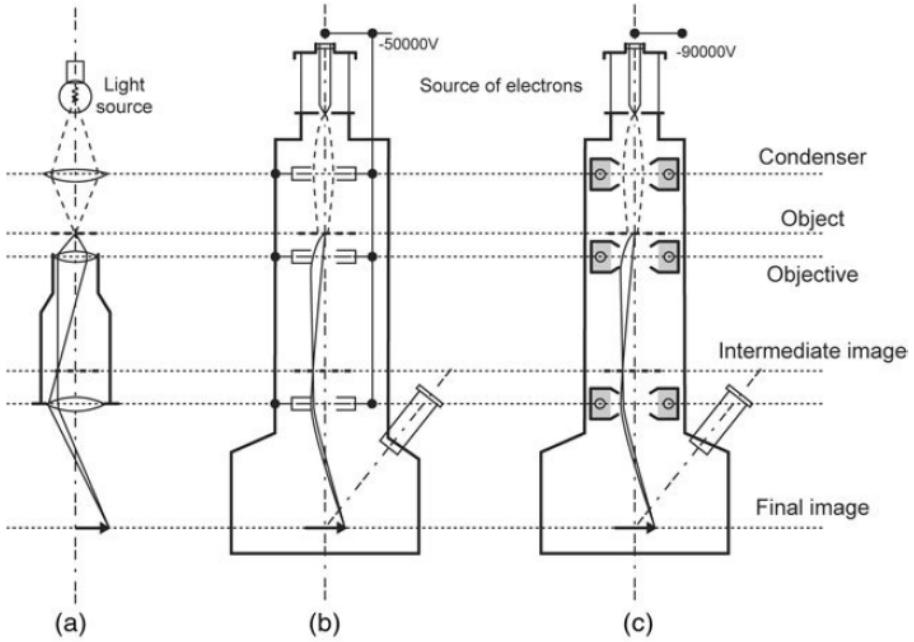

Fig.2.2. Comparison of a basic operation of (a) standard optical microscope, (b) an electrostatic version of electron microscope and (c) a magnetic coil version of electron microscopes.

The spatial resolution of this type of microscope is determined by the wavelength associated with the electrons and this wavelength may be 100,000 times smaller than optical wavelengths at the typical accelerating voltages used in electron microscopy [5].

TEM in a high-resolution (nanometer resolution) mode can be used with thin ultra-microtomed specimens 40–60 nm thick. Fine structural details, smaller than 1 nm are detectable by this microscope. In Fig.2.2 (b) and (c), the schematic diagram of a transmission electron microscope system is shown. The parallel illuminating electron beam is scattered by the object. The scattered beam passes through the convergent lens, L, and is focused in the intermediate image focal plane as an electron diffraction pattern. The final optical image is formed in the Gauss plane. For the magnified image to be a reliable Fourier synthesis, all of the beams must interfere whilst keeping their initial relative phases. The objective lens will

introduce additional phase shifts. These phase shifts vary as a function of the spherical aberration *Cs* of the lens, the diffraction angle, 2*θ*, of the beams relative to the optic axis and the defocus distance, *Δf* . The transfer function of the electron beam lens, *K*, has been shown to

$$K(u) = D(\lambda f u)e^{-i\chi(u)} \quad (1)$$

where $\chi(u) = \pi(^1/_2 C_s \lambda^3 u^4 - \lambda \Delta f u^4)$ and *D* is the characteristic function of the objective aperture, *χ(u)* is the aberration function, *u* is the spatial frequency (*u=2θ/λ*), *f* is the focal image distance and *λ* is the wavelength. The objective acts like a filter for spatial frequencies, selecting and modifying the phase of planar waves that can interfere in the image plane [6].

Typical acceleration voltages are *V*=120 kV, which gives the electron an energy, *E* = 120 keV (where 1 electronVolt, eV is equivalent to an energy of 1.6×10^{-19} Joules) and the representative wavelength, *λ*, for these electrons is 3.35×10^{-3} nm, computed from the non-relativistic De Broglie expression

$$\lambda = \frac{h}{\sqrt{2Em_e}} \quad (2)$$

where m_e is the electronic mass. Hence, the electron microscope has potentially, one of the highest spatial resolutions of all of the microscope techniques.

The electron microscope (like any other microscope) can be considered as an information channel that carries information from object to observer. The overall model for the electron microscope contains parameters, e.g. atomic coordinates which are unknown and which must be determined by experiment. Structure determination can be achieved by fitting the model to the experimental data in an iterative procedure in which the model parameters are systematically refined. By implication, details beyond the Rayleigh point resolution (and even beyond the information limit

of the microscope) may be extracted because, in the absence of noise (and assuming that the model is correct), the fitting procedure would be perfect and exact values of the model parameters would be obtained! In practice, however, results will always be limited by some noise component, e.g. the Poisson noise due to the counting statistics (quantum or shot noise) which is determined by the number of electrons in the illuminating beam. In scanning electron microscopes, low energy secondary electrons (E_e < 50 eV) are detected using a scintillator/pm tube detector. At these low energies, the secondary electrons can only escape, and be detected, from within a few nanometers of the surface of the specimen [7].

2.2. ATR-FTIR Spectroscopy

Infrared spectroscopy is a technique based on the vibrations of the atoms of a molecule. An infrared spectrum is commonly obtained by passing infrared radiation through a sample and determining what fraction of the incident radiation is absorbed at a particular energy. The energy at which any peak in an absorption spectrum appears corresponds to the frequency of a vibration of a part of a sample molecule.

Processes of change, including those of vibration and rotation associated with infrared spectroscopy, can be represented in terms of quantized discrete energy levels E_0, E_1, E_2, etc., as shown in Fig.2.3.

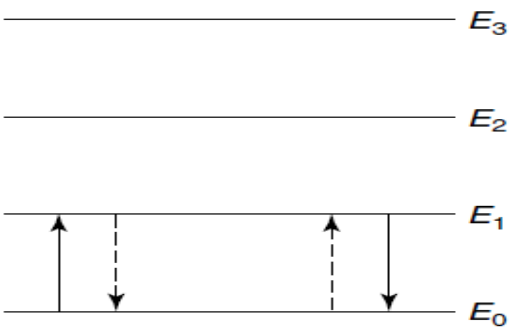

Fig.2.3. Illustration of quantized discrete energy levels.

Each atom or molecule in a system must exist in one or other of these levels. In a large assembly of molecules, there will be a distribution of all atoms or molecules among these various energy levels. The latter are a function of an integer (the quantum number) and a parameter associated with the particular atomic or molecular process associated with that state. Whenever a molecule interacts with radiation, a quantum of energy (or photon) is either emitted or absorbed. In each case, the energy of the quantum of radiation must exactly fit the energy gap $E_1 - E_0$ or $E_2 - E_1$, etc. The energy of the quantum is related to the frequency by the following:

$$\Delta E = h\nu \tag{3}$$

Hence, the frequency of emission or absorption of radiation for a transition between the energy states E_0 and E_1 is given by:

$$\nu = (E_1 - E_0)/h \tag{4}$$

Associated with the uptake of energy of quantized absorption is some deactivation mechanism whereby the atom or molecule returns to its original state. Associated with the loss of energy by emission of a quantum of energy or photon is some prior excitation mechanism. Both of these associated mechanisms are represented by the dotted lines in Fig.2.3.

The interactions of infrared radiation with matter may be understood in terms of changes in molecular dipoles associated with vibrations and rotations. The frequency of vibrational modes depends upon the stiffness of the bond and the masses of the atoms at each end of the bond. The stiffness of the bond can be characterized by a proportionality constant termed the force constant, k (derived from Hooke's law). The reduced mass, μ, provides a useful way of simplifying calculations by combining the individual atomic masses, and may be expressed as follows:

$$\left({}^{1}/_{\mu}\right) = \left({}^{1}/_{m_1}\right) + \left({}^{1}/_{m_2}\right) \tag{5}$$

where m_1 and m_2 are the masses of the atoms at the ends of the bond. A practical alternative way of expressing the reduced mass is:

$$\mu = m_1 m_2/(m_1 + m_2) \quad (6)$$

The equation relating the force constant, the reduced mass and the frequency of absorption is:

$$v = (1/2\pi)\sqrt{(k\ /\ \mu)} \quad (7)$$

This equation may be modified so that direct use of the wavenumber values for bond vibrational frequencies can be made, namely:

$$\bar{v} = (1/2\pi c)\sqrt{(k\ /\ \mu)} \quad (8)$$

where c is the speed of light.

A molecule can only absorb radiation when the incoming infrared radiation is of the same frequency as one of the fundamental modes of vibration of the molecule. This means that the vibrational motion of a small part of the molecule is increased while the rest of the molecule is left unaffected.

Vibrations can involve either a change in bond length (*stretching*) or bond angle (*bending*). Some bonds can stretch in-phase (*symmetrical* stretching) or out-of-phase (*asymmetric* stretching). If a molecule has different terminal atoms such as HCN, ClCN or ONCl, then the two stretching modes are no longer symmetric and asymmetric vibrations of similar bonds, but will have varying proportions of the stretching motion of each group. In other words, the amount of *coupling* will vary.

Bending vibrations also contribute to infrared spectra and these are summarized in Fig.2.4.

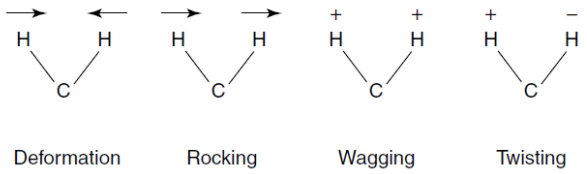

Fig.2.4. Different types of bending vibrations.

It is best to consider the molecule being cut by a plane through the hydrogen atoms and the carbon atom. The hydrogens can move in the same direction or in opposite directions in this plane, here the plane of the page. For more complex molecules, the analysis becomes simpler since hydrogen atoms may be considered in isolation because they are usually attached to more massive, and therefore, more rigid parts of the molecule [8]. This results in *in-plane* and *out-of-plane* bending vibrations, as illustrated in Fig.2.5.

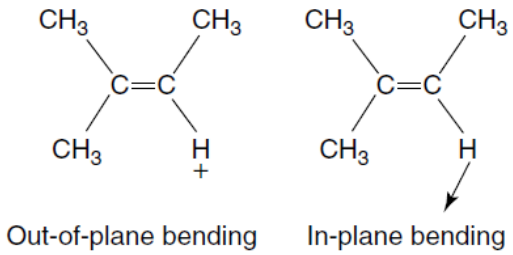

Fig.2.5. Out-of-plane and in-plane bending vibrations.

Fourier-transform infrared (FTIR) spectroscopy is based on the idea of the interference of radiation between two beams to yield an *interferogram*. The latter is a signal produced as a function of the change of pathlength between the two beams. The two domains of distance and frequency are interconvertible by the mathematical method of *Fourier-transformation* [9].

The essential equations for a Fourier-transformation relating the intensity falling on the detector, *I(*δ*)*, to the spectral power density at a particular wavenumber, v, given by *B(*.v*)*, are as follows:

$$I(\delta) = \int_{-\infty}^{+\infty} B(\bar{\nu}) \cos(2\pi\bar{\nu}\delta)\, d\bar{\nu} \tag{9}$$

which is one half of a cosine Fourier-transform pair, with the other being:

$$B(\bar{\nu}) = \int_{-\infty}^{+\infty} I(\delta)\cos(2\pi\bar{\nu}\delta)\,d\delta \tag{10}$$

These two equations are interconvertible and are known as a Fourier-transform pair. The first shows the variation in power density as a function of the difference in pathlength, which is an interference pattern. The second shows the variation in intensity as a function of wavenumber. Each can be converted into the other by the mathematical method of *Fourier-transformation*.

Attenuated total reflectance (ATR) spectroscopy utilizes the phenomenon of *total internal reflection* (Fig.2.6).

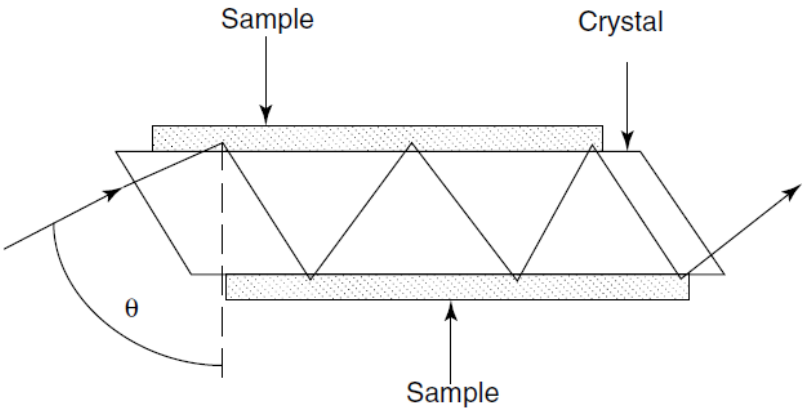

Fig.2.6. Schematic of a typical attenuated total reflectance cell.

A beam of radiation entering a crystal will undergo total internal reflection when the angle of incidence at the interface between the sample and crystal is greater than the critical angle, where the latter is a function of the refractive indices of the two surfaces. The beam penetrates a fraction of a wavelength beyond the reflecting surface and when a material that selectively absorbs radiation is in close contact with the reflecting surface, the beam loses energy at the wavelength where the material absorbs. The resultant attenuated radiation is measured and plotted as a function of wavelength by the spectrometer and gives rise to the absorption spectral

characteristics of the sample [10]. The depth of penetration in ATR spectroscopy is a function of the wavelength, λ, the refractive index of the crystal, n_2, and the angle of incident radiation, θ. The depth of penetration, d_p, for a non-absorbing medium is given by the following:

$$d_p = (\lambda/n_1)/\{2\pi[sin\theta - (n_1/n_2)^2]\} \quad (11)$$

where n_1 is the refractive index of the sample.

The crystals used in ATR cells are made from materials that have low solubility in water and are of a very high refractive index. Such materials include zinc selenide (ZnSe), germanium (Ge) and thallium–iodide (KRS-5). Different designs of ATR cells allow both liquid and solid samples to be examined [10].

2.3. Small Angle X-ray Scattering (SAXS)

Small angle X-ray scattering (SAXS) is a small angle scattering technique where the elastic scattering of X-rays by a sample which has structure in the nanometer-range, is recorded at very low angles (0.1 - 10°). This angular range contains information about the shape and size of macromolecules, pore sizes, unit cell distances of liquid crystalline phases etc.

In a SAXS instrument a monochromatic beam of X-rays is brought to a sample from which some of the X-rays scatter, while most go through the sample without interacting with it. The scattered X-rays form a scattering pattern which is then detected at a detector which is typically a 2-dimensional flat X-ray detector situated behind the sample perpendicular to the direction of the primary beam that initially hit the sample. The scattering pattern contains the information on the structure of the sample.

Elastic interactions are characterized by zero energy transfers, such that the final wave vector kf is equal in modulus to ki. The relevant

parameter to analyze the interaction is the momentum transfer or scattering vector q=ki-kf, given by equation:

$$q = 4\pi\sin(\theta) / \lambda \quad (12)$$

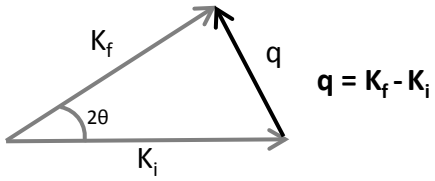

Fig.2.7. Schematic representation of the scattering vector

where *2θ* is the angle between the incident X-ray beam and the detector measuring the scattered intensity, and λ is the wavelength of the X-rays.

With X-ray scattering experiments characteristic interferences are generated from an ordered microstructure [11]. A typical interference pattern arises due to specific repeat distances of the associated interlayer spacings *d*. According to Bragg's equation *d* can be calculated:

$$d = n\lambda/2sin\gamma \quad (13)$$

where n is an integer and nominates the order of the interference, and γ is the angle under which the interference occurs (reflection conditions are fulfilled).

From Bragg's equation it can be seen that the interlayer spacing *d* is inversely proportional to the angle of reflection γ. Large terms for *d* in the region of long-range order can be measured by small-angle X-ray diffraction (SAXD), while small terms for *d* in the region of short-range order can be investigated by wide-angle X-ray diffraction (WAXD). SAXD is the most appropriate technique for the exact determination of the distances of interlayer spacings of liquid crystalline systems. The short-range order of crystalline nano-suspensions can be detected by WAXD. Interferences can be detected by using either film detection, or scintillation counters or

position-sensitive detectors. However, in addition to interference detection, and subsequent calculation of interlayer spacings of the crystalline material, the SAXS method enables the sequence of the interferences and thus the type of ordering to be detected [12].

Small-angle scattering (SAXS) is a powerful technique for examining nanostructures formed by the self-assembly of surfactants and block copolymers. SAXS is extensively used to identify morphologies in the self-assembled structures from the sequence of Bragg reflections observed. Table 1 lists the positions of peaks for the equilibrium structures observed in various liquid crystal structures. Multiple orders of Bragg reflection are observed for strongly segregated samples. Weakly segregated samples may only exhibit the lower order peaks, which can lead to ambiguities in phase identification. This can be circumvented by supplementary information from a complementary technique, for example, transmission electron microscopy. Alternatively, shear alignment of a sample can enhance the information content in a SAXS pattern, and facilitate the identification of morphology even for a weakly segregated sample. SAXS methods are well suited to investigate the structure of micelles because their size is typically ~5–100 nm, which leads to scattering at small angles[13].

Table 1 Peak positions (expressed as q/q*) of Bragg reflections for various structures.

Structure	**Ratio (q/q*)**
Lam	1, 2, 4, 5, 6,.....
Hex (*p6mm*)	1,√3, √4, √7, √9, √12,.....
BCC (*Im3m*)	1, √2, √3, √4, √5, √6,.....
FCC (*Fm3m)*	1, √4/3, √8/3, √11/3, √12/3, √16/3,.....
Gyr (*Ia3d*)	1, √4/3, √7/3, √8/3, √10/3, √11/3,.....

2.4. Rheology of gels

A gel system is composed of molecules that form a network and these molecules are linked either by chemical crosslinks, similar in strength to the molecular bonds, or physical links, which are considerably weaker. This definition covers a wide range of systems from proteins, lipids, and surfactants to polymers [14-15].

Experimentally, rheology is the study of the effects of shear on a system. The response of a system can comprise of two basic components. The system can either acts as a spring, returning the energy imparted to it, or it can act as a damper and dissipate the applied energy as heat. These two behaviours are termed elastic and viscous behavior, respectively. Gels show both these effects and are thus viscoelastic materials [16].

Let us consider a cube of material of height, *h*, with a fixed base. When a force, *F*, is applied to the top of the material's surface, it causes a deformation, *du*

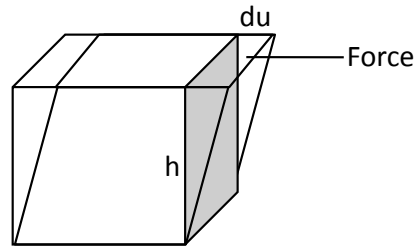

Fig.2.8. The effect of a shear force, the horizontal scale is exaggerated.

The shear strain deformation, or strain as it is simplified, is written as:

$$\gamma = du/h \tag{14}$$

There are no units for strain, and it is often expressed as a percentage. The applied force per unit area is the shearing stress, or shear

stress, measured in Pascals. The shear modulus, *G*, can be defined as the ratio of the shearing force to the shearing strain amplitude:

$$G = \sigma/\gamma \tag{15}$$

In general *G* is a complex quantity. If the cube is a viscous liquid, when we apply a force we now get a constant flow rather than just a deformation. This can be described as a strain changing as a function of time. The rate of change of strain is known as the shear rate, and generally has units of reciprocal seconds.

The viscosity is defined as:

$$\eta = Shear\ rate/Shear\ stress \tag{16}$$

The combination of hydrophobic blocks and hydrophilic blocks causes the systems to associate intermolecularly to form transient networks. A transient network allows for the hydrophobic end groups to detach from the micelles. Once detached, a chain is free to move independent of the rest of the network. Motion of the chains is governed by Rouse dynamics with a characteristic time, τ_R.

So, relaxation time = detachment time +Rouse time.

$$\tau = \beta_0^{-1} + \tau_R \tag{17}$$

The relaxation time when the stress and elongation have reached equilibrium is equal to η/G, where *G* is the modulus.

$$\gamma_{total} = S_{elastic} + \gamma_{viscous} \tag{18}$$

This can be expressed as

$$d\gamma/dt = S/\eta + dS/dt \cdot 1/G \tag{19}$$

i.e. Rate of strain is equal to zero under conditions of constant stress. So,

$$S/\eta + dS/dt.1/G = 0 \tag{20}$$

Assuming $S=S_0$ at time zero

$$S = S_0 \cdot e^{-t/\tau} \tag{21}$$

So, according to the Maxwell model, under conditions of constant strain, the stress will decrease exponentially with time and at the relaxation time will be equal to 1/e, of its original value.

In the Maxwell model the viscoelastic moduli are given by:

$$G^{'}(\omega) = (G_{\infty}\omega^2\tau^2)(1+\omega^2\tau^2)(\text{Storage modulus}) \quad (22)$$

$$G^{''}(\omega) = (G_{\infty}\omega\tau)(1+\omega^2\tau^2)(\text{Loss modulus}) \quad (23)$$

ω – Angular frequency (rad s^{-1})

τ – Stress relaxation time.

$$\tan\delta = G^{''}/G' \quad (24)$$

This ratio is *loss tangent*, and is a measure of the energy loss per cycle.

In general *G* is both a complex quantity, comprising of storage (real) (*G'*) and loss (imaginary) (*G''*) components and frequency dependent, showing vastly different behavior at low shear rates and high shear rate [17].

As concentration is increased, the ‘‘symmetric’’ diblocks such as PEO-PPO-PEO copolymers, which have a roughly equal number of hydrophobic and hydrophilic groups show a progression in the following order [18]:

Isotropic micellar ⟶ cubic micellar ⟶ hexagonal ⟶ lamellar structure

This is analogous to the phase behavior seen in surfactant solutions. The phase behavior of PEO-containing copolymers corresponds to fascinating rheological properties; the most notable is formation of a cubic gel from low viscosity solutions as the temperature is increased. Rheological ‘phase boundaries’ can be measured for several copolymers which show transitions between sols, ‘soft gels,’ and ‘hard gels’. The sol–hard gel transition corresponds to the formation of a close-packed

micellar gel, described above. The soft gels, on the other hand, show a fractal structure consistent with the idea of a percolated network of micelles [19]. The soft gel transition has also been ascribed to a spherical-to-cylindrical micelle transition [20-21] or the occurrence of defects in the cubic phase [22-23].

2.5. References

[1] W. Haase, D. Demus und L. Richter: Textures of Liquid Crystals. Verlag Chemie, Weinheim, New York 1978. 228 Seiten, Preis: DM 185, Berichte der Bunsengesellschaft für physikalische Chemie, 84 (1980) 1271-1271.

[2] M. Wlodzimierz Sulek, A. Bak, The Effect of Liquid Crystalline Structures on Antiseizure Properties of Aqueous Solutions of Ethoxylated Alcohols, Int J Mol Sci, 11 (2010) 189-205.

[3] S. Radhika, B.K. Sadashiva, V.A. Raghunathan, Occurrence of transition between lamellar antiferroelectric and columnar ferroelectric phases in achiral seven-ring bent-core compounds derived from 5-methoxyisophthalic acid, Ferroelectr, 364 (2008) 20-32.

[4] C.W. Oatley, W.C. Nixon, R.F.W. Pease, Scanning Electron Microscopy, in: L. Marton (Ed.) Advances in Electronics and Electron Physics, Academic Press, 1966, pp. 181-247.

[5] P. Goodhew, F. Humphreys, R. Beanland, Electron microscopy and analysis, Taylor & Francis Group, 2001.

[6] M. Hajibagheri, Electron microscopy methods and protocols, Humana Pr Inc, 1999.

[7] J. Bozzola, L. Russell, Electron microscopy: principles and techniques for biologists, Jones & Bartlett Pub, 1999.

[8] B. Stuart, Infrared spectroscopy: fundamentals and applications, Wiley, 2004.

[9] P. Griffiths, J. De Haseth, Fourier transform infrared spectrometry, Wiley-Interscience, 2007.

[10] K.A. Oberg, A.L. Fink, A New Attenuated Total Reflectance Fourier Transform Infrared Spectroscopy Method for the Study of Proteins in Solution, Anal Biochem, 256 (1998) 92-106.

[11] K. Fontell, Liquid crystallinity in lipid-water systems, Molecular Crystals and Liquid Crystals, 63 (1981) 59-82.

[12] A. Bradley, C. Hardacre, J. Holbrey, S. Johnston, S. McMath, M. Nieuwenhuyzen, Small-angle X-ray scattering studies of liquid crystalline 1-alkyl-3-methylimidazolium salts, Chem Mater, 14 (2002) 629-635.

[13] C. Müller-Goymann, Physicochemical characterization of colloidal drug delivery systems such as reverse micelles, vesicles, liquid crystals and nanoparticles for topical administration, Eur J Pharm Biopharm, 58 (2004) 343-356.

[14] J. Fairclough, A. Norman, 7 Structure and rheology of aqueous gels, Annual Reports Section" C"(Physical Chemistry), 99 (2003) 243-276.

[15] Y. Osada, K. Kajiwara, H. Ishida, Gels handbook, Academic Press London, 2001.

[16] C. Macosko, R. Larson, Rheology: principles, measurements, and applications, Wiley-Vch New York, 1994.

[17] C. Daniel, I.W. Hamley, M. Wilhelm, W. Mingvanish, Non-linear rheology of a face-centred cubic phase in a diblock copolymer gel, Rheologica Acta, 40 (2001) 39-48.

[18] I.W. Hamley, Amphiphilic diblock copolymer gels: the relationship between structure and rheology, Philos Transact A Math Phys Eng Sci, 359 (2001) 1017-1044.

[19] H. Li, G.-E. Yu, C. Price, C. Booth, E. Hecht, H. Hoffmann, Concentrated Aqueous Micellar Solutions of Diblock Copoly(oxyethylene/oxybutylene) E41B8: A Study of Phase Behavior, Macromolecules, 30 (1997) 1347-1354.

[20] S. Hvidt, E.B. Joergensen, W. Brown, K. Schillen, Micellization and Gelation of Aqueous Solutions of a Triblock Copolymer Studied by Rheological Techniques and Scanning Calorimetry, J Phys Chem, 98 (1994) 12320-12328.

[21] E.B. Jørgensen, S. Hvidt, W. Brown, K. Schillén, Effects of salts on the micellization and gelation of a triblock copolymer studied by rheology and light scattering, Macromolecules, 30 (1997) 2355-2364.

[22] J.A. Pople, I.W. Hamley, J.P.A. Fairclough, A.J. Ryan, B.U. Komanschek, A.J. Gleeson, G.E. Yu, C. Booth, Ordered phases in aqueous solutions of diblock oxyethylene/oxybutylene copolymers investigated by simultaneous small-angle X-ray scattering and rheology, Macromolecules, 30 (1997) 5721-5728.

[23] L. Derici, S. Ledger, S.M. Mai, C. Booth, I.W. Hamley, J.S. Pedersen, Micelles and gels of oxyethylene-oxybutylene diblock copolymers in aqueous solution: The effect of oxyethylene-block length, Phys Chem Chem Phys, 1 (1999) 2773-2785.

3. MICROSPHERES SUSPENDED IN PLURONIC F127 GEL

3.1. Introduction

Among the different types of drug delivery systems being proposed recently, microspheres composed of biodegradable polymers for controlled release applications are extensively studied [1]. Gelatin is one of the common natural polymers used in the fabrication of particulate drug delivery systems such as microspheres [2-4]. It is a well known natural polymer derived from collagen which possesses good biodegradability and biocompatibility [2, 5-6]. Moreover, it has been extensively used in various contemporary pharmaceutical dosage forms, and it is included on the FDA list of inactive ingredients [7]. Gelatin exhibits polyion complexation properties which can be utilized in the formulation of the sustained release of numerous charged pharmacologically active molecules including proteins [5-6]. Different cross-linking methods have been reported for gelatin microspheres (GMs) in order to alter the toxicity associated with cross-linking agents [8].

In this context, it should be remarked that GMs, due to their biodegradability, are not expected to fulfill all requirements of an effective controlled release, in terms of pharmacokinetic protocols. Burst release cannot be avoided unless a protection that slows down the degradation process is adopted. To obtain sustained release drug delivery systems, combinations of microspheres and gel systems have been attempted previously by several authors. Examples include 5-Fluorouracil in chitosan microspheres and PF127 gel [9], insulin in calcium-alginate microspheres and PF127 gel [10], Baclofen in Poly(lactide-co-glycolide) (PLGA) microspheres dispersed in chitosan and PF127 gels [11], timolol maleate in Poly(adipic anhydride) microspheres and gelrite gel [12], oxybenzone in gelatin microspheres and aloe vera gel [13].

The present work focuses on GMs dispersed in the thermosensitive Pluronic F127 (PF127) gel matrix. The concentrated aqueous solutions (20-40 % w/v) of Pluronic F127 (PF127), a synthetic triblock copolymer, show thermoreversible properties due to interactions between different segments of the copolymer along with hydration strength. Above the Krafft temperature, that was found to be approximately 12 ºC [14-15], PF127 molecules (concentration around, 20 % w/v) form O/W micelles. The micelle structure consists of almost spherical arrangement of copolymer with a dehydrated polypropylene oxide core and an outer shell of hydrated swollen polyethylene oxide chains. With increasing temperature ordered packing of micelles leads to gelation of aqueous solution of PF127 [16]. PF127 gels can be useful to enhance the stability and the protection of proteins. They do not show any inherent myotoxicity with single or multiple injections [17]. This polymer has been reported in literature for delivery of various protein/peptide drugs such as insulin [18], urease [19], interleukin-2 [20], epidermal growth factor [21], bone morphogenic protein (BMP) [22], and basic fibroblast growth factor (bFGF) [23]. Most release profiles show sustained release kinetics over several hours.

The aim of the present work was to investigate the effect on morphology and release performance of two different crosslinking methods in the preparation of GMs loaded with lysozyme chosen as a model protein. To the best of our knowledge, the combination of GMs and PF127 gel has never been reported. Lysozyme is a small antibacterial protein with molecular weight of 14.4 kD useful for the treatment of prosthetic valve endocarditis [24-25]. Another important aim of this work was to investigate the release performance modifications produced by suspending the lysozyme loaded GMs in PF127 gel, and to ascertain that lysozyme does not lose its activity due to the preparation conditions of the formulation or during the release. Scanning Electron Microscopy (SEM), ATR-Fourier

Transform Infrared (FTIR) Spectroscopy and Small-Angle X-Ray Scattering (SAXS) techniques along with rheological measurements were used to characterize morphology and physico-chemical properties of the formulations. The quantification of lysozyme loading and release was performed through lysozyme activity assay using *Micrococcus lysodeikticus* bacterial suspension [26].

3.2. Materials and methods

3.2.1. Materials

Hen egg white lysozyme (isoelctric point ~11), gelatin B (isoelectric point 4.7-5.2), D-glucose, Span 80, acetone, Pluronic F127, potassium dihydrogen orthophosphate and dipotassium hydrogen phosphate were purchased from Sigma aldrich. Millipore filtered and distilled water was used wherever required.

3.2.2. Preparation of gelatin microspheres

Glucose cross-linked gelatin microspheres (GluGM) and glutaraldehyde cross-linked gelatin microspheres (GAGM) were prepared with and without lysozyme loading. Both types of GMs were prepared by thermal gelation method as first described by Tabata and Ikada and later modified by several authors [2, 27-28]. For GluGM, 400 mg of D-glucose was dispersed in 20 ml of an aqueous gelatin B solution (20 %, w/v, preheated at 40 ^{0}C) and the dispersion was added drop wise to mixture of soya oil and Span 80 (1 % v/v) while stirring the mixture at 1000 rpm at 80 ^{0}C for 10 min. This gave water in oil (W/O) emulsion. Stirring was continued for further 10 min while decreasing the temperature to 15 ^{0}C. Then 150 ml of acetone was added to dehydrate and flocculate the microspheres. After 10 min of stirring microspheres were then filtered through sintered glass

filter and washed with 250 ml of acetone to remove residual oil. GluGMs were dried under vacuum to remove acetone. For preparing, lysozyme loaded GluGM (LGluGM), 100 mg of lysozyme was dissolved in gelatin and glucose-D solution. In case of GAGM, first gelatin microspheres without cross-linking were obtained through the same procedure as that of GluGM without the addition of sugar. These GMs were then mixed with 0.22 M glutaraldehyde prepared in aqueous ethanol solution (90 % v/v) with stirring for 45 min and then with 99.8 % ethanol for 4 hours to remove excess of glutaraldehyde. GAGMs were vacuum dried to evaporate residual ethanol. For preparing lysozyme loaded GAGMs (LGAGM), GAGMs were suspended in 10 mg/ml of lysozyme prepared in phosphate buffer pH 7.4 for 24 hours. The resulting LGAGMs were separated from the lysozyme solution and freeze dried. All the microspheres were stored in closely packed glass vial.

3.2.3. Lysozyme activity

Lysozyme activity was measured by a method reported in literature [26]. *Micrococcus lysodeikticus* (Sigma) bacterial cell suspension was used to quantitatively determine the bioactivity of the enzyme. Lysozyme is known to digest the cell wall of bacteria. The bacterial cells were dispersed in potassium phosphate buffer (66 mM, pH 6.24) in the concentration of 0.015% w/v. It was further diluted with the same buffer so that initial absorbance was approximately 1.50 at 450 nm. An appropriately diluted lysozyme solution (0.1 ml) was added into 2.5 ml of bacterial suspension and the absorbance at 450 nm was recorded every 15 s during a total incubation period of 5 min at 25 °C. The bioactive lysozyme concentration was determined by the following equation

$$Units/\ ml\ lysozyme = \frac{(\Delta E_{450nm}/\min Test - \Delta E_{450nm}/\min Blank)(df)}{(0.001)(0.1)} \quad (1)$$

where ΔE_{450nm}/min is the reduction in the absorbance at 450 nm per minute, *df* is the dilution factor, 0.001 is the change in absorbance at 450 nm as per the unit definition of lysozyme activity, 0.1 is volume (in ml) of lysozyme used for the assay.

3.2.4. Drug loading and encapsulation ratio of microspheres

Both types of lysozyme loaded gelatin microspheres (5 mg) were dispersed in 10 ml distilled water with the help of magnetic stirrer. The concentration of bioactive lysozyme was monitored till it becomes constant by the method described in section 3.2.3. The drug loading (L_D) and encapsulation ratio (E_D) were determined by using following equations:

$$L_{D=} \frac{Actual\ loaded\ amount\ of\ lysozyme\ \ obtained\ by\ extraction\ \times 100}{Amount\ of\ microspheres} \quad (2)$$

$$E_{D=} \frac{Actual\ loaded\ amount\ of\ lysozyme\ \ obtained\ by\ extraction\ \times 100}{Amount\ of\ lysozyme\ added\ to\ the\ preparation} \quad (3)$$

3.2.5. Preparation of gel and microsphere/gel suspension

PF127 gel was prepared by dissolving 20 % w/v of PF127 powder in distilled water for 12 to 24 hours at 4 ^{0}C in refrigerator. This method of preparation is called as ‘cold method’ [29]. The lysozyme was dissolved in distilled water for preparing lysozyme loaded PF127 gel. Lysozyme loaded gelatin microspheres were added to PF127 gel to form gelatin microsphere in PF127 gel formulation just before the experiment.

3.2.6. Microscopy

The prepared gelatin microspheres were observed under scanning electron microscope to study shape and surface properties. The gelatin microspheres were sprinkled onto a double adhesive tape fixed on aluminium stage. Fixed microspheres were spattered with platinum film. Examination of microspheres was performed with a scanning electron microscope FE Hitachi S4000 operating at 15–20 KV.

3.2.7. ATR-FTIR studies

ATR-FTIR studies were conducted with a Bruker Tensor 27 spectrophotometer equipped diamond ATR accessory and DTGS (deuteriotriglycine sulphate) detector. Each spectrum was an average of 128 scans at resolution of 4 cm^{-1} from wavenumber 4000 to 400 cm^{-1}. The Opus spectroscopic software was used for data handling.

3.2.8. Rheology

Rheological measurements were performed with rheometer (Malvern Kinexus, Worcestershire, UK) using cone-plate geometry CP4/40 and a 200 µm gap operating in the oscillation mode. The frequency and shear stress was set as 0.1 Hz and 0.5 Pa. The temperature ramp was performed from 5-40 ºC at 1 ºC/min rate. The sampling interval was set 5 seconds. The oscillatory measurements gave the information about the rheological parameters such as elastic or storage modulus (G') and the loss or viscous modulus (G''). Sol-gel transition temperature was determined for all the gel samples.

3.2.9. SAXS experiments

Small-angle X-ray diffraction was recorded with a S3-MICRO SWAXS camera system (HECUS X-ray Systems, Graz, Austria). Cu Kα

radiation of wavelength 1.542 Å was provided by a GeniX X-ray generator, operating at 50 kV and 1 mA. A 1D-PSD-50 M system (HECUS X-ray Systems, Graz, Austria) containing 1024 channels of width 54.0 μm was used for detection of scattered X-rays in the small-angle region. The working q-range ($Å^{-1}$) was $0.003 \leq q \leq 0.6$, where $q = 4\pi \sin(\theta) \lambda^{-1}$ is the modulus of the scattering wave vector. The distance between the sample and detector was 235 mm. Solutions were usually taken from storage under refrigerator, heated to the required temperature and allowed 15 min to equilibrate. A few milligrams of the sample were enclosed in a stainless steel sample holder using a polymeric sheet (Bratfolie, Kalle) window. The diffraction patterns were recorded at 37 °C for 3 hours. To minimize scattering from air, the camera volume was kept under vacuum during the measurements. Silver behenate (CH_3-$(CH_2)_{20}$-COOAg) with a d spacing value of 58.38 Å was used as a standard to calibrate the angular scale of the measured intensity. The lattice parameters (*a*) were determined for the cubic phases from the linear fits of the reciprocal spacing ($1/d_{hkl}$) of the various reflections versus the sum of the Miller indexes $(h^2 + k^2 + l^2)^{1/2}$. For a correct assignment the plot passes through the origin, and the slope is 1/a, where 'a' is the lattice parameter.

3.2.10. In vitro release studies

For gelatin microspheres alone, 5 mg weighed amount lysozyme loaded GM was put in test tube along with 5 ml of release media. Aliquot of 2 ml sample of the supernatant solution after a brief centrifugation was withdrawn at predetermined time-points and replaced with 2 ml fresh phosphate buffer.

Membrane-less diffusion system was used for studying the release of lysozyme from LGAGM and LGluGM suspended in PF127 gel [30]. Accurately weighed 1 g sample of each type was put in a flat-bottomed vial

(internal diameter about 18 mm) followed by gently adding 1 ml of phosphate buffer (pH 7.4) on the surface of gels, and then the vial was shaken in a thermostatic shaker under 37 °C at 100 rpm. Complete supernatant solution was withdrawn at predetermined time-points and replaced with equal amount of fresh phosphate buffer. The concentration of bioactive lysozyme in the supernatant solution was determined using the method described in section 3.2.3. In order to estimate the lysozyme release from lysozyme loaded gelatin microspheres, unloaded microspheres were subjected to same release conditions to obtain the actual release.

3.3. Results and discussion

3.3.1. Preparation of gelatin microspheres

Gelatin microspheres are normally prepared by the simple method of thermal gelation, also referred as emulsification-solvent-extraction method. In order to reduce the immediate quick dissolution of gelatin, and hence a burst release of the drug encapsulated within the microspheres, several cross-linking methods have been proposed. Chemical cross-linking of gelatin is frequently adopted by many researchers to decrease the solubility of GMs and consequently to decrease the rate of release of drugs from the microspheres. Di- or polyaldehydes used as cross-linking agents are known to give excellent microspheres for controlling release properties of encapsulated drug. However, these cross-linking agents lead to several undesirable toxic side effects, if traces of them remain after crosslinking and/ or if they form toxic products after reaction with the encapsulated drug. To overcome this problem several ‘natural’ cross-linking agents, for example sugars or sugar-derived compounds have been attempted for the preparation of microspheres with modified release profiles of the encapsulated drugs. The two representative compounds of chemical cross-

linkers (i.e. Di- or polyaldehydes and sugars) for gelatin microspheres selected for this study are glutaraldehyde and D-glucose. There are several different mechanisms proposed for cross-linking of gelatin using glutaraldehyde or D-glucose. In case of crosslinking by glutaraldehyde, because of aldehyde functional groups, it is suggested that reaction occurs mainly with the ε-amino groups of gelatin lysyl residues, ultimately forming the GAGM i.e. glutaraldehyde crosslinked gelatin microsphere (Fig.3.1.a). In case of D-glucose, a possible mechanism of reaction is that the sugar aldehyde group reacts with the free ε-amino groups of gelatin molecule producing aminoglycoside, which further reacts with another amine group producing the GluGM i.e. glucose crosslinked gelatin microsphere (Fig.3.1.b).

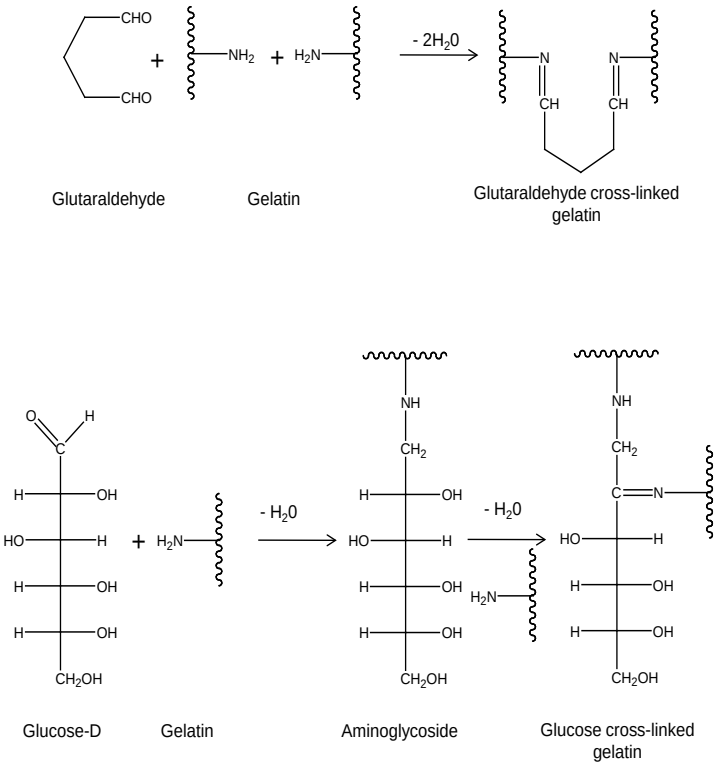

Fig.3.1. Cross-linking reaction of gelatin with (a) glutaraldehyde and (b) D-glucose.

Lysozyme has isoelectric pH of ~11, therefore, when it is adsorbed on the gelatin surface, it can react through the mechanism of poly-ion complexation. Gelatin B (isoelectric pH 4.7-5.2) was preferred over gelatin A (isoelectric pH 7.0-9.0) due to its higher anionic nature.

Table 1 Loading and entrapment ratio of lysozyme loaded gelatin microspheres.

	L_D (%)	E_D (%)
LGAGM	7.0 ± 0.2	7.0 ± 0.2
LGluGM	1.96 ± 0.04	98 ± 2

The loading and encapsulation efficiencies of the two types of GMs viz. LGAGM and LGluGM, used in this study differed significantly from each other as reported in Table 1. These differences are mainly due to different methods used for loading the lysozyme into the microspheres. In case of LGAGMs, the loading of lysozyme was done after preparing the GAGMs. In case of LGluGMs, lysozyme was added before the emulsification in the aqueous gelatin and glucose solution. In a latter case, almost all the lysozyme was loaded successfully with entrapment efficiency (E_D) equal to 98 ± 2 %. For LGAGMs, the E_D was lower since excess amount of lysozyme was used for loading procedure. Nevertheless, E_D of LGAGMs (7.0 ± 0.2 %) was lower. Conversely, its loading capacity (L_D) was significantly higher (7.0 ± 0.2 %) than that of LGluGMs (1.96 ± 0.04 %). It is noteworthy that in both the cases, the lysozyme did not lose its biological activity during the harsh conditions of formulation as determined through the methods described above (Section 3.2.3).

3.3.2. Microscopy

The lysozyme loaded GMs obtained through the two different cross-linking procedures described in section 3.2.1, were dried under vacuum and

then further characterized by SEM technique. The images of both types of microspheres revealed that they were nearly spherical in shape (Fig.3.2.a and d) with some differences in external surface texture (Fig.3.2.b and e). The LGAGMs were smoother than the LGluGMs. LGluGMs showed a wavy surface with the presence of small plaques. Our observation about the surface morphology of glucose and glutaraldehyde crosslinked microspheres is consistent with the literature [2, 27]. These differences in surface properties could be the effect of different cross-linking agent.

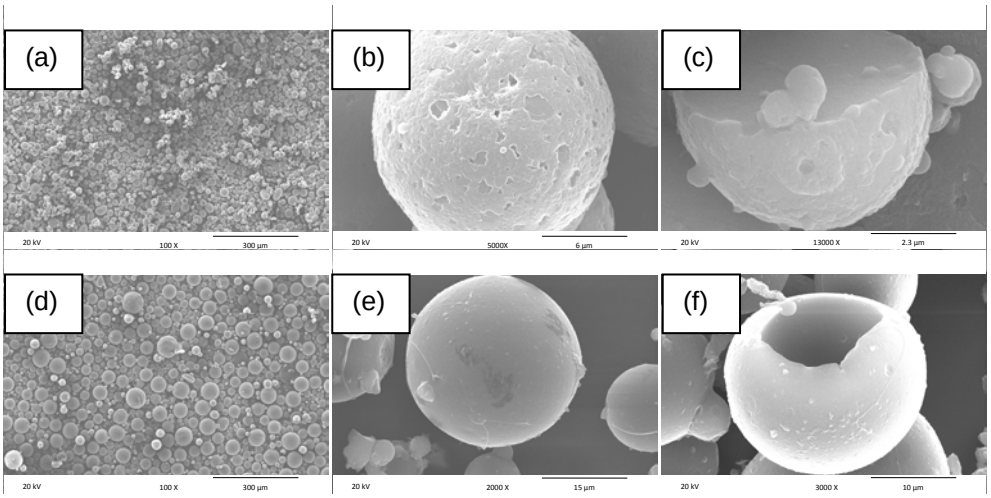

Fig.3.2. SEM micrographs of the lysozyme loaded glucose (LGluGM) (a, b and c) and glutaraldehyde (LGAGM) (d, e and f) crosslinked gelatin microspheres.

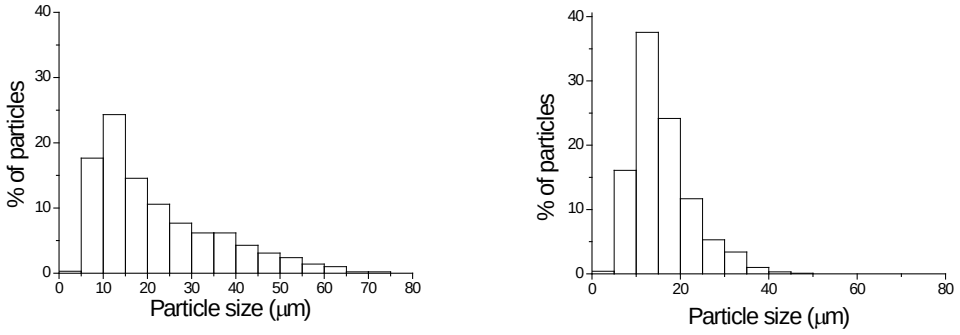

Fig.3.3. Size distribution histograms for (a) lysozyme loaded glutaraldehyde (LGAGM) and (b) glucose (LGluGM) crosslinked gelatin microspheres.

The formulation parameters which can significantly affect the particle size, surface morphology, and dispersion of gelatin microspheres are the concentration of gelatin solution, the concentration of the emulsifier, the W/O ratio, the emulsifying time, and the stirring speed [31]. Therefore, concentration of gelatin solution as 20 % w/v, concentration of emulsifier (Span 80) as 1 % v/v, W/O ratio as 0.05, emulsifying time 10 min and stirring speed 1000 rpm were kept constant in order to study the effect of the two different crosslinking agents on the release properties.

The image analysis of SEM micrographs leads to obtain size distribution and other interesting features induced by the different cross-linkers. Fig.3.3.a and b shows size distribution histograms for LGAGM and LGluGM, respectively. It is clear from the size distribution histograms that the particle size distribution of LGAGM and LGluGM were different. Both types of gelatin microspheres showed log-normal size distribution.

Table 2 Size distribution parameters for LGluGM and LGAGM.

Parameter	LGluGM (µm)	LGAGM (µm)
Mean	15.91	22.06
Standard Deviation	6.63	13.68
Minimum	4.80	2.72
Median	14.50	17.39
Maximum	48.02	70.49
D_{90}^{*}	25.23	42.65

* 90 % of particles are of size less than (µm)

Table 2 summarizes the various size distribution parameters for the two types of GMs investigated. For LGAGM and LGluGM, mean particle size was approximately 22 µm and 16 µm, respectively. In case of LGAGM D_{90} (90% of microspheres are smaller than that) was about 43 µm whereas in case of LGluGM it was about 25 µm. This clearly shows that the

microspheres formed with glucose as crosslinking agent were relatively smaller in size than those with glutaraldehyde. The reason for this difference could also be attributed to the different methods adopted for the production of microspheres. For LGluGM, glucose was added before the emulsification step whereas in case of LGAGM, crosslinking by glutaraldehyde was done after the formation of uncrosslinked gelatin microspheres. The crosslinking procedure involves suspension of microspheres in the glutaraldehyde ethanol solution for 4 hours. During this time, it is likely that some of the microspheres swell by absorbing considerable amount of ethanol inside them. This results in the formation of cavities inside the microspheres, which can be identified in SEM micrograph. These microspheres did not collapse or shrink even after freeze drying. An example can be seen in Fig.3.2.f, where the cross-section of a large particle gives a clear evidence of a cavity. In addition it was noteworthy that when these microspheres were suspended in aqueous medium some of them floated on the surface due to the cavity inside them. The cross-section of LGluGM shows that there is no cavity inside the GM (Fig.3.2.c).

3.3.3. ATR-FTIR studies

ATR-FTIR technique was used to get qualitative information on the degree of crosslinking of gelatin microspheres prepared with the two different cross-linking agents. The infrared spectra of uncross-linked gelatin microspheres (GMs) and lysozyme loaded gelatin microspheres cross-linked by glucose (LGlUGM) and glutaraldehyde (LGAGM) are shown in Fig.3.4. The IR spectra of all the GMs show the characteristic absorption peaks of protein due to NH and CO stretching. The NH stretching also referred as Amide A peak is observed at about 3300 cm^{-1} and CO stretching peaks, also referred as Amide I, II and III, were found at about

1650, 1550 and 1240 cm^{-1}, respectively. The intensity of the CO stretching peaks was very high when glutaraldehyde was used for cross-linking, followed by glucose, thus indicating that more carboxyl groups were activated for LGAGM than for LGluGM. An additional strong absorption peak, characteristic of an aldimine stretching vibration, is observed at about 1450 cm^{-1}. The formation of aldimine functional groups in case of glucose and glutaraldehyde crosslinking of gelatin has already been mentioned in the reaction mechanism. This confirms the occurrence of cross-linking reaction but with significant differences in the degree of cross-linking. Glutaraldehyde clearly favors the cross-linking reaction.

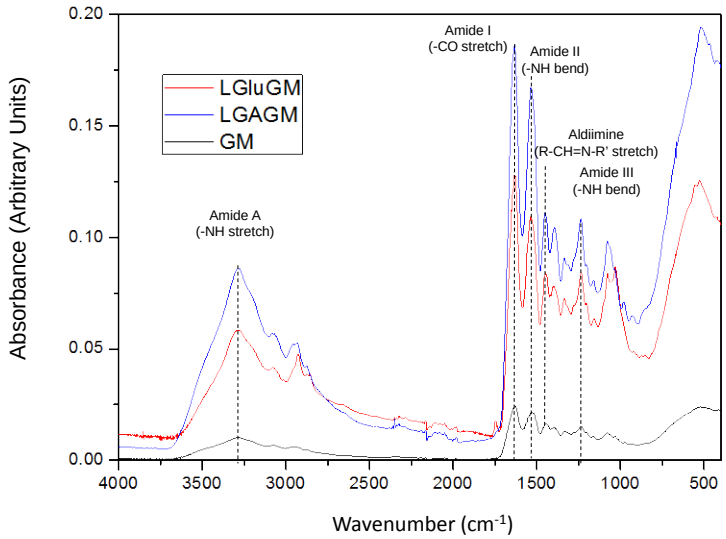

Fig.3.4. ATR-FTIR spectra of (a) lysozyme loaded glutaraldehyde cross-linked (LGAGM); (b) lysozyme loaded glucose cross-linked (LGluGM) and (c) uncross-linked gelatin microspheres without lysozyme (GM).

3.3.4. Rheological characterization

In order to understand the sol-gel transition process and viscoelastic behavior of Pluronic F127 thermosensitive gels, rheological characterization was performed according to other works reported in literature [32-35]. Rheological data reported in Fig.3.5 show the sol-gel transition

temperatures of 20 % w/v PF127 alone and in the presence of LGAGM and LGluGM; these temperatures were found to be 21.90, 21.87 and 21.86 ºC respectively as shown in Table 3. The thermoreversible sol-gel transition of PF127 solutions occurs due to close micellar packing. It is worth noting that when the LGluGM or LGAGM are added to the PF127 solutions, the micelles become more closely packed and the volume fraction of PF127 copolymer molecules decreases as reported in Table 4. Consequently a weakening of the elastic modulus of the gels may result.

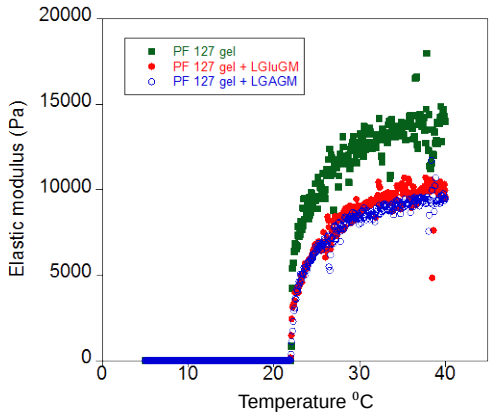

Fig.3.5. Change of elastic modulus as a function of temperature for (from top to bottom) (a) 20 % w/v PF127, (b) 20 % w/v PF127–0.5 % w/v LGluGM and (c) 20 % w/v PF127–0.5 % w/v LGAGM.

Table 3 Phase transition temperature and complex viscosity data for PF127 gel, PF127 gel with LGluGM and LGAGM.

Sample	Transition temperature (ºC)	Viscosity (PaS) with increasing temperature (ºC)		
		20	25	35
PF	21.90	0.105	15544.86	21650.36
PF+LGAGM	21.87	0.078	10393.58	14524.34
PF+LGluGM	21.86	0.083	11023.00	16551.24

Viscosity data at increasing temperature were obtained through the oscillatory measurements in order to ascertain the practical application of final formulations.

Table 3 summarizes relevant rheological and viscosity parameters. It can be noted that the viscosity at 20 ºC was very low in all cases. This implies that these formulations have the desired characteristic of being liquid at lower temperature. Viscosity increases sharply at room temperature and further at 30 ºC. At the investigated temperatures, i.e. 20, 25 and 30 ºC, complex viscosity was significantly lower when either LGAGM or LGluGM were added to the PF127 solutions.

3.3.5. SAXS

Above the sol-gel transition temperature, the PF127-water systems show peculiar features that are not typical for gels. Indeed the close micellar packing produces a long-range ordered nanostructure that is a discrete cubic liquid crystal. The structural characterization was done according to the methods reported in ref [36]. The PF127 nanostructure was determined by the relative positions of the Bragg peaks in the SAXS diffraction patterns.

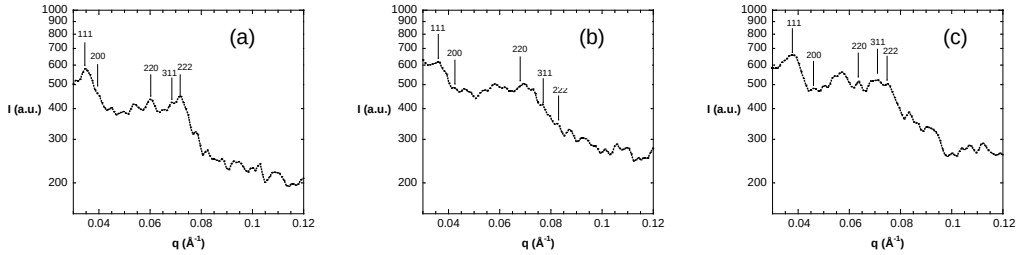

Fig.3.6. SAXS patterns of (a) PF127 20 % w/v gel (b) PF127 20 % w/v gel with 0.5 % w/v lysozyme loaded glucose crosslinked gelatin microspheres (c) PF127 20 % w/v gel with 0.5 % w/v lysozyme loaded glutaraldehyde crosslinked gelatin microspheres.

Fig.3.6 shows the SAXS patterns of (a) PF127 20 % w/v gel, (b) PF127 20 % w/v gel with 0.5 % w/v LGluGMs and (c) PF127 20 % w/v gel with 0.5 % w/v LGAGMs. The three patterns are strikingly similar and show at least five weak Bragg peaks with relative positions in ratios $\sqrt{3} : 2 : \sqrt{8} :$

√11 : √12... which can be indexed as hkl = 111, 200, 220, 311, 222 reflections of a face centered cubic phase of Fm3m space group (Q_{225}). Although the SAXS pattern is essentially dominated by a Fm3m structure, several weak non-indexable peaks are visible.

Two parameters are characteristic of the nanostructure of the liquid crystalline phases: the lattice parameter *a*, and the interfacial area per PEO block, a_p. In the normal micellar cubic structure the interfacial area per PEO block can be calculated from:

$$a_p = (36\pi n_u f^2)^{1/3} \frac{v_p}{2\Phi_{\mathrm{p}}\,\mathrm{a}} \tag{4}$$

where n_u is the number of spherical micelles in the cubic cell, *f* is the apolar volume fraction, v_p is the volume of one PF127 molecule, Φ_p is the copolymer volume fraction in the system and *a* is the lattice parameter. The apolar volume fraction *f*, is given by:

$$f = 0.34\Phi_{\mathrm{p}} \tag{5}$$

where 0.34 is the volume fraction of the PPO block in the PF127 molecule (PPO weight fraction = 0.30). To convert the weight fractions of the components into volume fractions, the bulk densities of the copolymer (1.05 g/cm3), water and additives are used. The volume of one molecule is 20000 Å3. The aggregation number of the micelles, N_{agg}, defined as the number of P127 molecules per micelle can be determined using:

$$N_{agg} = \frac{\Phi_p\, a^3}{n_u v_p} \tag{6}$$

In these equations n_u = 4 for the unit cell of the face-centered lattice consisting of four micelles.

Mortensen et al have shown that 20 % w/v PF127 gel may have face centered cubic (fcc) or body centered cubic (bcc) ordering depending on the proportion of diblock copolymer in the commercial triblock copolymer, with as-received samples forming fcc structured gels and purified samples

forming bcc gels [37]. Recently, Chaibundit et al found that with as-received PF 127, fcc structure is formed and with the addition of 10-30% ethanol, it changes to bcc structure [38]. Our results are in agreement with the reported findings; since all samples used in this study were prepared with the as-received PF127, a fcc structure was found. No significant variations in the nanostructure of PF127 gel were found after inclusion of GMs; indeed small differences in lattice parameter are within 5 % of error (Table 4).

Table 4 PF127 volume fraction (Φ_p), apolar volume fraction (f), lattice parameter (a*)*, interfacial area (a_p) and aggregation number (N_{agg}) obtained from SAXS data for PF127 gel, PF127 gel with LGAGM and LGluGM.

Sample name	PF127/W/GM Ratio	Φp	f	Space group	a (Å)	a_p(Å^2)	N_{agg}
PF	20/80/0	0.192	0.065	Fm3m	294 ± 9	238	56
PF+LGAGM	19.9/79.6/0.5	0.183	0.062	Fm3m	281 ± 12	244	45
PF+LGluGM	19.9/79.6/0.5	0.183	0.062	Fm3m	281 ± 2	235	50

This result implies that lysozyme, if any diffused from GMs and/or GMs themselves is/are not affecting significantly the discrete cubic LC structure of PF127 gel.

3.3.6. In vitro release studies

In vitro release studies performed on gelatin microspheres showed that both types of cross-linked microspheres showed burst release. About 51 % and 89 % of lysozyme was released in the first hour of release experiment in case of LGAGM and LGluGM, respectively. This difference in burst release of lysozyme from LGAGM and LGluGM could be attributed to the differences in degree of cross-linking of gelatin microspheres. Gelatin microspheres are known to swell in aqueous medium due to hydration. Glutaraldehyde and glucose forms bridges in polymeric chains of gelatin. Therefore, the extent of swelling process depends upon the degree of

cross-linking. If the degree of cross-linking is higher, more bridges are formed and microspheres swell less. Swelling of microspheres can cause increased mobility of encapsulated lysozyme, and hence diffusion from the microspheres into the release medium, occurs. Since glutaraldehyde has shown higher cross-linking density than glucose, lysozyme was released at higher rate in case of glucose crosslinked microspheres compared to glutaraldehyde crosslinked microspheres.

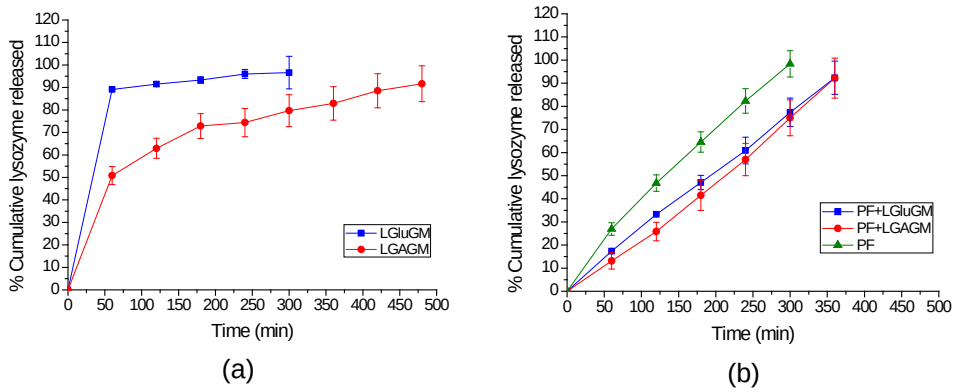

Fig.3.7. *In vitro* release of lysozyme from (a) lysozyme loaded gelatin microspheres crosslinked by glutaraldehyde (LGAGM) and glucose (LGluGM); and (b) PF127 20 % w/v with lysozyme (PF), lysozyme loaded glutaraldehyde (PF + LGAGM) and glucose (PF + LGluGM) cross-linked gelatin microspheres

The release of lysozyme from LGluGM and LGAGM suspended in PF127 gel was slower, in comparison also to lysozyme dissolved in PF127 gel (Fig.3.7.b). PF127 gel released almost all the lysozyme in 5 hours, whereas the GMs suspended in PF127 gel could extend the release for another 1 hour. The reason for the slower release of lysozyme from the GMs suspended in PF127 gel could be the increased path required for lysozyme to pass through the micellar gel matrix before releasing into the buffer medium. It can be noted in Fig.3.7.b that during the initial 2 hours of release experiment, LGluGM suspended in PF127 gel released significantly more lysozyme (33 ± 0.34 %) in comparison to LGAGM suspended in

PF127 gel (approximately 26 ± 4 %). This effect could be related to burst release of lysozyme from LGluGM (Fig.3.7.a). It is worth mentioning that after this initial burst release from LGluGM suspended in PF127 gel, the lysozyme was slowly released from both the GMs.

Burst release of encapsulated drugs from microspheres is an unwanted phenomenon. To limit the burst release, some authors has suggested use of higher concentration of cross-linking agents. But, this has its inherent disadvantages, as cross-linking agents at high concentration will give rise higher toxicity or interact with the encapsulated drugs.

3.4. Conclusions

The results of this study allow to point out that the cross-linking of gelatin with glutaraldehyde and D-glucose produced two different cross-linked structures. Although, the shape of microspheres was spherical in both the cases, the surface texture and size distribution was clearly distinct. The infrared spectroscopy analysis showed that the degree of cross-linking density was significantly different for the two types of microspheres obtained. Lysozyme, without losing its biological activity, was successfully loaded, although loading and encapsulation was significantly different for the two types of microspheres. The nanostructure of 20 % w/v PF127 gel was found to be a Fm3m type cubic discrete liquid crystal; that was not significantly modified upon gelatin microspheres addition. PF127 gel has higher elastic modulus and complex viscosity than the microspheres in gel formulations. The suspension of GMs in PF127 gel allowed for a more sustained release of lysozyme. Finally, it should be remarked that the combination of these two different formulation systems into one can give more options to control the drug release.

3.5. References

[1] M.-L. Manca, S. Mourtas, V. Dracopoulos, A.M. Fadda, S.G. Antimisiaris, PLGA, chitosan or chitosan-coated PLGA microparticles for alveolar delivery?: A comparative study of particle stability during nebulization, Colloids and Surfaces B: Biointerfaces, 62 (2008) 220-231.

[2] R. Dinarvand, S. Mahmoodi, E. Farboud, M. Salehi, F. Atyabi, Preparation of gelatin microspheres containing lactic acid--effect of cross-linking on drug release, Acta Pharm, 55 (2005) 57-67.

[3] K. Ulubayram, I. Eroglu, N. Hasirci, Gelatin microspheres and sponges for delivery of macromolecules, J Biomater Appl, 16 (2002) 227-241.

[4] Z.S. Patel, M. Yamamoto, H. Ueda, Y. Tabata, A.G. Mikos, Biodegradable gelatin microparticles as delivery systems for the controlled release of bone morphogenetic protein-2, Acta Biomaterialia, 4 (2008) 1126-1138.

[5] S. Young, M. Wong, Y. Tabata, A.G. Mikos, Gelatin as a delivery vehicle for the controlled release of bioactive molecules, J. Controlled Release, 109 (2005) 256-274.

[6] K. Mladenovska, E.F. Kumbaradzi, G.M. Dodov, L. Makraduli, K. Goracinova, Biodegradation and drug release studies of BSA loaded gelatin microspheres, Int. J. Pharm., 242 (2002) 247-249.

[7] S. Singh, K.V. Rama Rao, K. Venugopal, R. Manikandan, Alteration in dissolution characteristics of gelatin-containing formulations, Pharm. Tech., (2002) 36-58.

[8] M.A. Vandelli, M. Romagnoli, A. Monti, M. Gozzi, P. Guerra, F. Rivasi, F. Forni, Microwave-treated gelatin microspheres as drug delivery system, J. Controlled Release, 96 (2004) 67-84.

[9] A.P. Rokhade, N.B. Shelke, S.A. Patil, T.M. Aminabhavi, Novel hydrogel microspheres of chitosan and pluronic F-127 for controlled release of 5-fluorouracil, J. Microencapsulation, 24 (2007) 274-288.

[10] Y. Wang, J.-Q. Gao, F. Li, S.-H. Ri, W.-Q. Liang, Triblock copolymer Pluronic®F127 sustains insulin release and reduces initial burst of microspheres—in vitro and in vivo study, Colloid Poly. Sci., 285 (2006) 233-238.

[11] F. Lagarce, N. Faisant, J.-C. Desfontis, L. Marescaux, F. Gautier, J. Richard, P. Menei, J.-P. Benoit, Baclofen-loaded microspheres in gel suspensions for intrathecal drug delivery: In vitro and in vivo evaluation, Eur. J. Pharm. Biopharm., 61 (2005) 171-180.

[12] A.-C. Albertsson, J. Carlfors, C. Sturesson, Preparation and characterisation of poly(adipic anhydride) microspheres for ocular drug delivery, J. Appl. Poly. Sci., 62 (1996) 695-705.

[13] M. Patel, S.K. Jain, A.K. Yadav, D. Gogna, G.P. Agrawal, Preparation and Characterization of Oxybenzone-Loaded Gelatin Microspheres for Enhancement of Sunscreening Efficacy, Drug Delivery, 13 (2006) 323 - 330.

[14] M.J. Song, D.S. Lee, J.H. Ahn, D.J. Kim, S.C. Kim, Dielectric behavior during sol-gel transition of PEO-PPO-PEO triblock copolymer aqueous solution, Polymer Bulletin, 43 (2000) 497-504.

[15] G. Wanka, H. Hoffmann, W. Ulbricht, Phase Diagrams and Aggregation Behavior of Poly(oxyethylene)-Poly(oxypropylene)-Poly(oxyethylene) Triblock Copolymers in Aqueous Solutions, Macromolecules, 27 (1994) 4145-4159.

[16] G. Dumortier, J. Grossiord, F. Agnely, J. Chaumeil, A Review of Poloxamer 407 Pharmaceutical and Pharmacological Characteristics, Pharm. Res., 23 (2006) 2709-2728.

[17] Y. Liu, W.-L. Lu, J.-C. Wang, X. Zhang, H. Zhang, X.-Q. Wang, T.-Y. Zhou, Q. Zhang, Controlled delivery of recombinant hirudin based on thermo-sensitive Pluronic® F127 hydrogel for subcutaneous administration: In vitro and in vivo characterization, J. Controlled Release, 117 (2007) 387-395.

[18] M. Morishita, J.M. Barichello, K. Takayama, Y. Chiba, S. Tokiwa, T. Nagai, Pluronic® F-127 gels incorporating highly purified unsaturated fatty acids for buccal delivery of insulin, International Journal of Pharmaceutics, 212 (2001) 289-293.

[19] E.A. Pec, Z.G. Wout, T.P. Johnston, Biological activity of urease formulated in poloxamer 407 after intraperitoneal injection in the rat, Journal of Pharmaceutical Sciences, 81 (1992) 626-630.

[20] T.P. Johnston, M.A. Punjabi, C.J. Froelich, Sustained Delivery of Interleukin-2 from a Poloxamer 407 Gel Matrix Following Intraperitoneal Injection in Mice, Pharmaceutical Research, 9 (1992) 425-434.

[21] M.D. Dibiase, C.T. Rhodes, Formulation and Evaluation of Epidermal Growth Factor in Pluronic F-127 Gel, Drug Development and Industrial Pharmacy, 22 (1996) 823-831.

[22] J.H. Jeon, D.A. Puleo, Alternating release of different bioactive molecules from a complexation polymer system, Biomaterials, 29 (2008) 3591-3598.

[23] J.J. Yoon, H.J. Chung, T.G. Park, Photo-crosslinkable and biodegradable Pluronic/heparin hydrogels for local and sustained delivery of angiogenic growth factor, Journal of Biomedical Materials Research Part A, 83A (2007) 597-605.

[24] A.J. Kuijpers, G.H.M. Engbers, P.B. van Wachem, J. Krijgsveld, S.A.J. Zaat, J. Dankert, J. Feijen, Controlled delivery of antibacterial proteins from biodegradable matrices, J. Controlled Release, 53 (1998) 235-247.

[25] M.S. Bhattacharyya, P. Hiwale, M. Piras, L. Medda, D. Steri, M. Piludu, A. Salis, M. Monduzzi, Lysozyme Adsorption and Release from Ordered Mesoporous Materials, J. Phys. Chem. C, 114 (2010) 19928-19934.

[26] Y. Lin, J. Sun, G. Jiang, J. Zan, F. Ding, In vitro Evaluation of Lysozyme-loaded Microspheres in Thermosensitive Methylcellulose-based Hydrogel, Chin. J. Chem. Eng., 15 (2007) 566-572.

[27] R. Cortesi, C. Nastruzzi, S.S. Davis, Sugar cross-linked gelatin for controlled release: microspheres and disks, Biomaterials, 19 (1998) 1641-1649.

[28] Y. Tabata, Y. Ikada, Synthesis of Gelatin Microspheres Containing Interferon, Pharm. Res., 6 (1989) 422-427.

[29] I.R. Schmolka, Artificial skin I. Preparation and properties of pluronic F-127 gels for treatment of burns, J. Biomed. Mater. Res., 6 (1972) 571-582.

[30] Y. Yang, J. Wang, X. Zhang, W. Lu, Q. Zhang, A novel mixed micelle gel with thermo-sensitive property for the local delivery of docetaxel, J. Controlled Release, 135 (2009) 175-182.

[31] R. Sun, J. Shi, Y. Guo, L. Chen, Studies on the particle size control of gelatin microspheres, Front. Chem. Chin., 4 (2009) 222-228.

[32] J. Yun Chang, Y.-K. Oh, H. Soo Kong, E. Jung Kim, D. Deuk Jang, K. Taek Nam, C.-K. Kim, Prolonged antifungal effects of clotrimazole-containing mucoadhesive thermosensitive gels on vaginitis, J. Controlled Release, 82 (2002) 39-50.

[33] J.Y. Chang, Y.-K. Oh, H.-g. Choi, Y.B. Kim, C.-K. Kim, Rheological evaluation of thermosensitive and mucoadhesive vaginal gels in physiological conditions, Int. J. Pharm., 241 (2002) 155-163.

[34] G. Grassi, A. Crevatin, R. Farra, G. Guarnieri, A. Pascotto, B. Rehimers, R. Lapasin, M. Grassi, Rheological properties of aqueous Pluronic-alginate systems containing liposomes, J. Colloid Interface Sci, 301 (2006) 282-290.

[35] Y. Liu, Y.-y. Zhu, G. Wei, W.-y. Lu, Effect of carrageenan on poloxamer-based in situ gel for vaginal use: Improved in vitro and in vivo sustained-release properties, Eur. J. Pharm. Biopharm., 37 (2009) 306-312.

[36] R. Ivanova, B. Lindman, P. Alexandridis, Evolution in Structural Polymorphism of Pluronic F127 Poly(ethylene oxide)−Poly(propylene oxide) Block Copolymer in Ternary Systems with Water and Pharmaceutically Acceptable Organic Solvents: From “Glycols” to “Oils”†, Langmuir, 16 (2000) 9058-9069.

[37] K. Mortensen, W. Batsberg, S. Hvidt, Effects of PEO−PPO Diblock Impurities on the Cubic Structure of Aqueous PEO−PPO−PEO Pluronics Micelles: fcc and bcc Ordered Structures in F127, Macromolecules, 41 (2008) 1720-1727.

[38] C. Chaibundit, N.M.P.S. Ricardo, N.M.P.S. Ricardo, C.A. Muryn, M.-B. Madec, S.G. Yeates, C. Booth, Effect of ethanol on the gelation of aqueous solutions of Pluronic F127, Journal of Colloid and Interface Science, 351 (2010) 190-196.

4. ORDERED MESOPOROUS MATERIALS

4.1. Introduction

Ordered mesoporous materials (OMMs) have outstanding textural and structural features [1] that make them suitable hosts for bioactive molecules [2]. They have high surface area (about 1000 m^2/g) a highly ordered, and hence a highly reproducible structure, with uniform pore size (2 – 50 nm) which is comparable with the diameter of many bio-macromolecules. Most of previous works concerning the use of OMMs as sorbents for bio-macromolecules were aimed to stably immobilize an enzyme into the pores to obtain a stable and active biocatalyst [3-4] for potential industrial,[5-6] environmental,[7] or biosensing applications [8].

Innovative emerging applications are the use of OMMs in different nanomedicine topics, namely, carriers for the release of drugs and bioactive agents [9] and tissue engineering [10]. A drug delivery system is capable of releasing a carried bioactive agent in a specific location at a specific rate.

The use of OMMs for biocatalysis or controlled release depends on the fact that the interaction between the macromolecule and the sorbent surface is strong or weak, respectively. Consequently, given a bioactive agent, the chemical surface of the sorbent material has an important effect on the strength of the interaction, and hence on the possible application [5]. In addition, it is relevant that OMMs surface can be easily modified by a wide number of suitable functionalizing agents[11-12] that allow for tailoring the sorbent surface to get the desired, weak or strong, interaction with the adsorbing molecule [13]. Moreover, the surface interaction can be modulated by the suitable choice of the pH,[3, 14] the ionic strength [14] and also the type of salt [15-16] of the adsorbing solution.

SBA-15 and similar materials have been studied as delivery systems for different locations. Most researchers focused the attention in the oral

therapy, studying the controlled release of ibuprofen,[17] nimodipine,[18] itraconazole,[19] and many poorly soluble drugs [20]. Vallet-Regì and coworkers - taking advantage of the bioactive behavior of mesoporous silica, that can be covered by a layer of hydroxyapatyte[21-22] and thus used as bioceramics for bone tissue regeneration - deeply studied the local release of drugs for bones disease [12, 23-26]. Lopez et al. used ordered mesoporous silica for the storage and release of valproic acid and sodic phenytoin in the brain of rats [27].

An important issue for the use of OMMs as drug delivery systems concerns their toxicity and biocompatibility. Hudson et al. found that subcutaneous injection of some OMMs in rats resulted in a general good biocompatibility as determined through histological investigations. In contrast, intra-peritoneal and intra-venous injections in mice caused death [28].

Another key point for the application of OMMs in drug delivery systems is the stability of the matrix in the releasing medium. Very recently Izquierdo-Barba et al. investigated the stability of SBA-15 like materials in selected aqueous media mimicking body fluids. They found that, although the mesoporous structure of SBA-15 was partially lost after 60 days in all tested media, organically modified SBA-15 samples exhibited a higher resistance to lixiviation [29].

Here we report the characterization through TEM, SAXS, N_2-adsorption/desorption isotherms, ATR-FTIR, and potentiometric titrations of two different OMMs, namely: SBA-15 and MSE, and their use for the adsorption and the *in vitro* controlled release of a model protein - hen egg white lysozyme (Lyz) - in physiological conditions (pH = 7.4, t = 37°C). The effect of the different chemical surface and the adsorbing pH is investigated. Besides the structural features, it will be shown that the different material surface can affect both the loading amount and the

kinetics of the release. Finally, a comparison of the stability of the two matrices towards the lixiviation effect of the release medium is presented.

4.2. Materials and methods

4.2.1. Materials

Chemicals for the synthesis and modification of OMMs, tetraethylorthosilicate (TEOS, 98%), pluronic copolymer 123 (EO20PO70EO20), 1,2-bis(trimethoxysilyl)ethane (BTMSE) (96%) and buffer components, sodium hydrogencarbonate (99%), Na_2HPO4 (99%), and NaH_2PO4 (99%), were purchased from Sigma-Aldrich. Lysozyme from hen egg white (92717 U/mg) was purchased from Fluka.

4.2.2. Characterization of OMMs and lysozyme

SBA-15 mesoporous silica and MSE mesoporous organosilica were synthesized according to the methods reported in refs [30] and [31], respectively. SBA-15 and MSE were characterized with the following techniques. SAXS patterns were recorded (1200 s) with a S3-MICRO SWAXS camera system (HECUS X-ray Systems, Graz, Austria). Cu Kα radiation of wavelength 1.542 Å was provided by a GeniX X-ray generator, operating at 50 kV and 1 mA. A 1D-PSD-50 M system (HECUS X-ray Systems, Graz, Austria) containing 1024 channels of width 54.0 µm was used for detection of scattered X-rays in the small-angle region. Transmission electron microscopy (TEM) images were obtained on a JEOL 100S microscope. Finely ground samples were placed directly onto formvar-coated electron microscopy nichel grids. Textural analysis was carried out on a Thermoquest-Sorptomatic 1990, by determining the N_2 adsorption/desorption isotherms at 77 K. Before analysis the sample was out-gassed overnight at 40 °C. The specific surface area, the total pore volume and the pore size distribution were assessed by the BET [32] and

BJH [33] methods respectively. ATR-FTIR studies were conducted with a Bruker Tensor 27 spectrophotometer equipped diamond-ATR accessory and DTGS (deuteriotriglycine sulphate) detector. A number of 128 scans at resolution of 4 cm^{-1} were averaged from wavenumber 4000 to 400 cm^{-1}. The Opus spectroscopic software was used for data handling. Surface charge densities of SBA-15 and MSE were determined through potentiometric titrations according to the procedure reported in ref [15]. The theoretical titration curve of lysozyme and the corresponding theoretical p*I* were obtained through PROPKA 2.0 software [34-35]. Lysozyme images in Fig.4.5.a-d were made with VMD software support. VMD is developed with NIH support by the Theoretical and Computational Biophysics group at the Beckman Institute, University of Illinois at Urbana-Champaign.

4.2.3. Loading of lysozyme.

To load lysozyme on SBA-15 and MSE, 0.2 g of the mesoporous sample were suspended in 10 mL of aqueous solution of lysozyme (10 mg/mL) prepared in 10 mM phosphate buffer pH 7.0 or 10 mM sodium hydrogen carbonate buffer at pH 9.6, and soaked for 96 hours with shaking at 100 rpm and 37°C. The concentration of lysozyme was measured by UV spectrophotometer at a wavelength of 280 nm. The amount of lysozyme loaded onto the samples was determined according to the change of concentration before and after soaking. After loading, the powders were quickly and thoroughly washed with water and dried under vacuum. The loading of lysozyme - *LLyz* (mg/g) – on mesoporous material was calculated according the following formula:

$$loading = \frac{[Lysoz_i]V - [Lysoz_r]V - [Lysoz_w]V_w}{m_s} \quad (1)$$

where, [Lysoz$_i$] is the protein concentration in the initial solution ($mg_{lysozyme}/mL_{solution}$) method; [Lysoz$_r$] is the residual concentration of protein in solution ($mg_{lysozyme}/mL_{solution}$); [Lysoz$_w$] is the protein concentration of remained in the washing solution ($mg_{lysozyme}/mL_{solution}$); V is the volume of the lysozyme solution (mL), V_w is the washings volume (mL), and m_s is the mass of support (g).

4.2.4. *In vitro* lysozyme release studies

The *in vitro* lysozyme release from the loaded materials was studied in phosphate buffer solution (PBS) (pH 7.4 , 50 mM), by suspending 50 mg of lysozyme loaded SBA-15 (or MSE) in 100 mL of PBS and maintained at 37°C in an orbital shaker (100 rpm). These experimental conditions were chosen according to what previously reported [36]. At fixed time intervals, 5 mL of the releasing solution was withdrawn, and an identical volume of a fresh PBS solution was added to maintain sink conditions. Lysozyme concentration in each of the collected samples was measured at 280 nm using a Cary UV-Vis spectrophotometer. The amount of lysozyme released at time *t,* M_t, was determined from the appropriate calibration line (with an absorption coefficient ε_{280} = 2.803 ml mg^{-1} cm^{-1}). The total amount of lysozyme incorporated in the material was taken as M_0, thus, the percentage of the lysozyme released was expressed as M_t/M_0(%). An exponential decay model was used for the fitting of the experimental data according to ref. [37].

$$\frac{M_t}{M_0} = A(1 - e^{-k_1 t}) \tag{2}$$

where, A is the maximal mass percentage released and k1 is the release rate constant. The correlation coefficient (r) was calculated to evaluate the accuracy of the fitting procedure.

4.3. Results and discussion

4.3.1. OMMs and protein characterization

4.3.1.1. OMMs characterization

The two investigated OMMs present a different surface from the chemical point of view. SBA-15 is a silica-based mesoporous structure, hence its surface is constituted by silanols. MSE is a periodic mesoporous organosilica in whose synthesis silicon atoms are alternatively connected by means of -Si-O-Si- and -Si-CH_2-CH_2-Si- groups. The presence of the methylene groups confers a higher hydrophobic character to the material compared to SBA-15. The different chemical composition of OMMs was qualitatively confirmed by ATR-FTIR spectroscopy (Fig.4.1).

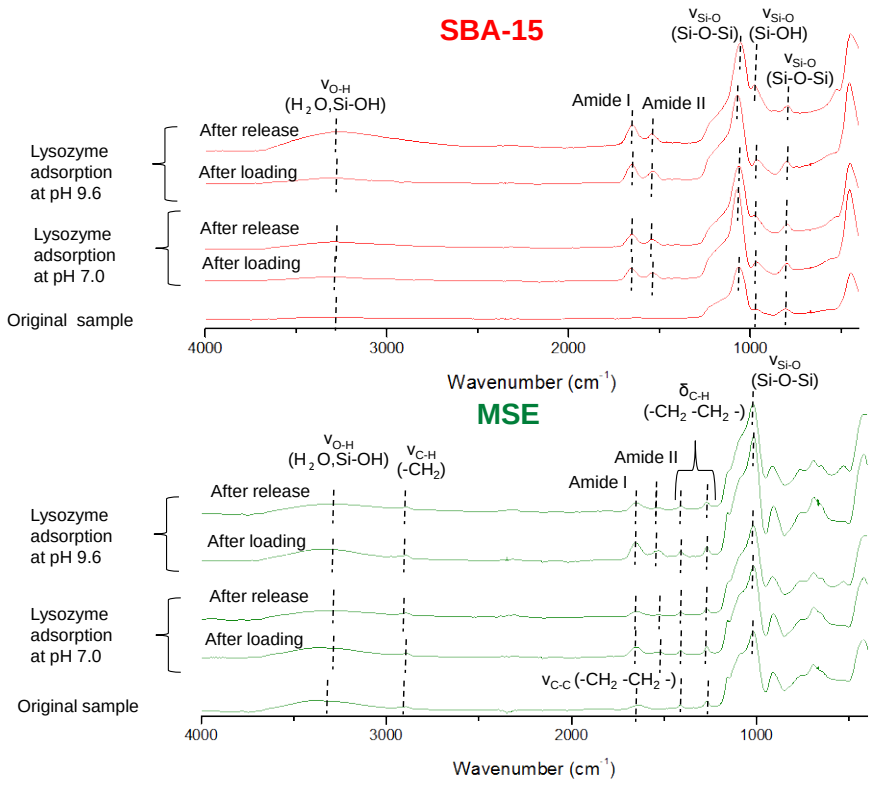

Fig.4.1. ATR-FTIR spectra of original OMMs after lysozyme loading (pH 7 and 9.6) and release (*T* = 37 °C and pH 7.4).

Both materials present an intense band at 1070 cm^{-1} due to Si-O stretching, one less intense at 450 cm^{-1} due to Si-O-Si bending, and also a band at 950 cm^{-1} due to silanols. In addition, MSE shows bands due stretching vibrations at 2916 cm^{-1} (ν_{C-H}) and 1645 cm^{-1} (ν_{C-C}), and to bending vibrations (δ_{C-H}) at 1412 and 1271 cm^{-1}, respectively.

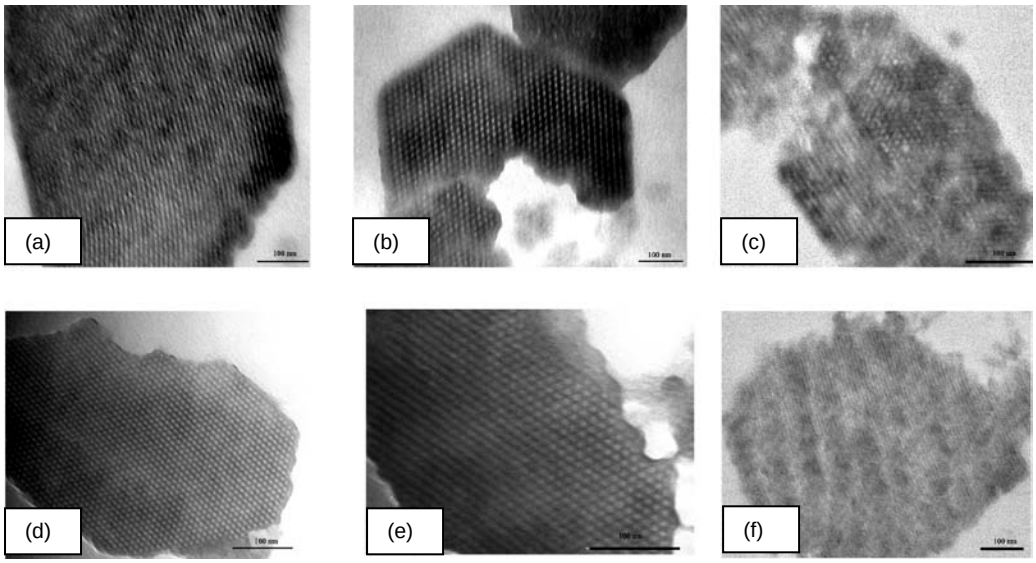

Fig.4.2. TEM images of OMMs. (a,b) original SBA-15; (c) SBA-15 sample after Lyz release; (d,e) orginal MSE; (f) MSE sample after Lyz release.

Fig.4.2 shows the TEM micrographs of the two materials. For SBA-15 the side view (Fig.4.2.a) shows that the material is constituted by cylindrical channels, and the top view (Fig.4.2.b) shows the ordered hexagonal array of the pores. MSE particles (Fig.4.2d and 4.2.e) were less regular than those of SBA-15 but the ordered hexagonal structure can clearly be seen also in this case. SAXS analysis carried out on OMMs shows the typical pattern of a hexagonal phase where an intense peak due to (1 0 0) plane and other two less intense peaks due to (1 1 0) and (2 0 0) planes occur (Fig.4.3). From SAXS measurements the lattice spacing *(a*) of

the two structures was determined, this was 112 Å for SBA-15 and 119 Å for MSE (Table 1).

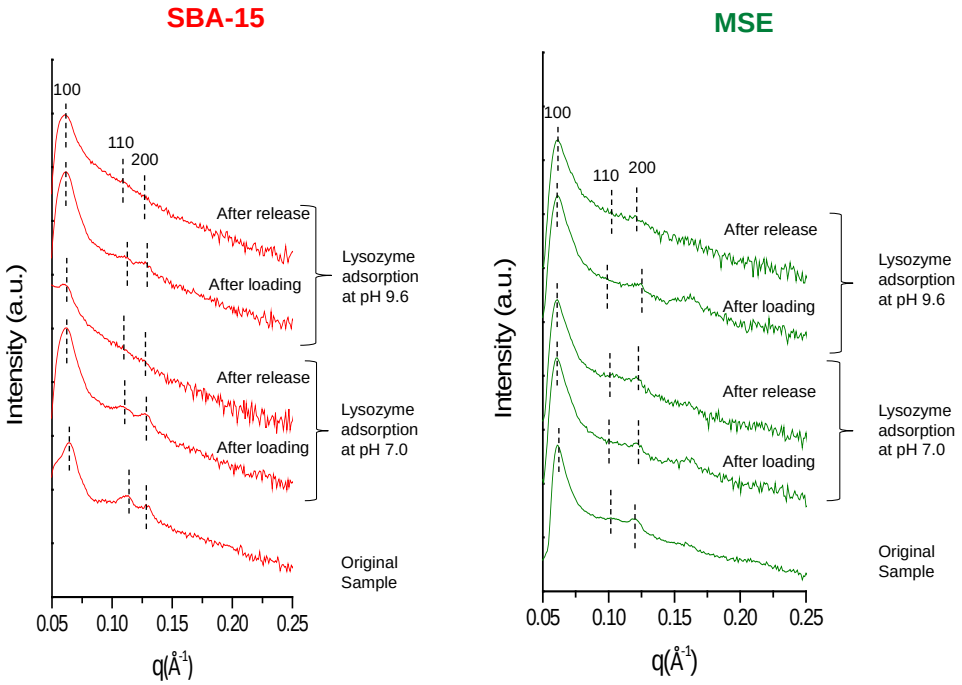

Fig.4.3. SAXS Pattern of OMMs after lysozyme loading (at pH 7.0 and 9.6) and after in vitro release (pH 7.4, *T* = 37 °C)

Table 1 Characterization of OMMs Obtained Through N_2-Adsorption/Desorption Isotherms and SAXS.

	S_{BET} [a] (m^2/g)	V_p [b] (cm^3/g)	d_{BJH} [c] (Å)	d_{BJH} [d] (Å)	a [e] (Å)
SBA-15	718	1.2	86	65	112
MSE	1752	2.2	76	58	119

[a] Specific surface area calculated by the BET method; [b] cumulative pore volume; [c] pore diameter calculated by applying BJH method to the data of the adsorption branch; [c] pore diameter calculated by applying BJH method to the data of the desorption branch; [d] lattice parameter calculated by the equation $a=2d_{100}/\sqrt{3}$, where d_{100} is the spacing of the (1 0 0) plane of hexagonal (*p6mm*) array of pores.

The OMMs were then characterized through N_2 adsorption/desorption isotherms. Both samples show a type IV isotherm, with a steep increase typical of mesoporous solids at a relative pressure around 0.70-0.75 (Fig.4.4.a). The presence of a hysteresis cycle, defined by IUPAC as H1, is closely associated with channel-like mesopores [38]. Table 1 reports the specific surface area (S_{BET}), the total pore volume (V_p), calculated by BET method [32]. SBA-15 had a S_{BET} = 718m2/g, a Vp= 2.1 cm^3/g; a very high value of surface area, S_{BET} = 1752 m2/g and V_p= 2.2 cm^3/g was obtained for MSE. The pore size distribution (d_{BJH}) of the materials was calculated from both adsorption and desorption branches of the isotherms through the BJH model. A d_{BJH} = 86 Å (adsorption branch) and d_{BJH} = 65 Å were obtained for SBA-15, whereas a d_{BJH} = 76 Å and d_{BJH} = 58 Å were obtained for MSE. Although the BJH model is known to underestimate the diameter of the mesopores, it is still the most used calculation method because software using more accurate models (i.e., NLDFT) [39] is not easily available.

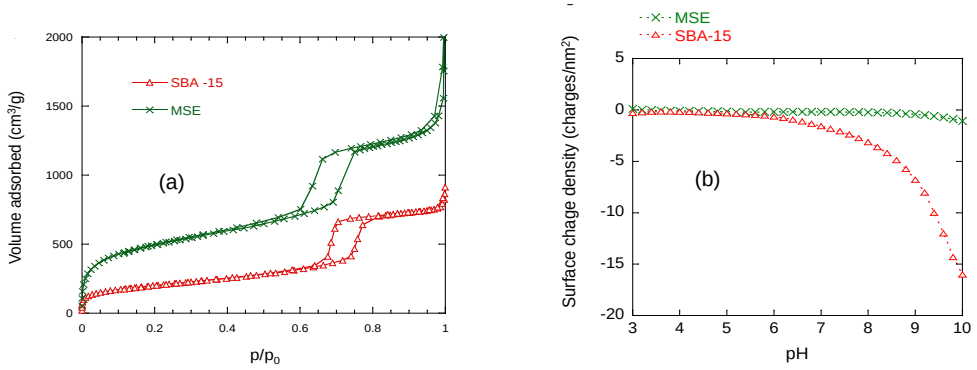

Fig.4.4. Characterization of SBA-15 and MSE. (a) N_2-adsorption/desorption isotherms; (b) Surface charge density versus pH.

The last characterization of the ordered mesoporous materials was the determination of surface charge density as a function of pH that was carried out through potentiometric titration; results are displayed in

Fig.4.4.b. SBA-15 surface was practically neutral from pH 3 to pH 5-6, whereas at higher pH it became negatively charged due to the acidic behavior of surface silanols. According to its hydrophobic nature, the surface charge density of MSE was practically zero up to pH 9, and then becoming only slightly negative charged at basic pH (> 8) values.

4.3.1.2. Protein characterization

The model protein used for this work was hen egg white lysozyme (E.C.3.1.1.17). Lysozyme belongs to the family of hydrolases and its biological function is the hydrolysis of polysaccharides constituting bacterial cell wall. It is a globular protein consisting of 129 residues (MW=14.3 kDa) in the form of five α-helices, three antiparallel β-sheets and a large number of random coils and β-turns. Four disulfide bridges are responsible for the stabilization of the structure of the protein that displays an ellipsoidal shape with a large cleft acting as active site. Its dimensions (19×25×43 Å) allows for the adsorption into the pores of both investigated materials.

As shown below, the adsorption and the release processes of Lyz are strongly dependent on the intermolecular interactions between the protein and OMMs surfaces. Hence, the amino acid composition of Lyz, shown in Fig.4.5, plays a fundamental role. Charged amino acids are mainly located on the protein surface, the basic amino acids being more abundant (Fig.4.5.a) than the acidics (Fig.4.5.b). Uncharged amino acids are more abundant than those charged: non polar residues are less exposed at the hydrophilic external surface with respect to polar amino acids as illustrated in Fig.4.5.c, and 4.5.d. Fig.4.5.e reports the number of different types of amino acids (basic, acidic, polar, and non polar). The presence of a higher number of basic residues with respect to acidic residues is reflected by the high isoelectric point of the protein (pI ~ 11),

and by the theoretical protein charge as a function of pH reported in Fig.4.5.f.

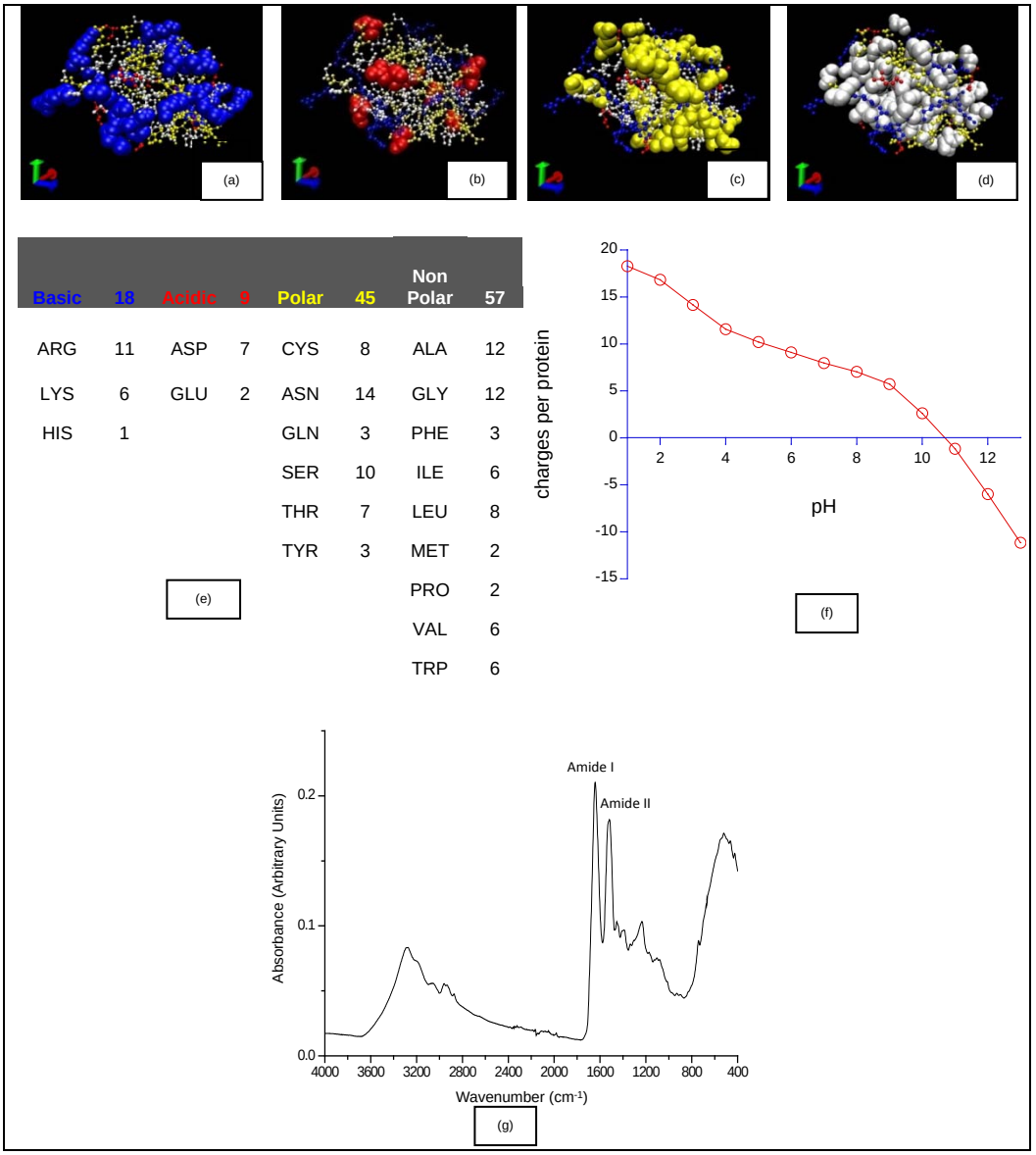

Fig.4.5. Hen Egg Whyte Lysozyme characterization by taking the amino acid composition available at protein data bank (1LYZ.pdb). Structural representation of the amino acid residues by using VMD (video molecular dynamics) of (a) basic amino acids; (b) acidic amino acids; (c) polar (uncharged) amino acids; (d) non polar amino acids. (e) Number of amino acid of different classes ; (f) theoretical titration curve of lysozyme obtained through PROPKA 2.0 software; (g) ATR-FTIR spectrum.

4.3.2. Adsorption of lysozyme on OMMs

The adsorption of Lyz on the two OMMs matrices was carried out by suspending a weighed amount of them in a Lyz solution at 37°C. The effect of pH was also investigated by dissolving lysozyme powder in two different buffer solutions at pH 7.0 and 9.6. The higher pH was chosen because the maximal loading is usually obtained in proximity of the protein isoelectric point [3, 40]. Unfortunately we could not use pH 11 since, at a so high pH, silica becomes soluble in the solution. Hence, pH 9.6 was chosen as the best compromise between these two exigencies. Lyz adsorption was determined through UV spectroscopy ($\lambda_{max=}$ 280 nm), and loading was calculated, according to eq. (1), as the difference between protein concentration in the buffer solution at the beginning and at the end of the adsorption process.

The adsorption of lysozyme on the OMMs was also qualitatively demonstrated by means of ATR-FTIR spectroscopy. FTIR spectrum of free lysozyme shows the two typical bands of proteins namely, amide I at 1643 cm^{-1}, and amide II at 1522 cm^{-1} (Fig.4.5.g). The same bands, although a bit shifted in frequency (amide I: 1653 cm^{-1}; amide II: 1537 cm^{-1}), occur in the spectra of the Lyz-loaded OMMs as shown in Fig.4.1.

The experimental results for Lyz loading on the OMMs at pH 7 and 9.6 are reported in Table 2. Lyz loading at pH 7.0 was 587 mg/g for SBA-15 and 450 mg/g for MSE, whereas at pH 9.6 it was 646 mg/g for SBA-15 and 500 mg/g for MSE. These results deserve some comments. Let us take into account the experimental surface charge densities of OMMs at pH 7.0 and 9.6 (Table 2) and lysozyme theoretical charge (+8.0 at pH 7.0, and +3.7 at pH 9.6) taken by the graph shown in Fig.4.4.b.

Table 2 Lysozyme Loading and Release parameters on OMMs and their surface charge densities (σ) at the adsorption pH.

OMM	Adsorption pH	σ (charges/nm^2)	L_{Lyz}[a] (mg/g)	A[b] (%)	k_1[c] (X 10^{-6} s^{-1})	R[d]	a_{ads}[e] (Å)	a_{rel}[f] (Å)
SBA-15	7	-1.6	587±63	43±2	5±0.8	0.986	116	121
SBA-15	9.6	-12.0	646±34	46±2	14±3	0.958	117	119
MSE	7	-0.2	450±48	17.2±0.3	139±28	0.990	119	119
MSE	9.6	-0.7	500±50	28.6±0.5	81±8	0.989	119	119

[a] Loading of adsorbed lysozyme [b] Maximal amount of released lysozyme; [c] release rate constant (n=2, data is represented as avg±SD) t; [d] correlation coefficient; [e] lattice parameter after lysozyme adsorption; [f] Lattice parameter after lysozyme release.

Electrostatic forces seem to be the leading interactions in the adsorption of positively charged Lyz on negatively charged SBA-15. At pH 9.6 a higher loading is obtained due to the lower electrostatic repulsion among lysozyme molecules [3]. If electrostatics was the only type of intermolecular interaction involved the low charge carried by MSE at both pH values, due to its hydrophobic character, would lead to a very low loading of lysozyme. Nevertheless, although lower than that of SBA-15, MSE reached a quite high loading likely due to the establishment and the action of non electrostatic forces (i.e. van der Waals, London) between hydrophobic groups at MSE and lysozyme surfaces.

Besides, the ionic strength of the adsorbing solution and of the release medium can have important effects. Hudson et al. showed that increasing the ionic strength disfavored the adsorption of cytochrome c and xylanase on SBA-15, whereas an initial decrease followed by an increase was observed for the same enzyme on MSE [14]. Essa et al. showed that the effect of ionic strength is not univocal for a protein/adsorbent pair (i.e., myoglobin/SBA-15), but different results are obtained at different adsorbing pHs.39 Very recently, we found that lysozyme adsorption on functionalized

SBA-15 depends not only on the ionic strength of the solution but also on the type of salt. We could order the effectiveness of anions and cations on promoting protein adsorption according to the Hofmeister series [41]. The involved phenomena are complicated but can be easily explained invoking Collins' empirical law of matching water affinities [42]. Briefly, ionic strength can either promote or disfavor adsorption, depending on the nature (dispersion and/or electrostatic) of protein-adsorbent interactions. Concerning the textural properties, pore size is an important parameter that can affect protein adsorption. Serra et al. investigated the immobilization of *Candida antarctica* lipase B on OMMs having different pore sizes [38]. They found that, during the adsorption process, diffusion limitations occurred when the pore size was similar to the enzyme size, but these disappeared when the pore diameter was around twice the largest enzyme dimension. On the basis of these findings and OMM's pore size (Table 1), we would expect an easier adsorption due to faster mass diffusion of lysozyme (dimensions: 19 × 25 × 43 Å) in SBA-15 compared to that in MSE. In any case, because we carried out the adsorption process for a long time (96 h), even a very slow diffusion should take place. Concerning the other textural properties, the surface area and the pore volume are higher for MSE than that for SBA-15 and should lead to a higher loading for the former compared to the latter. Exactly the opposite occurs (Table 2), likely because enzyme molecules occupy a small fraction of the total volume and surface [38]. It can be substantially concluded that the obtained loadings are mainly due to surface properties (charges and hydrophobic/ hydrophilic character) rather than to textural properties.

4.3.3. Release of lysozyme

In vitro release of Lyz from OMMs was carried out, for about 30 days, in a phosphate buffer solution at pH 7.4 and 37°C to mimick

physiological conditions. Samples were withdrawn at fixed times and analyzed by UV spectroscopy. Experimental results of release, shown in Fig.4.6, were fitted by means of eq. (2) that allowed determining the maximal mass percentage released *A*, and the release rate constant k_1. These data are listed in Table 2. A very different behavior between MSE and SBA-15, also modulated by the adsorption pH, was observed. SBA-15 is the material that releases the highest percentage of Lyz ($A_{pH\ 9.6}$ = 46%; $A_{pH\ 7.0}$ = 43%) followed by MSE ($A_{pH\ 9.6}$ = 28.6%; $A_{pH\ 7.0}$ = 17.2%). The maximal amount of release was higher for samples where Lyz was adsorbed at pH 9.6 both for SBA-15 and MSE.

Table 2 reports also the kinetic release constants k_1 as determined by the fitting procedure of experimental data. Lyz molecules adsorbed on MSE were released faster (k_1 = 139 μs^{-1} at pH 7.0; k_1 = 81 μs^{-1} at pH 9.6) than those adsorbed on SBA-15 (k_1 = 5 μs^{-1} at pH 7.0; k_1 = 14 μs^{-1} at pH 9.6).

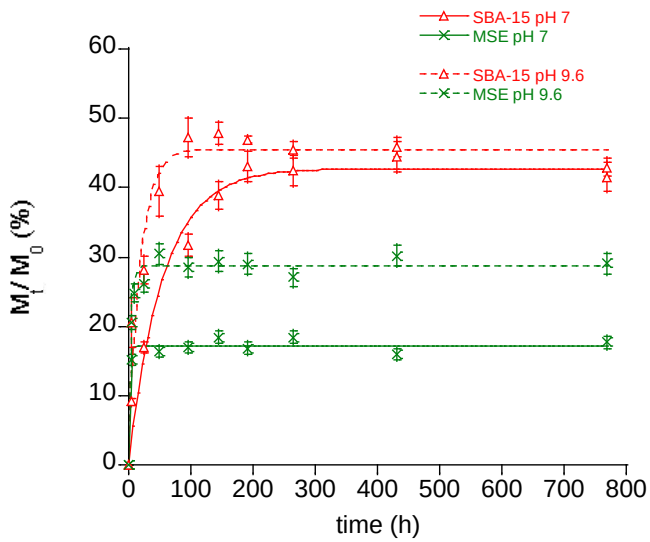

Fig.4.6. Release of lysozyme from OMMs. (pH 7.4, t=37°C)

The fact that more than 50% of adsorbed lysozyme was not released is not surprising. The reason is evidently due to the strength of the

interactions between the surfaces of the protein and the hosting material. Indeed, there are several works in which enzymes are immobilized by physical adsorption for biocatalytic purposes [4, 8, 14, 43-44]. In those works, desorption is an unwanted effect that is different than what is needed for release studies. The amount of lysozyme released depends on the choice of the protein-adsorbent pair. Very recently, Nieto et al. found that the amount of released BSA was strongly dependent on the chemical groups present on the SBA-15 surface [13]. Here, although electrostatic interactions lead to a higher Lyz loading with SBA-15, this kind of interaction is not able to retain the protein when in contact with the releasing medium. A rather burst release occurs. On the other hand, nonelectrostatic forces, responsible for lysozyme adsorption on the more hydrophobic MSE, are likely to adsorb more strongly than protein molecules that, hence, are less available for release. There is also a modulation effect due to the adsorption pH that increases both the loading and release as it approaches the isoelectric point of the protein. The higher release rates observed for MSE matrixes at both pHs, compared to SBA-15, are likely to be due to the high burst release of Lyz adsorbed on the outer surface of the MSE particles. Nevertheless, it can be remarked that burst release from MSE occurs at a much lower extent (and for a much shorter time) than that from SBA-15. Another effect, not investigated here, might be obtained with other release medium. In the literature, different media having the same pH but higher ionic strength (i.e., 0.9% NaCl)13 or SBF (simulated body fluid) have been used.44 We may expect that a change in the ionic strength, and also the ionic composition, of the release medium would strongly affect both the release trends and the material stability [29]. For example, if the lysozyme-SBA-15 interaction is mainly based on electrostatics, we might expect an increased release at higher ionic strength due to salt adsorption at the protein and adsorbent charged groups. The opposite effect would be

expected for MSE due to the hydrophobic interaction with lysozyme. In any case, the effects observed here, due to different chemical composition of the adsorbent and a different pH of adsorption, are quite remarkable since they affect the amount and the rate of lysozyme release.

4.3.4. OMMs stability in the release medium

The stability of OMM samples after 32 days of in vitro release in the release medium (pH 7.4 and 37 °C) was studied through FTIR, SAXS, and TEM. FTIR analysis (Fig.4.1) shows that there is no appreciable change in the OMM spectra after release with respect to those after lysozyme loading at the two pH values (7.0 and 9.6). The amide I and amide II bands are still present according to the fact that a substantial amount of lysozyme molecules is still adsorbed in the matrixes. In fact, looking at TEM micrographs (Fig.4.2c and f), it appears that the ordered structure of SBA-15 is partially destroyed due to the lixiviation action of the physiological medium. Effects at much lower extent are observed for MSE, which seems to be more resistant toward lixiviation. A similar result was found by Izquierdo-Barba et al., who focused on the in vitro stability of SBA-15 in different physiological media [29]. Matrix lixiviation observed by TEM was furthermore confirmed by SAXS measurements. Fig.4.3 shows that a significant decrease of the intensity of the second- and third-order diffraction peaks occurs after Lyz release experiments. This could be due to the partial loss of the ordered hexagonal structure. This intensity loss was less important for MSE, in agreement with the lower degree of dissolution of the matrix observed in TEM pictures. Moreover, the comparison between the lattice parameters, obtained from SAXS analysis, reported in Tables 1 and 2, points out an interesting result; the original SBA-15 has a lattice parameter of 112 Å that increases to 116 Å after Lyz adsorption at pH 7 (117 Å at pH 9.6) and to 121 Å after Lyz release (119 Å at pH 9.6). On the

contrary, MSE retains a constant lattice parameter of 119 Å during all steps of the study, thus confirming its higher resistance to the lixiviating action of both the adsorption and the release media. From these results, besides the initial burst release due to Lyz adsorbed on the outer surface of both OMMs, a different mechanism of lysozyme release from the two matrixes can be suggested. Indeed, in the case of SBA-15, Lyz release is enhanced by the swelling of the channels due to the nucleophilic attack of water to siloxane groups, whereas for MSE, release is mainly due to the diffusion of Lyz molecules outside of the pores.

As a matter of fact, Izquierdo-Barba et al. found that the functionalization of the SBA-15 surface was a good procedure to enhance the structural stability [29]. Here, the use of a more hydrophobic structure, without the need of any post synthesis functionalization, allowed a similar result to be reached.

4.4. Conclusions

The present work focuses on two OMMs having similar structure and texture but different chemical composition and surface properties. These OMMs can be used for the adsorption and the release of lysozyme, a therapeutic protein. Among others, a peculiar advantage of these OMMs is the narrow range of pore sizes that constitutes the crucial size-selective parameter to address guest molecules adsorption. The use of BTMSE as the organosilica precursor produces the MSE OMM that shows a hexagonal matrix as well as SBA-15, but with a slightly smaller pore size and larger surface area. It should be remarked that the small reduction of the pore size does not prevent the adsorption of protein molecules whose maximal dimension is 43 Å. Indeed, this fact does not modify Lyz loading significantly, although the very different nature of the surface, in terms of surface charge, also implies different types of host-guest (surface-protein)

interactions. The van der Waals interactions, mainly involved in the adsorption/release process at the Lyz/MSE interface, seem to produce stronger protein binding than the electrostatic forces that dominate the Lyz/SBA-15 interface. As a matter of fact, this strong protein binding in the Lyz-loaded MSE matrix decreases both the time over which burst release occurs and the released amount of protein significantly. It is remarkable that a short burst release, in all cases, suggests that only a small amount of adsorbed protein is located on the outer surface of the OMM particle. Another very significant parameter that affects both adsorption and release is the pH of the adsorbing solution. This allows for a potential modulation of the global performance, in terms of the loaded amount of protein, and the rate of release. In other words, a personalized sustained release may be produced. Another important consideration concerns the longer shelf life in the physiological medium observed for MSE compared to that for SBA-15. Silica materials tend to dissolve in biological fluids, and this can develop toxicity when accumulation above certain concentrations occurs [28]. Hence, if a silica-based drug delivery system has to be projected in view of possible innovative applications (cf. protein drug delivery) and performances (cf. sustained release), it is relevant to introduce structural features that can prolong the shelf life and attenuate dangerous, though not fatal, side effects.

Finally, the last comment in favor of the MSE OMM being used as a sustained drug release carrier is given by the relatively easy and reproducible synthesis; this is a peculiar feature of all OMMs that does not involve any postsynthesis functionalization step.

4.5. References

[1] M.E. Davis, Ordered porous materials for emerging applications, Nature, 417 (2002) 813-821.

[2] S. Hudson, J. Cooney, E. Magner, Proteins in Mesoporous Silicates, Angew. Chem. Int. Ed., 47 (2008) 8582-8594.

[3] A. Salis, D. Meloni, S. Ligas, M.F. Casula, M. Monduzzi, V. Solinas, E. Dumitriu, Physical and chemical adsorption of Mucor javanicus lipase on SBA-15 mesoporous silica. Synthsis, structural characterization, and activity performance, Langmuir, 21 (2005) 5511-5516.

[4] M. Hartmann, D. Jung, Biocatalysis with enzymes immobilized on mesoporous hosts: the status quo and future trends, J Mater Chem, 20 (2010) 844-857.

[5] A. Salis, M.S. Bhattacharyya, M. Monduzzi, V. Solinas, Role of the support surface on the loading and the activity of Pseudomonas fluorescens lipase used for biodiesel synthesis, J. Mol. Catal. B: Enzym., 57 (2009) 262-269.

[6] A. Salis, M.F. Casula, M.S. Bhattacharyya, M. Pinna, V. Solinas, M. Monduzzi, Physical and Chemical Lipase Adsorption on SBA-15: Effect of Different Interactions on Enzyme Loading Catalytic Performance, ChemCatChem, 2 (2010) 322-329.

[7] A. Salis, M. Pisano, M. Monduzzi, V. Solinas, E. Sanjust, Laccase from Pleurotus sajor-caju on functionalised SBA-15 mesoporous silica: Immobilisation and use for the oxidation of phenolic compounds, J. Mol. Catal. B: Enzym., 58 (2009) 175-180.

[8] M. Hartmann, Ordered Mesoporous Materials for Bioadsorption and Biocatalysis, Chem Mater, 17 (2005) 4577-4593.

[9] S. Wang, Ordered mesoporous materials for drug delivery, Micropor. Mesopor. Mater., 117 (2009) 1-9.

[10] M. Vallet-Regí, Nanostructured mesoporous silica matrices in nanomedicine, Journal of Internal Medicine, 267 (2010) 22-43.

[11] J.M. Rosenholm, M. Lindén, Wet-Chemical Analysis of Surface Concentration of Accessible Groups on Different Amino-Functionalized Mesoporous SBA-15 Silicas, Chem. Mater., 19 (2007) 5023-5034.

[12] A. Nieto, F. Balas, M. Colilla, M. Manzano, M. Vallet-Regí, Functionalization degree of SBA-15 as key factor to modulate sodium alendronate dosage, Micropor. Mesopor. Mater., 116 (2008) 4-13.

[13] A. Nieto, M. Colilla, F. Balas, M.a. Vallet-Regí, Surface Electrochemistry of Mesoporous Silicas as a Key Factor in the Design of Tailored Delivery Devices, Langmuir, 26 (2010) 5038-5049.

[14] S. Hudson, E. Magner, J. Cooney, B.K. Hodnett, Methodology for the Immobilization of Enzymes onto Mesoporous Materials, J Phys Chem B, 109 (2005) 19496-19506.

[15] A. Salis, D.F. Parsons, M. Bostrom, L. Medda, B. Barse, B.W. Ninham, M. Monduzzi, Ion Specific Surface Charge Density of SBA-15 Mesoporous Silica, Langmuir, 26 (2010) 2484–2490.

[16] A. Salis, M.S. Bhattacharyya, M. Monduzzi, Specific Ion Effects on Adsorption of Lysozyme on Functionalized SBA-15 Mesoporous Silica, J. Phys. Chem. B, (2010).

[17] S.W. Song, K. Hidajat, S. Kawi, Functionalized SBA-15 Materials as Carriers for Controlled Drug Delivery:Influence of Surface Properties on Matrix Drug Interactions, Langmuir, 21 (2005) 9568-9575.

[18] H. Yu, Q.-Z. Zhai, Mesoporous SBA-15 molecular sieve as a carrier for controlled release of nimodipine, Micropor. Mesopor. Mater., 123 (2009) 298-305.

[19] R. Mellaerts, K. Houthoofd, K. Elen, H. Chen, M. Van Speybroeck, J. Van Humbeeck, P. Augustijns, J. Mullens, G. Van den Mooter, J.A. Martens, Aging behavior of pharmaceutical formulations of itraconazole on SBA-15 ordered mesoporous silica carrier material, Micropor. Mesopor. Mater., 130 (2010) 154-161.

[20] M. Van Speybroeck, V. Barillaro, T.D. Thi, R. Mellaerts, J. Martens, J. Van Humbeeck, J. Vermant, P. Annaert, G. Van den Mooter, P. Augustijns, Ordered mesoporous silica material SBA-15: A broad-spectrum formulation platform for poorly soluble drugs, J. Pharm. Sci., 98 (2009) 2648-2658.

[21] A. Díaz, T. López, J. Manjarrez, E. Basaldella, J.M. Martínez-Blanes, J.A. Odriozola, Growth of hydroxyapatite in a biocompatible mesoporous ordered silica, Acta Biomaterialia, 2 (2006) 173-179.

[22] J. Andersson, S. Areva, B. Spliethoff, M. Lindén, Sol-gel synthesis of a multifunctional, hierarchically porous silica/apatite composite, Biomaterials, 26 (2005) 6827-6835.

[23] M. Vallet-Regi, A. Ràmila, R.P. del Real, J. Pérez-Pariente, A New Property of MCM-41: Drug Delivery System, Chem. Mater., 13 (2001) 308-311.

[24] A.L. Doadrio, J.C. Doadrio, J.M. Sánchez-Montero, A.J. Salinas, M. Vallet-Regí, A rational explanation of the vancomycin release from SBA-15 and its derivative by molecular modelling, Micropor. Mesopor. Mater., 132 (2010) 559-566.

[25] A.L. Doadrio, E.M.B. Sousa, J.C. Doadrio, J. Pérez Pariente, I. Izquierdo-Barba, M. Vallet-RegI, Mesoporous SBA-15 HPLC evaluation for controlled gentamicin drug delivery, J. Contr. Rel., 97 (2004) 125-132.

[26] M. Colilla, M. Manzano, M. Vallet-Regí, Recent advances in ceramic implants as drug delivery systems for biomedical applications, Int. J Nanomed., 4 (2008) 403-414.

[27] T. López, E.I. Basaldella, M.L. Ojeda, J. Manjarrez, R. Alexander-Katz, Encapsulation of valproic acid and sodic phenytoin in ordered mesoporous SiO2 solids for the treatment of temporal lobe epilepsy, Opt. Mater., 29 (2006) 75-81.

[28] S.P. Hudson, R.F. Padera, R. Langer, D.S. Kohane, The biocompatibility of mesoporous silicates, Biomaterials, 29 (2008) 4045-4055.

[29] I. Izquierdo-Barba, M. Colilla, M. Manzano, M. Vallet-Regí, In vitro stability of SBA-15 under physiological conditions, Microporous Mesoporous Mater, 132 (2010) 442-452.

[30] D. Zhao, J. Feng, Q. Huo, N. Melosh, G.H. Fredrickson, B.F. Chmelka, G.D. Stucky, Triblock Copolymer Syntheses of Mesoporous Silica with Periodic 50 to 300 Angstrom Pores, Science, 279 (1998) 548-552.

[31] X.Y. Bao, X.S. Zhao, X. Li, P.A. Chia, J. Li, A Novel Route toward the Synthesis of High-Quality Large-Pore Periodic Mesoporous Organosilicas, The Journal of Physical Chemistry B, 108 (2004) 4684-4689.

[32] S. Brunauer, P.H. Emmett, E. Teller, Adsorption of Gases in Multimolecular Layers, J Am Chem Soc, 60 (1938) 309-319.

[33] E.P. Barrett, L.G. Joyner, P.P. Halenda, The Determination of Pore Volume and Area Distributions in Porous Substances. I. Computations from Nitrogen Isotherms, J Am Chem Soc, 73 (1951) 373-380.

[34] H. Li, A.D. Robertson, J.H. Jensen, Very fast empirical prediction and rationalization of protein pKa values, Proteins, 61 (2005) 704-721.

[35] D.C. Bas, D.M. Rogers, J.H. Jensen, Very fast prediction and rationalization of pKa values for protein–ligand complexes, Proteins, 73 (2008) 765-783.

[36] I. Izquierdo-Barba, M. Vallet-Regí, N. Kupferschmidt, O. Terasaki, A. Schmidtchen, M. Malmsten, Incorporation of antimicrobial compounds in mesoporous silica film monolith, Biomaterials, 30 (2009) 5729-5736.

[37] A. Nieto, M. Colilla, F. Balas, M.a. Vallet-Regi, Surface Electrochemistry of Mesoporous Silicas as a Key Factor in the Design of Tailored Delivery Devices, Langmuir, 26 (2010) 5038-5049.

[38] E. Serra, A. Mayoral, Y. Sakamoto, R.M. Blanco, I. Díaz, Immobilization of lipase in ordered mesoporous materials: Effect of textural and structural parameters, Microporous Mesoporous Mater, 114 (2008) 201-213.

[39] P.I. Ravikovitch, D. Wei, W.T. Chueh, G.L. Haller, A.V. Neimark, Evaluation of Pore Structure Parameters of MCM-41 Catalyst Supports and Catalysts by Means of Nitrogen and Argon Adsorption, J Phys Chem B, 101 (1997) 3671-3679.

[40] H. Essa, E. Magner, J. Cooney, B.K. Hodnett, Influence of pH and ionic strength on the adsorption, leaching and activity of myoglobin immobilized onto ordered mesoporous silicates, J. Mol. Catal. B: Enzym., 49 (2007) 61-68.

[41] A. Salis, M.S. Bhattacharyya, M. Monduzzi, Specific Ion Effects on Adsorption of Lysozyme on Functionalized SBA-15 Mesoporous Silica, J Phys Chem B, 114 (2010) 7996-8001.

[42] K.D. Collins, G.W. Neilson, J.E. Enderby, Ions in water: Characterizing the forces that control chemical processes and biological structure, Biophys Chem, 128 (2007) 95-104.

[43] J. He, Y. Xu, H. Ma, D.G. Evans, Z. Wang, X. Duan, Inhibiting the leaching of lipase from mesoporous supports by polymerization of grafted vinyl groups, Microporous Mesoporous Mater, 94 (2006) 29-33.

[44] S. Hudson, J. Cooney, B.K. Hodnett, E. Magner, Chloroperoxidase on Periodic Mesoporous Organosilanes:Immobilization and Reuse, Chem Mater, 19 (2007) 2049-2055.

5. MONOOLEIN BASED FORMULATIONS FOR CAFFEINE

5.1. Introduction

One of the successful and novel area of research in drug delivery that aims to enhance therapeutic efficacy, bioavailability and avoid adverse effects of the drugs is transdermal/topical drug delivery [1]. Different approaches such as iontophoresis [2], sonophoresis [3], transdermal gels [4] nanoemulsions [5] and chemical enhancers [6] have been used to enhance skin permeation and bioavailability of drugs. Surfactants, a category of chemical enhancers, can form liquid crystalline (LC) phases in the presence of water. Lyotropic LC formulations based upon use of biocompatible lipids have been studied for drug delivery of a wide number of small molecules as well as proteins and peptides [7]. Emulsions stabilized by LC phases are one of the most promising approaches for transdermal/topical delivery of drugs and cosmetics. It presents many advantages over conventional creams and ointments such as higher storage stability, good production feasibility, higher thermodynamic stability and absence of organic solvents [8-12].

LC phases of monoolein present interesting properties for drug delivery system across the skin and mucosa. Monoolein is a biocompatible and bioadhesive chemical enhancer and has the ability to incorporate compounds independently of their solubility. It can protect drugs from physical and enzymatic degradation and sustain their delivery [13]. It is non-irritant, non-toxic and safe to the skin and fall under generally recognized as safe (GRAS) category [14]. It is useful for transdermal/topical drug delivery since it promotes ceramide extraction and enhancement of lipid fluidity in the stratum corneum region of the skin [15]. Moreover, it swells in water and depending on water content and temperature several LC phases can be formed, including lamellar, bicontinuous cubic and

hexagonal phases. The lamellar and bicontinuous cubic phases of monoolein and water are formed at room temperature, and have been shown to accommodate and sustain the release of drugs with various physical and chemical properties [7, 16-17]. The reverse hexagonal phase of monoolein and water is obtained only at high temperatures, unless a third nonpolar component (e.g. triglycerides or oleic acid) is added to the system [18]. Also this phase presents the ability to sustain the delivery of incorporated compounds [19]. Earlier, it has been showed that an emulsion prepared by dispersing water in the LC medium shows a long-term shelf life [11]. The stability of such a system towards phase separation is high. The use of thermodynamically stable LC phases, preferentially lamellar or hexagonal microstructure, allows the dispersion of many types of liquids [11].

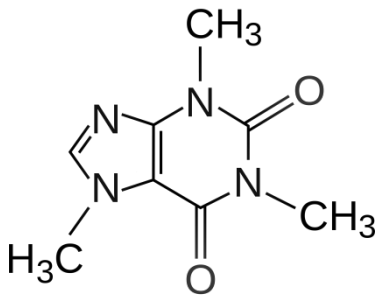

Fig.5.1. Chemical structure of caffeine

Model small molecular weight (194.19 Da) water soluble (21.7 mg/ml) drug caffeine is often used in the release kinetics experiments from emulsions and microemulsions [20-22]. The chemical structure of caffeine is represented in Fig.5.1. It is non-irritant and compatible with lipidic membranes. It has several therapeutic and cosmetic applications. It has been investigated in the treatment of neonatal apnea [23], in the prevention of neurodegenerative disorders [24], in the treatment of skin cancer [25]

and in the anti-cellulite activity by stimulation of fat metabolism [26]. Several commercially available topical formulations contain about 3% caffeine [20].

The aim of this study was to investigate the microstructure and physico-chemical properties of W/O emulsion, lamellar, reverse hexagonal, and bicontinuous cubic LC formulations prepared with primarily monoolein and caffeine solution (CS). In order to prepare reverse hexagonal LC formulations and emulsions stabilized by liquid crystals, triolein was used as non-polar component. The emulsion and different LC phases were obtained according to the monoolein-water phase diagram and ternary phase diagram of monoolein, triolein and water [11, 27]. *In vitro* release properties of caffeine from these formulations were investigated.

5.2. Materials and methods

5.2.1. Materials

Monoolein (MO) (98.1 wt.%) was kindly provided by Danisco Ingredients, Brabrand, Denmark. Triolein (TRI) with technical purity of 65 wt.% (this reagent contains also 1,3- and 1,2-diglycerides, monoglycerides; the fatty acid chain composition is 90 wt.% as oleic acid and 10 wt.% as linoleic acid), was from Sigma. Caffeine (99 wt.%) was obtained from Sigma. Distilled water (W), passed through a Milli-Q water purification system (Millipore), and deuterated water from Fluka were used to prepare the samples.

5.2.1. Preparation of formulations

The formulations were prepared according to the components and composition given in Table 1. Caffeine solution (CS) used for preparing the formulations was prepared with the fixed concentration of 10 mg/ml in water (W) or deuterated water (D_2O). The samples for NMR experiments were prepared using D_2O instead of W.

Table 1 Components and composition of formulation.

Formulation	Composition	Ratio	Amount of caffeine (mg)/g of formulation
I	MO/TRI/W/CS	63/11/19/7	0.7
II	MO/TRI/CS	69/11/20	2.0
III	MO/CS	85/15	1.5
IV	MO/CS	70/30	3.0
V	MO/TRI/CS	80/11/9	0.9

For preparation of formulation I, MO (3.77 g) was melted in a glass test tube (80 ml Duran Schott, Germany) at about 40 °C and TRI (0.66 g) was added subsequently. A small amount (approximately 200 μl) of W was added to this mixture and vortexing was done at approximately 2500 rpm for about 5 min. This was repeated till the total volume of W added becomes 1110 μl. This sample was centrifuged for about 20 minutes at 2000 rpm. It was kept in incubator at 25 °C overnight to achieve equilibrium. A small amount (approximately 200 μl) of CS (10 mg/ml) was added to the LC phases and again vortexing was done. A total of 450 μl of CS was added and vortexing was done each time. Finally sample was centrifuged at 1000 rpm for 10 minutes in order to settle down the emulsion stuck on the wall of glass tube. Formulation II was prepared similarly using CS instead of W for the formation of LC phase. For the preparation of formulation III and IV, CS was mixed with monoolein according to the composition mentioned in Table 1.

5.2.2. Polarized light microscopy (PLM)

The anisotropic LC phases were observed by optical microscopy (Zeiss Axioplan 2) in polarized light at 25 ± 1 °C. The obtained patterns were compared with the typical textures of other surfactants [28].

5.2.3. Nuclear Magnetic Resonance (NMR)

^{2}H NMR measurements were performed by a Bruker Avance 7.05 T spectrometer at the operating frequency of 300 MHz at 25 °C. A standard variable temperature control unit (with an accuracy of 0.5 °C) was used. ^{2}H NMR spectra were periodically recorded, without lock, to verify the achievement of equilibrium and to characterize the LC microstructure in mono- or multiphase samples.

Nuclei with a spin quantum number $I \geq 1$, such as ^{14}N or ^{2}H, have an electric quadrupolar moment that can interact with nonzero net electric field gradients giving multiple resonance of $2I$ peaks, which in the case of oriented anisotropic LC phases are separated by the splitting:

$$\Delta\nu_q = (3/m)P_b\chi S_b \quad (1)$$

where m = 4 and m = 8 apply for the lamellar and hexagonal phase, respectively, P_b is the fraction of the observed nucleus in the bound state, χ is the quadrupolar coupling constant, and S_b = ½(3cos$^2\nu_D$ - 1) is the order parameter related to the average time orientation (ν_D) of the nucleus with respect to the surfactant chain axis. For water molecules, P_b is linearly dependent on the surfactant/water (S/W) molar ratio and thus equation 1 can be rewritten as

$$\Delta\nu_q = (3/m)\, n_b(S/W)\chi S_b \quad (2)$$

where n_b is the number of bound water molecules per polar head. The inner and outer peaks correspond to the nuclei orientations at 90° and 0°. Each sample was left for 30 min in the NMR probe to ensure thermal equilibrium and alignment in the magnetic field before recording the spectra at 25 °C.

5.2.3. SAXS experiments

Small-angle X-ray scattering (SAXS) diffraction patterns were recorded with a S3-MICRO SWAXS camera system (HECUS X-ray Systems, Graz, Austria). Cu K_α radiation of wavelength 1.542 Å was provided by a GeniX X-ray generator, operating at 50 kV and 1 mA. A 1D-PSD-50M system (HECUS X-ray system) containing 1024 channels of width 54 μm was used for detection of scattered X-rays in the small-angle region. The working *q*-range ($Å^{-1}$) was $0.003 \leq q \leq 0.6$, where $q = 4\pi \sin(\theta) \lambda^{-1}$ is the modulus of the scattering wave vector. To minimize scattering from air, the camera volume was kept under vacuum during the measurements. Silver behenate (CH_3-$(CH_2)_{20}$-COOAg) with a *d* spacing value of 58.38 Å was used as a standard to calibrate the angular scale of the measured intensity. The diffraction patterns were first recorded in increasing order of temperature i.e. 25, 32 and 37 ºC and latter it was decreased to original sample temperature of 25 ºC to study the effect of temperature on the stability of LC phases. A PC-controlled Peltier element was used for temperature stabilization and control of the sample. A few milligrams of the sample were enclosed in a stainless steel sample holder using a polymeric sheet (Bratfolie, Kalle) window. The distance between the sample and detector was 254 mm. The lattice parameter (*a*) of the different LC phases was determined using the relation $d = 2\pi/q = a/(h^2 + k^2 + l^2)^{1/2}$ from linear fits of the plots of *q* versus $(h^2 + k^2 + l^2)^{1/2}$, where *q* is the measured peak position and *h*, *k*, and *l* are the Miller indices. The lattice parameters are represented as mean ± standard deviation. Standard deviation was calculated by considering lattice parameter values for all the major peaks.

5.2.4. *In vitro* release studies

Caffeine release from W/O emulsion and LC formulations was monitored using Franz diffusion cells. Membrane diffusion was performed on cellulose membrane (MS® CA membrane filter, pore size 0.45 µm, Membrane Solutions, USA). Test material was applied to the membrane with a glass rod and a dose (1000 mg) of formulation was applied and the cells were covered with parafilm in order to avoid water evaporation. The receptor fluid phosphate buffer pH 7.4 (50 mM) was stirred constantly and maintained at 37 °C. Sodium azide (0.02% w/v) was added to the receptor fluid to prevent microbial growth. Membranes were allowed to equilibrate with the receptor phase for 2h before charging each donor compartment with the formulations. The sampling times investigated were 1, 2, 3, 4, 6, 8 and 24 h. Samples (2 ml) of receptor phase were withdrawn and each sample removed was replaced by an equal volume of fresh receptor phase. The diffusion experiment was performed 3 times for each formulation except if noted differently.

5.3. Results and discussion

5.3.1. Phase behaviour

Caffeine release from W/O emulsion and LC formulations was monitored using Franz diffusion cells. Membrane diffusion was performed on cellulose membrane (MS® CA membrane filter, pore size 0.45 µm, Membrane Solutions, USA). Test material was applied to the membrane with a glass rod and a dose (1000 mg) of formulation was applied and the cells were covered with parafilm in order to avoid water evaporation. The receptor fluid phosphate buffer pH 7.4 (50 mM) was stirred constantly and maintained at 37 °C. Sodium azide (0.02% w/v) was added to the receptor fluid to prevent microbial growth. Membranes were

allowed to equilibrate with the receptor phase for 2h before charging each donor compartment with the formulations. The sampling times investigated were 1, 2, 3, 4, 6, 8 and 24 h. Samples (2 ml) of receptor phase were withdrawn and each sample removed was replaced by an equal volume of fresh receptor phase. The diffusion experiment was performed 3 times for each formulation except if noted differently.

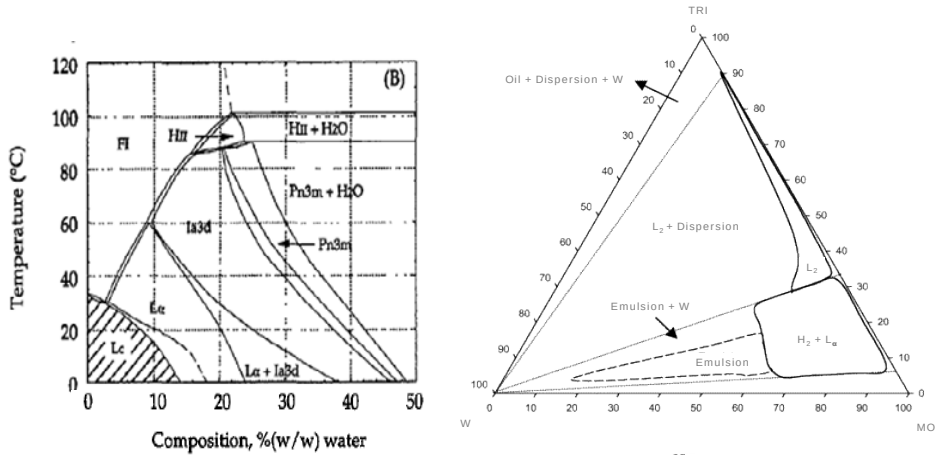

(a) (b)

Fig.5.2. (a) Phase diagram for MO/W system in the 0–120 °C temperature and 0–50% (w/w) water composition range, and (b) Schematic and phase diagram of the ternary system of MO/TRI/W at 25 °C.

5.3.2. Polarized light microscopy

The preliminary information about the phase behaviour of the emulsion and LC samples with CS instead of W was obtained using polarized light microscopy. The four different samples were selected with the intention of their possible application for drug delivery and composition for them is given in Table 1. As observed in Fig.5.3.a, formulation I was found to be W/O type emulsion with the presence of aqueous droplets surrounded by reverse hexagonal (H_2) phase with the characteristic fan-like texture. It can be seen in Fig.5.3.b that also formulation II shows fan like texture, characteristic of reverse hexagonal (H_2) phase. Fig.5.3.c clearly

shows maltese-crosses which is characteristic of lamellar (L_α) phase and hence validates lamellar LC structure of formulation III. Formulation IV did not show any pattern under the polarized light microscope as it was isotropic. This is typical of cubic phases. All the four types of samples prepared with CS exhibited similar microscopic pattern to the samples prepared according to MO/TRI/W and MO/W phase diagrams. This demonstrates that the caffeine added at the concentration of 10 mg/ml to the emulsion and LC samples did not cause significant phase transition among the four samples investigated here.

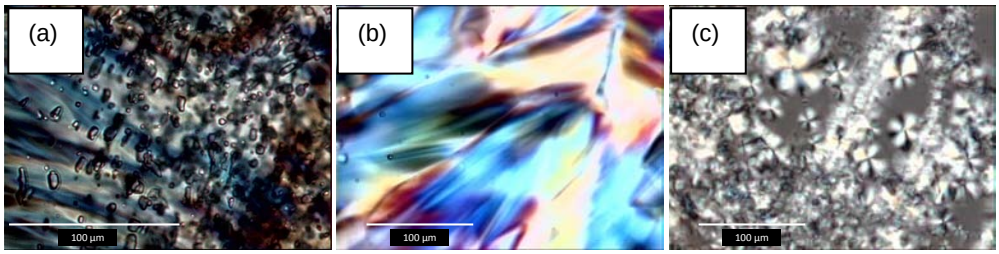

Fig.5.3. Polarized light microscopy at 25 º C (a) formulation I (320X magnification) (b) formulation II (200X magnification) and (c) formulation III (200X magnification).

5.3.2 ^{2}H NMR

^{2}H NMR spectra for the H_2+L_α two-phase and emulsion regions of MO/TRI/D are reported in reference [11]. It is known that the ^{2}H NMR spectra of samples prepared with D shows the quadrupolar splitting typical of anisotropic phases. Fig.5.4 (a) shows the results obtained for the W/O emulsion sample having the composition MO/TRI/D_2O/CS (63/11/19/7). A single isotropic signal due to isotropic solution (CS droplets of Fig.5.3.a) and the two clear quadrupolar splittings due to anisotropic LC phase can be observed, namely $\Delta\upsilon_{q1}$ = 501 Hz, $\Delta\upsilon_{q2}$ = 938 Hz, as expected from the H_2 phase which shows both 90° and 0° alignments. The results obtained for samples containing different amount of CS and having the composition MO/TO/CS (69/11/20) (formulation I) and (80/11/9) (formulation II) are

shown in Fig.5.4 (b) and (c), respectively. In the case of the sample with the higher amount of CS i.e. formulation I, two quadrupolar splittings, namely $\Delta\upsilon_{q1}$ = 576 Hz and $\Delta\upsilon_{q2}$ = 1050 Hz are observed suggesting again the presence H_2 LC structure. Sample with relatively less amount of CS i.e. MO/TO/CS (80/11/9) shows four quadrupolar splittings.

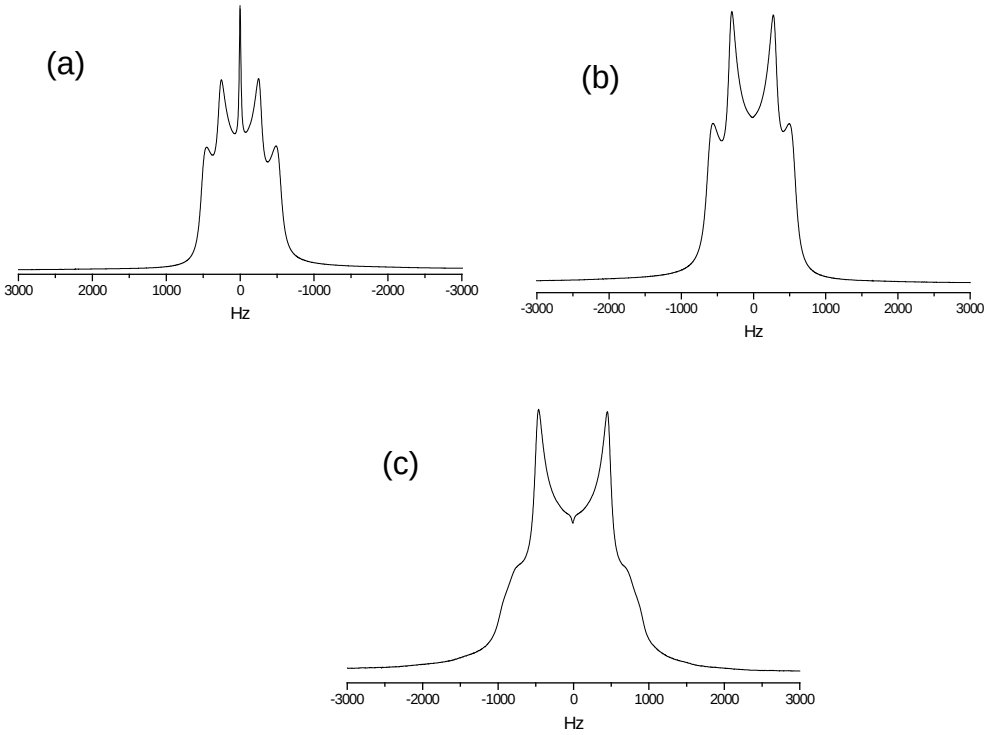

Fig.5.4. ^{2}H NMR spectra for (a) formulation I, (b) formulation II, and (c) formulation V.

The splittings $\Delta\upsilon_{q1}$ = 910 Hz and $\Delta\upsilon_{q2}$ = 1856 Hz could correspond to a predominant H_2 phase. The less intense splittings $\Delta\upsilon_{q3}$ = 1450 Hz and $\Delta\upsilon_{q4}$ = 3210 Hz could be due to presence of a L_α phase. Thus, this sample clearly shows the biphasic nature and validates the presence of both LC phases, H_2 and L_α, as reported previously [11]. It should be remarked that the splittings assigned to the H_2 and to the L_α LCs do not fulfil the predictions of equation 2 exactly. Substantially, $\Delta\upsilon_{q3}$ should be almost equal to $\Delta\upsilon_{q2}$. The reason of the anomalous values may be ascribed

to the presence of caffeine that, due to its shape, is likely to be preferentially located in the water layer of the lamellar phase rather than in the water cylinders of the reverse hexagonal phase. Caffeine partition should increase the effective thickness of the L_α, water layer, but subtracts water molecules, thus decreasing the surfactant/water (S/W) molar ratio; consequently the quadrupolar splitting decreases. Indeed, as depicted by equation 2, $\Delta\upsilon_q$ of D_2O in surfactant/water systems mainly depends on S/W, provided that enough hydration water molecules are present (n_b is constant). Generally $\Delta\upsilon_q$ decreases with increasing water content.

In conclusion, it can be suggested that the different partition of caffeine in the water domains of the L_α, and H_2 LC phases is responsible for the observed anomalous quadrupolar splittings of D_2O.

5.3.3. SAXS

Fig.5.5 and Table 2 show the SAXS patterns and lattice parameters for formulation I-IV. The SAXS study was performed to understand the effect of temperature on the LC structure of all formulations. The formulation I which was W/O type emulsion stabilized by LC phase showed peculiar results. We could not observe the peaks due to L_α phase, since it was mainly dominated by H_2 phase. The lattice parameter of this sample decreased from about 65 to 59 Å, when it was warmed from ambient temperature (25 °C) to physiological temperature (37 °C). It did not revert back to the original lattice parameter when temperature was decreased to the ambient temperature; rather it decreased slightly to 58 Å. This effect could be due to relatively less thermal stability of the emulsion in comparison to LC phases, alone. Formulation II and III showed typical scattering pattern of H_2 and L_α LC phases, respectively, from temperature 25 to 37 °C and even when they were brought back to ambient temperature (25 °C). Formulation II showed a slight decrease from 60 to 59 Å with

increase in temperature from 25 to 37 °C and it reversed back to 59 Å after decreasing temperature to 25°C. Formulation III is a lamellar phase, whose lattice parameter fluctuates in the range of 41.9-43.6 Å. Formulation IV showed bicontinuous cubic phase pattern of *Ia3d* type. In this case lattice parameter decreased significantly from about 146 to 142 Å with increasing temperature to physiological condition. It reverts back to the original lattice parameter with decreasing temperature to ambient conditions.

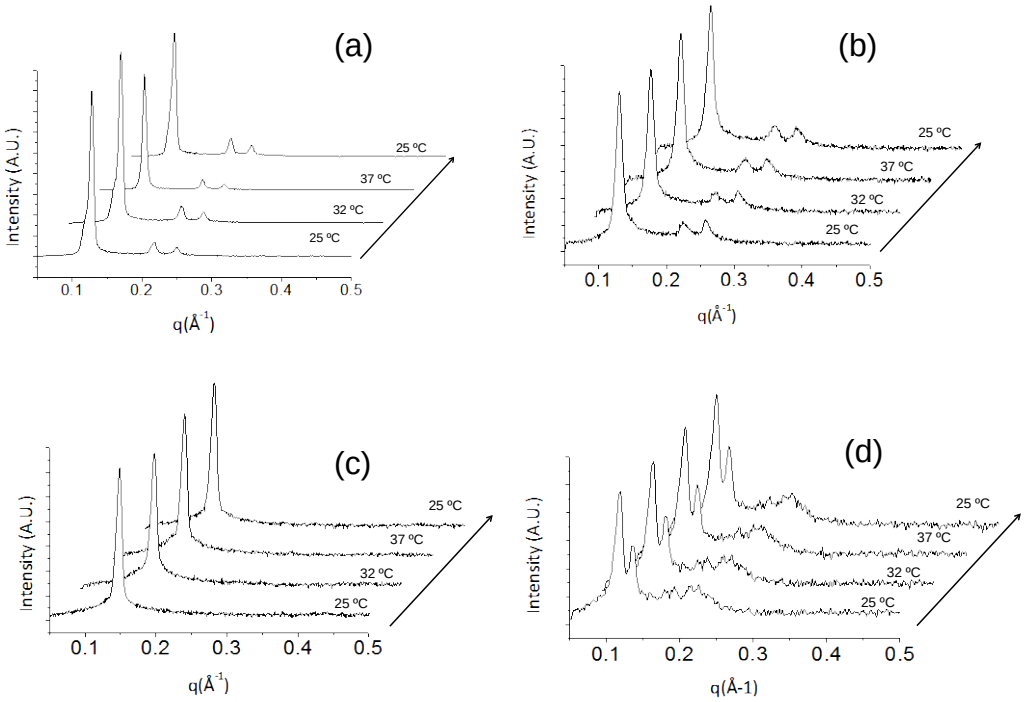

Fig.5.5. SAXS patterns with increase in temperature from 25, 32 to 37 ºC and then decreasing back to 25 ºC for formulation I (a), II (b), III (c) and IV (d).

Table 2 Effect of temperature on lattice parameters for formulation I-IV.

Temperature (ºC) →	*25*	*32*	*37*	*25*	*LC structure*
I	65.0 ± 0.5	63.5 ± 0.4	59.2 ± 0.6	57.6 ± 0.7	H_2
II	59.7 ± 0.2	59.6±0.6	58.6 ± 0.5	59.2 ± 0.2	H_2
III	43.0	41.9	43.6	42.4	L_α
IV	146.0 ± 1.0	145.0 ± 1.0	142.0 ± 0.2	144.8 ± 0.9	Ia3d

5.3.4. *In vitro* release of caffeine

The four formulations studied here had different loading capacities for caffeine, because of different water content in respective formulations. It can be observed from Table 1 that maximum loading of caffeine was obtained in case of formulation IV, which had 30% water and bicontinuous cubic LC structure. Formulation II and III had 20% and 15% water, and H_2 and L_α LC structure, respectively. In case of formulation I, although 26% water was added, only 7% water was used for caffeine loading because 19% water was required to form LC structure.

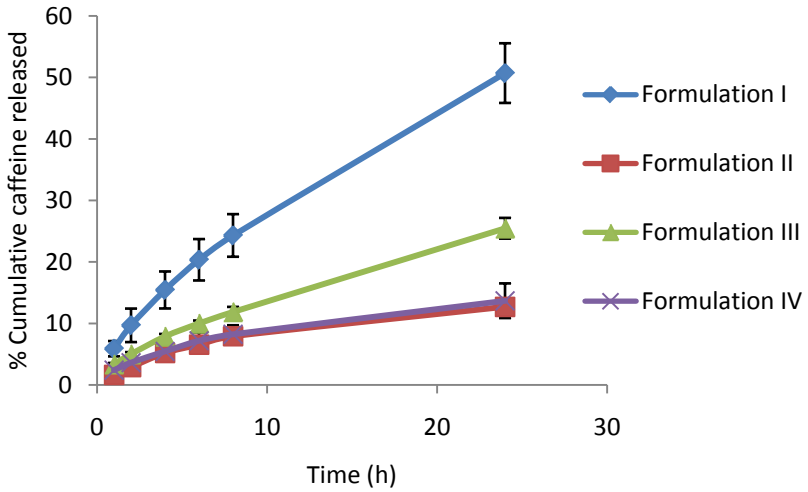

Fig.5.6. *In vitro* release of caffeine using Franz diffusion cell.

The *in vitro* release experiments show that about 50% of caffeine loaded was released in 24 hours in case of W/O emulsion (formulation I) samples. Lamellar LC formulation (formulation III) showed slower release than emulsion sample and only about 25% caffeine was released in 24 hours. Both reverse hexagonal LC formulation (formulation II) and bicontinuous cubic LC formulation (formulation IV) samples showed very slow and similar release pattern. In both cases at the end of experiment only about 15% release of caffeine was found. Hexagonal phases are more

viscous than lamellar phases. The bicontinuous cubic phases are very stiff, and they behave almost like a solid [29]. Thus, the release data obtained here can be correlated to viscosity of the different LC phases. The reason for highest release of caffeine from formulation I is that the caffeine might not have experienced considerable resistance from the LC phases, since it is mainly present in the water droplets of the emulsion.

Similarity between the release curves can further be elucidated by the similarity factor, F_2, described by FDA, which can be calculated using the following equation:

$$F_2 = 50 \times log\left\{\left[1 + \frac{1}{n}\sum_{t=1}^{n}(R_t - T_t)^2\right]^{-0.5} \times 100\right\} \quad (3)$$

where n is the number of time points, R_t is the amount released of a reference product and T_t is the amount released for the test product at time t. If F_2 is between 50 and 100, the two profiles are considered to be similar and bioequivalent [30].

When the release data for formulation I are compared with that of formulation II, III and IV, F_2 values were 36.5, 44.6 and 37 respectively. This proves that the formulation I, which is a W/O emulsion shows a completely different release pattern. Comparing the release data for formulation II with that of formulation III and IV, the calculated F_2 values are 61.3 and 96, respectively. This proves that formulation II, which has mainly reverse hexagonal structure, releases caffeine at a similar rate to that of formulation IV having bicontinuous cubic structure. The final amount released in case of formulation III (lamellar phase) (about25%) was found to be significantly higher than that from formulation II (reverse hexagonal phase) (about 15%), nevertheless the initial release for the first eight hours was very similar. Hence the F_2 comparison suggests that these two formulations are not significantly different in releasing caffeine. The F_2

value was found to be 63.4, when comparison between release data for formulation III (lamellar phase) and formulation IV (bicontinuous cubic phase) was done. This shows that formulation III and IV are also similar in releasing caffeine. Thus, only significant difference in release of caffeine is found in case of emulsion sample.

5.4. Conclusions

The monoolein based formulations for caffeine were characterized by polarized light microscopy, ^{2}H NMR and SAXS. The LC structure did not change, at a macroscopic level, as result of caffeine addition. SAXS study proved that temperature changes from ambient to physiological conditions and then reverting back to original temperature can cause significant variations in lattice parameter of LC phases that stabilize W/O emulsion system. The *in vitro* release of caffeine from these formulations was in the range of 15-50% of the loaded amount of the caffeine after 24 hours. This preformulation data can be used to design an appropriate topical/transdermal drug delivery system. Further studies are in progress to understand the diffusion across the biological membrane, and to obtain optimized procedures for the preparation of the formulations.

5.5. References

[1] R.B. Walker, E.W. Smith, The role of percutaneous penetration enhancers, Adv Drug Deliv Rev, 18 (1996) 295-301.

[2] R.H. Guy, Iontophoresis - Recent developments, J Pharm Pharm Sci, 50 (1998) 371-374.

[3] A. Boucaud, L. Machet, B. Arbeille, M.C. Machet, M. Sournac, A. Mavon, F. Patat, L. Vaillant, In vitro study of low-frequency ultrasound-enhanced transdermal transport of fentanyl and caffeine across human and hairless rat skin, Int J Pharm, 228 (2001) 69-77.

[4] S. Baboota, F. Shakeel, K. Kohli, Formulation and evaluation of once-a-day transdermal gels of diclofenac diethylamine, Methods Find Exp Clin Pharmacol, 28 (2006) 109-114.

[5] F. Shakeel, W. Ramadan, M.A. Ahmed, Investigation of true nanoemulsions for transdermal potential of indomethacin: characterization, rheological characteristics, and ex vivo skin permeation studies, J Drug Target, 17 (2009) 435-441.

[6] S.A. Ibrahim, S.K. Li, Effects of chemical enhancers on human epidermal membrane: Structure-enhancement relationship based on maximum enhancement (Emax), J Pharm Sci, 98 (2009) 926-944.

[7] J.C. Shah, Y. Sadhale, D.M. Chilukuri, Cubic phase gels as drug delivery systems, Adv Drug Deliv Rev, 47 (2001) 229-250.

[8] P. Tyle, S.G. Frank, Phytosterol Stabilized Emulsions: Interpacial Complexation and Structural Investigations, Drug Dev Ind Pharm, 16 (1990) 1605-1618.

[9] A. Otto, J.W. Wiechers, C.L. Kelly, J.C. Dederen, J. Hadgraft, J. du Plessis, Effect of emulsifiers and their liquid crystalline structures in emulsions on dermal and transdermal delivery of hydroquinone, salicylic acid and octadecenedioic acid, Skin Pharmacol Physiol, 23 (2010) 273-282.

[10] A. Semenzato, A. BaÙ, C. Dall'Aglio, M. Nicolini, A. Bettero, I. Calliari, Stability of vitamin A palmitate in cosmetic emulsions: influence of physical parameters, Int J Cosmet Sci, 16 (1994) 139-147.

[11] S. Mele, S. Murgia, F. Caboi, M. Monduzzi, Biocompatible Lipidic Formulations: Phase Behavior and Microstructure, Langmuir, 20 (2004) 5241-5246.

[12] L. Brinon, S. Geiger, V. Alard, J.F. Tranchant, T. Pouget, G. Couarraze, Influence of lamellar liquid crystal structure on percutaneous diffusion of a hydrophilic tracer from emulsions, J Cosmet Sci, 49 (1998) 1-11.

[13] L.B. Lopes, J.L.C. Lopes, D.C.R. Oliveira, J.A. Thomazini, M.T.J. Garcia, M.C.A. Fantini, J.H. Collett, M.V.L.B. Bentley, Liquid crystalline phases of monoolein and water for topical delivery of cyclosporin A: Characterization and study of in vitro and in vivo delivery, Eur J Pharm Biopharm, 63 (2006) 146-155.

[14] A. Ganem-Quintanar, D. Quintanar-Guerrero, P. Buri, Monoolein: A Review of the Pharmaceutical Applications, Drug Dev Ind Pharm, 26 (2000) 809 - 820.

[15] T. Ogiso, M. Iwaki, T. Paku, Effect of various enhancers on transdermal penetration of indomethacin and urea, and relationship between penetration parameters and enhancement factors, J Pharm Sci, 84 (1995) 482-488.

[16] M.G. Lara, M.V.L.B. Bentley, J.H. Collett, In vitro drug release mechanism and drug loading studies of cubic phase gels, Int J Pharm, 293 (2005) 241-250.

[17] P. Geraghty, D. Attwood, J. Collett, Y. Dandiker, The in vitro release of some antimuscarinic drugs from monoolein/water lyotropic liquid crystalline gels, Pharm Res, 13 (1996) 1265-1271.

[18] J. Borné, T. Nylander, A. Khan, Phase Behavior and Aggregate Formation for the Aqueous Monoolein System Mixed with Sodium Oleate and Oleic Acid, Langmuir, 17 (2001) 7742-7751.

[19] M.G. Carr, J. Corish, O.I. Corrigan, Drug delivery from a liquid crystalline base across Visking and human stratum corneum, Int J Pharm, 157 (1997) 35-42.

[20] M. Dias, A. Farinha, E. Faustino, J. Hadgraft, J. Pais, C. Toscano, Topical delivery of caffeine from some commercial formulations, Int J Pharm, 182 (1999) 41-47.

[21] P. Clément, C. Laugel, J.-P. Marty, In vitro release of caffeine from concentrated W/O emulsions: effect of formulation parameters, Int J Pharm, 207 (2000) 7-20.

[22] P. Clément, C. Laugel, J.-P. Marty, Influence of three synthetic membranes on the release of caffeine from concentrated W/O emulsions, J Control Release, 66 (2000) 243-254.

[23] M. Amato, M. Isenschmid, P. Hüppi, Percutaneous caffeine application in the treatment of neonatal apnoea, Eur J Pediatr, 150 (1991) 592-594.

[24] J.-F. Chen, K. Xu, J.P. Petzer, R. Staal, Y.-H. Xu, M. Beilstein, P.K. Sonsalla, K. Castagnoli, N. Castagnoli, Jr, M.A. Schwarzschild, Neuroprotection by Caffeine and A2A Adenosine Receptor Inactivation in a Model of Parkinson's Disease, J. Neurosci., 21 (2001) 143RC-.

[25] A.H. Conney, Y.P. Lu, Y.R. Lou, M.T. Huang, Inhibitory effects of tea and caffeine on UV-induced carcinogenesis: Relationship to enhanced apoptosis and decreased tissue fat, European Journal of Cancer Prevention, 11 (2002) S28-S36.

[26] C. Bertin, H. Zunino, J.C. Pittet, P. Beau, P. Pineau, M. Massonneau, C. Robert, J. Hopkins, A double-blind evaluation of the activity of an anti-cellulite product containing retinol, caffeine, and ruscogenine by a combination of several non-invasive methods, J Cosmet Sci, 52 (2001) 199-210.

[27] J. Briggs, H. Chung, M. Caffrey, The temperature-composition phase diagram and mesophase structure characterization of the monoolein/water system, J Phys II, 6 (1996) 723-751.

[28] F.B. Rosevear, The microscopy of the liquid crystalline neat and middle phases of soaps and synthetic detergents, J Am Oil Chem Soc, 31 (1954) 628-639.

[29] G. Montalvo, M. Valiente, E. Rodenas, Rheological Properties of the L Phase and the Hexagonal, Lamellar, and Cubic Liquid Crystals of the CTAB/Benzyl Alcohol/Water System, Langmuir, 12 (1996) 5202-5208.

[30] X. Cheng, R. Liu, Y. He, A simple method for the preparation of monodisperse protein-loaded microspheres with high encapsulation efficiencies, Eur J Pharm Biopharm, 76 (2010) 336-341.

CONCLUDING REMARKS

In last few decades, smart nanostructured materials, for instance, triblock copolymers with thermoreversible properties, silica nanoparticles with different organic functionalizations, and lipids possessing ability to form different lyotropic liquid crystalline structures, have drawn attention to obtain novel drug delivery systems. These drug delivery systems are highly advantageous over conventional pharmaceutical dosage forms, since they can be tailor-made to achieve controlled release of therapeutic drug molecules.

In this PhD thesis, the use of different non-ionic surfactants to prepare and characterize smart nanostructured drug delivery systems was investigated. The focus was on the evaluation of effectiveness of these systems to modulate the *in vitro* release properties of a model protein such as lysozyme and, a small drug molecule such as caffeine.

Chapter 3 discusses the system consisting of gelatin microspheres suspended in thermoreversible Pluronic F127 (PF 127) gel. The characterization of the gelatin microspheres (GMs) crosslinked by two different cross-linkers *viz.* D-glucose and glutaraldehyde was done by Scanning Electron Microscopy (SEM) and ATR-FTIR technique. Evidence of the spherical shape and different degree of cross-linking was provided. Aqueous PF 127 gel (20 % w/v) with the presence and the absence of GMs, were, characterized for rheology and for gel microstructure by Small Angle X-ray Scattering (SAXS). Sol-gel transition temperature of PF 127 gel was mostly unaffected when either glucose or glutaraldehyde crosslinked microspheres were suspended in them. It was found about 22 ^{0}C indicating feasibility of formulations for therapeutic applications. SAXS study confirmed that the PF 127 gel microstructure was a discrete cubic liquid crystal of Fm3m type and it was not significantly affected by the presence of

0.5 % w/v of both the types of microspheres. The release of lysozyme from both types of crosslinked GMs was successfully controlled when they were suspended in PF127 gel.

Chapter 4 discusses about the application of ordered mesoporous materials (OMMs) as matrices for drug delivery systems. A comparison was made between the widely studied SBA-15 mesoporous silica with that of less investigated MSE mesoporous organosilica, towards the adsorption (at pH 7.0 and 9.6) and *in vitro* controlled release of lysozyme. Both OMMs have a hexagonal ordered mesoporous structure and texture, as confirmed by SAXS, TEM and N_2 adsorption isotherms, but differ for the chemical composition and surface charge density, as determined by ATR-FTIR spectroscopy and potentiometric titrations, respectively. Rather than the structural and textural features, the different chemical composition of SBA-15 and MSE seems to be responsible of the different lysozyme loading and release, and of the different stability towards the lixiviating action of the physiological medium.

Chapter 5 discusses the use of monoolein to form W/O emulsion and liquid crystalline formulations, including reverse hexagonal, lamellar, and bicontinuous cubic formulations. Caffeine, chosen as a model drug, was added to these formulations at the concentration of 10mg/ml. The formulations were then characterized by polarized light microscopy, NMR and SAXS. It was found that they did not change the liquid crystalline structure significantly due to the presence of caffeine. The loading capacity for caffeine solution in these formulations varied between 7 and 30% of the weight of the formulations. The *in vitro* release of caffeine from these formulations was in the range of 15-50% of the loaded amount of the caffeine after 24 hours. The preformulation data obtained here can be useful to design an appropriate topical/transdermal drug delivery system.